

1983

A study of single angle compression members

James Robert Callaway
Portland State University

Follow this and additional works at: https://pdxscholar.library.pdx.edu/open_access_etds



Part of the [Civil Engineering Commons](#), and the [Structural Engineering Commons](#)

Let us know how access to this document benefits you.

Recommended Citation

Callaway, James Robert, "A study of single angle compression members" (1983). *Dissertations and Theses*. Paper 3240.

<https://doi.org/10.15760/etd.3231>

This Thesis is brought to you for free and open access. It has been accepted for inclusion in Dissertations and Theses by an authorized administrator of PDXScholar. Please contact us if we can make this document more accessible: pdxscholar@pdx.edu.

AN ABSTRACT OF THE THESIS OF James Robert Callaway for the Master of Science in Engineering-Civil presented December 2, 1983.

Title: A Study of Single Angle Compression Members

APPROVED BY MEMBERS OF THE THESIS COMMITTEE:

[REDACTED]

Wendelin H. Mueller

[REDACTED]

Donald G. Howard

[REDACTED]

Leon Kempner

A study was undertaken to investigate the compressive capacity of a specific group of single angle members.

A review of existing literature and techniques was presented. Laboratory compression tests were performed on 22 angle members of four different sizes and two different lengths. Additional tests were performed to determine the yield strength of the material. The results, normalized with respect to the yield stress, were tabulated and discussed.

Two existing analytic models were used to attempt to predict the ultimate capacity of the test members. The first, an elastic method,

was based upon the AISC combined stress equation. The second, an inelastic method, was developed by Mueller and Erzurumlu of Portland State University. Comparisons were made with the results of the test program.

The results indicate that both analytic models give conservative predictions when pinned end conditions are assumed and unconservative results for fixed end conditions. For the test members with L/r ratios greater than 125, the elastic method results closely paralleled the test results but for the members with L/r ratios less than 125 the correlation was less consistent. The results of the inelastic technique closely paralleled the results of all the member tests.

A STUDY OF SINGLE ANGLE COMPRESSION MEMBERS

by

JAMES ROBERT CALLAWAY

A thesis submitted in partial fulfillment of the
requirements for the degree of

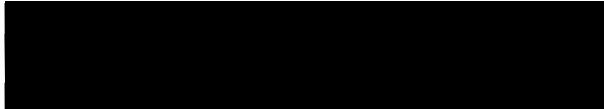
MASTER OF SCIENCE
in
ENGINEERING-CIVIL

Portland State University

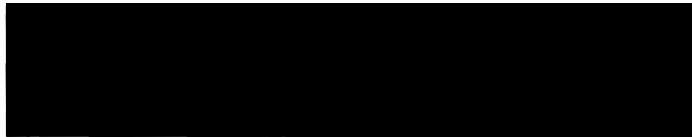
1983

TO THE OFFICE OF GRADUATE STUDIES AND RESEARCH:

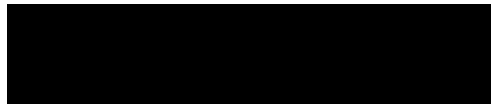
The members of the Committee approve the thesis of James Robert Callaway presented December 2, 1983.



Wendelin H. Mueller



Donald G. Howard

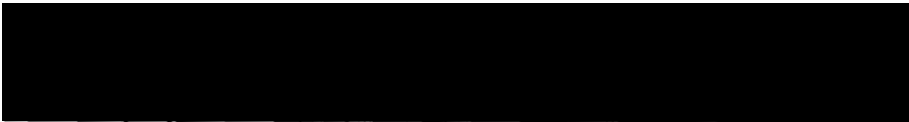


Leon Kempher

APPROVED:



Franz N. Rad, Head, Department of Civil Engineering



S.E. Rauch, Dean of Graduate Studies and Research

ACKNOWLEDGEMENTS

I would like to thank my advisor and friend, Dr. Wendelin Mueller, for providing his continual support and encouragement along with an occasional push, without which this project might never have been completed. Special thanks also to Microflect Company, and particularly Jim Kreitzberg, who gave me the encouragement and incentive to embark upon this project in the first place. Also, thanks to Steve Speer of Portland State University for his help with the testing, Beverly LaCrosse for her help with the drawings, Karen Mercer and Jodell Bayan for their efforts with the typing of this manuscript and, of course, to my wife, Linda.

TABLE OF CONTENTS

	PAGE
ACKNOWLEDGEMENTS	iii
LIST OF TABLES	v
LIST OF FIGURES	vi
CHAPTER	
I INTRODUCTION	1
II REVIEW OF THE LITERATURE	3
III TEST PROGRAM	9
Test Procedure	9
Test Results	13
Summary of Test Results	69
IV ANALYTICAL METHODS	72
Elastic Method	73
Inelastic Method	81
Summary of Analytical Methods	84
V CONCLUSIONS AND RECOMMENDATIONS	90
BIBLIOGRAPHY	93

LIST OF TABLES

TABLE		PAGE
I	Test Specimen Group, Number, Type and Dimensions	10
II	Summary of Test Results	14
III	Connection Eccentricity and Location of Shear Center	40
IV	Summary of Test Specimen Yield Strength Values	64
V	Connection Average Maximum Bearing Stresses	66
VI	Input Values for Elastic Solution	79
VII	Results of Combined Stress Solution	80
VIII	Input Values for Inelastic Solution	85
IX	Results of Inelastic Computer Solution	86

LIST OF FIGURES

FIGURE	PAGE
1. Classic Euler column	4
2. Schematic layout of test apparatus	11
3. Load vs displacement plot for test specimen 01-GT48-01	15
4. Load vs displacement plot for test specimen 02-GT48-01	16
5. Load vs displacement plot for test specimen 03-GT48-01	17
6. Load vs displacement plot for test specimen 20-GT48-01	18
7. Load vs displacement plot for test specimen 04-GT48-02	19
8. Load vs displacement plot for test specimen 05-GT48-02	20
9. Load vs displacement plot for test specimen 06-GT48-02	21
10. Load vs displacement plot for test specimen 19-GT48-02	22
11. Load vs displacement plot for test specimen 07-GT36-01	23
12. Load vs displacement plot for test specimen 08-GT36-01	24
13. Load vs displacement plot for test specimen 09-GT36-01	25
14. Load vs displacement plot for test specimen 17-GT36-01	26
15. Load vs displacement plot for test specimen 10-GT36-02	27
16. Load vs displacement plot for test specimen 11-GT36-02	28
17. Load vs displacement plot for test specimen 12-GT36-02	29
18. Load vs displacement plot for test specimen 18-GT36-02	30
19. Load vs displacement plot for test specimen 13-GT36-03	31
20. Load vs displacement plot for test specimen 14-GT36-03	32
21. Load vs displacement plot for test specimen 15-GT36-03	33

FIGURE	PAGE
22. Load vs displacement plot for test specimen 16-GT36-03	34
23. Load vs displacement plot for test specimen 21-GT36-01	35
24. Load vs displacement plot for test specimen 22-GT36-02	36
25. Typical load/displacement plot	37
26. Diagram of angle cross section and major axis	39
27. Typical midspan movement of test specimen cross section ...	42
28. Yield stress determination, test specimen 01-GT48-1	43
29. Yield stress determination, test specimen 02-GT48-1	44
30. Yield stress determination, test specimen 03-GT48-1	45
31. Yield stress determination, test specimen 20-GT48-1	46
32. Yield stress determination, test specimen 04-GT48-2	47
33. Yield stress determination, test specimen 05-GT48-2	48
34. Yield stress determination, test specimen 06-GT48-2	49
35. Yield stress determination, test specimen 19-GT48-2	50
36. Yield stress determination, test specimen 07-GT36-1	51
37. Yield stress determination, test specimen 08-GT36-1	52
38. Yield stress determination, test specimen 09-GT36-1	53
39. Yield stress determination, test specimen 17-GT36-1	54
40. Yield stress determination, test specimen 10-GT36-2	55
41. Yield stress determination, test specimen 11-GT36-2	56
42. Yield stress determination, test specimen 12-GT36-2	57
43. Yield stress determination, test specimen 18-GT36-2	58
44. Yield stress determination, test specimen 13-GT36-3	59
45. Yield stress determination, test specimen 14-GT36-3	60
46. Yield stress determination, test specimen 15-GT36-3	61

FIGURE

PAGE

47. Yield stress determination, test specimen 16-GT36-3	62
48. Yield stress determination, test specimen 21-GT36-1 and 22-GT36-1	63
49. Computer listing of numerical combined stress solution	77
50. Computer listing of exact combined stress solution	78
51. Plot of combined stress solution results	82
52. Plot of inelastic solution results	87

CHAPTER I

INTRODUCTION

The column is one of the most widely used structural elements in existence. Few structures, if any at all, lack column members.

The most common cross sections used for columns are pipes and wide flanges. Considerable research has been performed for these sections to develop analytical models and practical design methods. For other cross sectional shapes, such as single angles, very little research data is available.

Single angles are not generally recommended for use as compression members. This is primarily because of the inherently eccentric end connections. The American Institute of Steel Construction (AISC), in their Manual of Steel Construction, (5, pg. 3-48) does not encourage the use of single angle compression members because of the difficulty involved in evaluating their compressive capacity.

The worldwide tower industry, however, uses single angle compression members almost universally. This may seem to be a contradiction, but when the economics of material cost, ease of fabrication, and competitiveness of the marketplace are considered, angle sections have proven to be reliable and cost effective for this particular application.

Because towers are generally designed as space trusses, each individual component is designed for tension and compression loads only.

The effects of eccentric end conditions have historically been either neglected or simplified for ease of design. The American Society of Civil Engineers (ASCE), in their Design Manual for Steel Transmission Towers, does not have any provisions for evaluating the end connections for singly-bolted single angle struts.

For this particular report, a group of single angle compression members was obtained from the inventory of Microflect Co., Inc. of Salem, Oregon. These members were actual components of one of Microflect Company's standard guyed tower product lines.

In their actual application, the angle members are attached between the leg members of a guyed tower to develop a latticed mast. Their function is to transmit lateral wind shear loads along the length of the guyed mast to either the ground or to one of the guy cable attachment points. These shear loads result in substantial axial tension/compression loads in the single angle members. The connection at each end between tower members is made by means of a single bolt in one leg of the angles.

A consequence of this type of connection is partial end restraint of the member. This partial end restraint is not along a principal axis of the member cross section and, therefore, the effects of it cannot be easily evaluated.

This report compares the results of actual member tests with two analytical models and attempts to recommend a practical design procedure.

- problem e/end cond

CHAPTER II

REVIEW OF THE LITERATURE

The first major column theory was presented by Euler in 1744(1).

Euler's theory was based upon the following assumptions:

1. Constant cross-sectional area.
2. Homogeneous material.
3. The member in compression is simply supported at both ends.
4. The member is perfectly straight and loaded axially along its centroidal axis.
5. The material obeys Hooke's Law.
6. The curvature of the member is small, thus enabling it to be approximated by y'' .

Figure 1 depicts the classic Euler column. By summing moments about the midpoint of the infinitesimally deflected column and solving the resulting linear differential equation for the non-trivial solution, the following equation can be developed for the critical buckling load of a pinned end column:

$$P_{cr} = \frac{\pi^2 EI}{L^2}$$

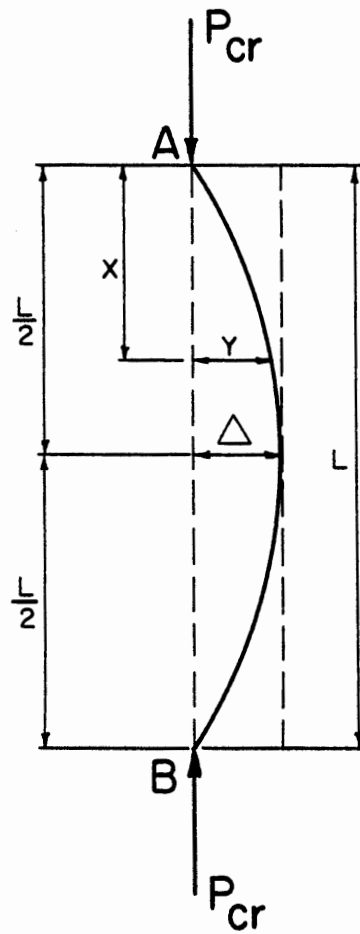


Figure 1. Classic Euler column

For slender columns where the compressive stress of the entire cross-section is below the proportional limit, Euler's formula has been shown to be correct. However, for short columns, Euler's formula is not valid since it implies that P_{CR} approaches infinity as the L/r ratio approaches zero.

In the late 19th century Engesser presented a modification to Euler's theory wherein he suggested that the constant modulus of elasticity, E , be replaced by an effective modulus of elasticity, E_t . The effective or tangent modulus, E_t , was to be taken as the tangent of the stress-strain curve at the stress level under consideration.

At the same time Considere (1) suggested that as a column begins to bend, the stress on the concave side of the cross-section increases in accordance with the tangent modulus, while the stresses on the convex side of the member decrease in accordance with Young's modulus.

Engesser, upon learning of Considere's work, revised his theory to what is now known as the reduced or double modulus theory.

In the development of the reduced modulus theory, the basic assumptions made by Euler were utilized along with two additions:

7. The same relationship exists between bending stresses and bending strains as exists between stress and strain in simple tension and compression.
8. Plane sections before bending remain plane after bending.

Utilizing a development similar to that of Euler, but including the effects upon the cross section, the critical buckling load according to the reduced modulus theory is:

$$P_r = \frac{\pi^2 E_r I}{L^2}$$

$$E_r = \frac{EI_1 + E_t I_2}{I}$$

where:

- I = moment of inertia of column cross-section
- I₁ = moment of inertia of tension zone taken about the neutral axis
- I₂ = moment of inertia of compression zone taken about the neutral axis
- E_t = tangent modulus of elasticity

In 1910 von Karman independently confirmed Engesser's work and performed tests which verified the double modulus theory. For the next 30 years the double modulus theory was assumed to be the correct theory for inelastic column action.

In 1947 Shanley (1,2,3) studied the tangent modulus and double modulus theories through the use of a simplified analytical model. He observed that a fundamental, yet unstated, assumption carried over from Euler's original theory to the double modulus theory was not correct. This assumption was that the column member remained perfectly straight until P_r was reached. This is in contradiction to the development of the reduced modulus wherein it is assumed that the member has finite curvature at P_r . Shanley stated that the tangent modulus load, P_t , is the maximum compressive load at which the member remains straight.

Precise tests have shown that Shanley's work is correct. Upon reaching the tangent modulus load, the axial compressive load can be increased further, but the column no longer remains straight.

The classical theories discussed heretofore all deal with perfectly straight, axially loaded, pinned-end columns. In actual practice, such columns do not exist. Many techniques have been developed which have expanded these classical theories to account for bent members, varying end conditions, and eccentrically applied axial loads. (1,2,3,4)

Chajes (1) presents a method for evaluating eccentrically loaded inelastic columns. Because of the difficulty inherent in obtaining a closed-form solution, the method suggested is a numerical procedure. This procedure is based upon two assumptions:

1. The axis of the column deflects in a half sinewave.
2. The stress varies linearly across the section.

In using Chajes method, a compressive extreme fibre stress is assumed, the corresponding material strain is obtained from the required stress-strain diagram, an equivalent modulus of elasticity is evaluated and the resulting compressive stress is evaluated. If the calculated value and the assumed value are within the desired tolerances, the process is complete.

Bleich (2) discusses a variety of methods that deal with eccentric inelastic column action. He states (1, pg. 44):

Careful analytical studies and comparative calculations made by Chwalla, Jezek and Fritsche indicate that the column strength is considerably influenced by the particular shape of the cross section.

The combination of the influence of the cross-sectional shape and the inherent difficulty in developing a general analytical method for determining the critical load has made it difficult to adequately design

eccentrically loaded columns. This situation is compounded further when a doubly eccentrically loaded column is under investigation.

Recent research, performed by Mueller and Erzurumlu (7), was directed towards the development of a computer model which would be able to predict the behavior of single angle members in the elastic, inelastic and post-buckling regions. They performed parametric studies on a single angle section, varying parameters such as L/r ratio, end connection eccentricity and fixity. The test results were then compared with the results of the computer model which was found to give excellent correlation.

This report will document the results of a series of tests performed on single angle compression members. A comparison of the test results with two different analytical models will be made. These two analytical models take into account the axial shortening of the member and the curvature resulting from the end moments. These end moments are a direct result of the inherent eccentric end connections of singly-bolted angle members. One analytical model assumes elastic material properties only, with the other including the effects of inelastic action. A summary discussion including a recommended design procedure completes the report.

CHAPTER III

TEST PROGRAM

Test Procedure

The purpose of this test program was to provide a data base of actual empirical results to which various analytical models could be compared and evaluated.

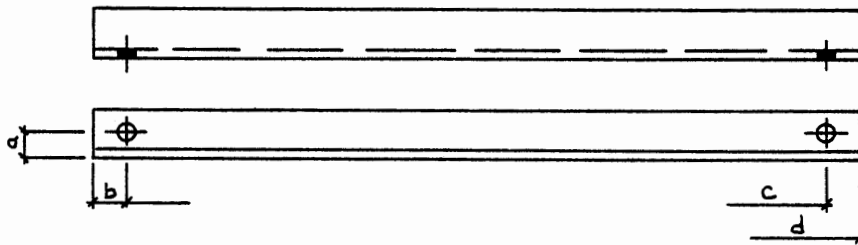
Twenty-two single angle specimens were tested to determine their individual maximum compressive load carrying capacity. The twenty-two specimens consisted of four each of five different pre-manufactured members and two specially modified members. These members consisted of combinations of four section types and two overall lengths. Table I indicates the member lengths, types, and test specimen numbers.

Each specimen had a single 11/16 inch diameter hole at each end. These holes were in the same leg of the angle. All specimens were fabricated from ASTM A36 steel and galvanized in accordance with ASTM A123 specifications.

Figure 2 shows a schematic layout of the test apparatus. The parallelogram members of the test frame were fabricated from double angle 8" x 8" x 3/4" sections. The test specimens were installed diagonally in the frame from corner A to corner C. Because the test specimens were of two different lengths, two adapter links were fabricated, allowing the test frame to translate sideways and provide the correct diagonal hole-to-hole length.

TABLE I

TEST SPECIMEN GROUP, NUMBER, TYPE AND DIMENSION



Group	Number	Angle size	a	b	c	d	L/r
A	01-GT48-1	2.5 x 2.5 x 0.1875	1.25	1.125	59.9375	61.0625	118.8
A	02-GT48-1	2.5 x 2.5 x 0.1875	1.25	1.125	59.9375	61.0625	118.8
A	03-GT48-1	2.5 x 2.5 x 0.1875	1.25	1.125	59.9375	61.0625	118.8
A	20-GT48-1	2.5 x 2.5 x 0.1875	1.25	1.125	59.9375	61.0625	118.8
B	04-GT48-2	2.0 x 2.0 x 0.1875	1.00	1.125	59.9375	61.0625	149.3
B	05-GT48-2	2.0 x 2.0 x 0.1875	1.00	1.125	59.9375	61.0625	149.3
B	06-GT48-2	2.0 x 2.0 x 0.1875	1.00	1.125	59.9375	61.0625	149.3
B	19-GT48-2	2.0 x 2.0 x 0.1875	1.00	1.125	59.9375	61.0625	149.3
C	07-GT36-1	1.75 x 1.75 x 0.125	1.00	1.125	50.625	51.75	142.7
C	08-GT36-1	1.75 x 1.75 x 0.125	1.00	1.125	50.625	51.75	142.7
C	09-GT36-1	1.75 x 1.75 x 0.125	1.00	1.125	50.625	51.75	142.7
C	17-GT36-1	1.75 x 1.75 x 0.125	1.00	1.125	50.625	51.75	142.7
D	10-GT36-2	2.0 x 2.0 x 0.125	1.00	1.125	50.625	51.75	124.4
D	11-GT36-2	2.0 x 2.0 x 0.125	1.00	1.125	50.625	51.75	124.4
D	12-GT36-2	2.0 x 2.0 x 0.125	1.00	1.125	50.625	51.75	124.4
D	18-GT36-2	2.0 x 2.0 x 0.125	1.00	1.125	50.625	51.75	124.4
E	13-GT36-3	2.0 x 2.0 x 0.1875	1.00	1.125	50.625	51.75	125.7
E	14-GT36-3	2.0 x 2.0 x 0.1875	1.00	1.125	50.625	51.75	125.7
E	15-GT36-3	2.0 x 2.0 x 0.1875	1.00	1.125	50.625	51.75	125.7
E	16-GT36-3	2.0 x 2.0 x 0.1875	1.00	1.125	50.625	51.75	125.7
F	21-GT36-1	1.75 x 1.75 x 0.125	0.875	1.125	50.625	51.75	142.7
F	22-GT36-1	1.75 x 1.75 x 0.125	0.875	1.125	50.625	51.75	142.7

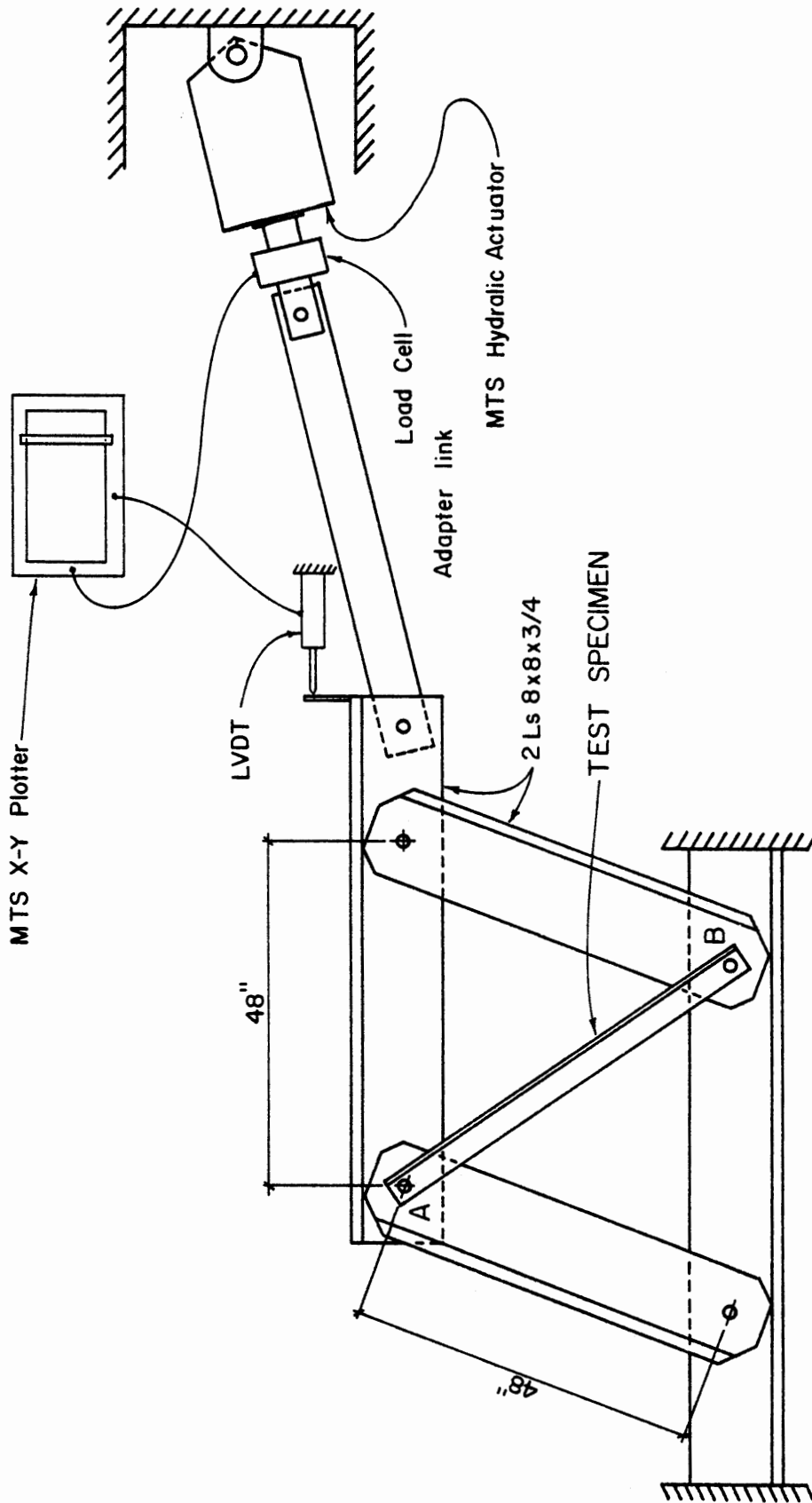


Figure 2. Schematic layout of test apparatus

The end connections were designed to simulate an actual tower installation where they would be bolted, by means of a single bolt, to the outstanding leg of another tower member.

The hydraulic actuator, which is controlled by the MTS has a load cell built into the mechanism. This load cell is placed in series with the actuator providing a direct reading of the applied load. To measure the movement of the test apparatus, an LVDT was utilized and located as shown in Figure 2.

The load cell and LVDT readings were output to the MTS X-Y plotter with the load cell on the ordinate and the LVDT on the abscissa. Because of the geometry of the test frame, the readings from the load cell and the LVDT were not the true load and displacement values of the test specimen. To obtain the actual test specimen load and displacement values, two geometric correction coefficients, C_1 and C_2 , were developed.

The following procedure was used during the testing of each specimen:

1. The member was placed in the test frame, and the nut at each end was installed "finger tight".
2. The member was pre-loaded to approximately 500 lbs. compression.
3. The installation nuts were tightened with a socket wrench using a "turn of the nut" method, wherein the nut is brought to a "snug" fit and then tightened $1/4$ to $1/3$ more turns.

4. The member was loaded under strain control at a rate of approximately 1 strain/sec.
5. A continuous plot of applied MTS load vs. frame translation was made.
6. The plot was monitored and when the member load peaked, indicating compressive failure, the test was terminated.

Test Results

The MTS load vs. frame translation plot, for each of the 22 test specimens, is shown in Figures 3 thru 24. Each plot includes the load vs. axial shortening curve for each specimen obtained through the application of the geometric correction coefficients. Table II summarizes the ultimate loads and displacements of Figures 3 thru 24.

Figure 25 shows a load/displacement plot typical of those obtained from the tests. There were four basic segments common to each of the plots.

1. Each curve exhibited a portion similar to segment AB, this was attributed to the frame seating. Frame seating is the elimination of any looseness due to the fabrication tolerances of the test frame and connection tolerances.
2. Curve segment BC results from the axial elastic shortening of the test specimen combined with axial shortening resulting from the end moment induced curvature.
3. Curve segment CD represents three phenomena. First, the inelastic yielding of the member initiated by the

TABLE II

SUMMARY OF TEST RESULTS

GROUP	NUMBER	P (MTS) Kips	(MTS) Inches	C ₁ *	P Kips	C ₂ *	Inches
A	01-GT48-1	13.4	0.935	1.22	16.3	1.23	1.150
A	02-GT48-1	13.7	0.945	1.22	16.7	1.23	1.162
A	03-GT48-1	13.3	0.725	1.22	16.2	1.23	0.892
A	20-GT48-1	13.1	0.720	1.22	16.0	1.23	0.886
B	04-GT48-2	8.60	0.455	1.22	10.5	1.23	0.560
B	05-GT48-2	9.05	0.450	1.22	11.0	1.23	0.554
B	06-GT48-2	9.00	0.500	1.22	11.0	1.23	0.615
B	19-GT48-2	9.38	0.540	1.22	11.4	1.23	0.664
C	07-GT36-1	7.88	0.405	0.991	7.81	1.03	0.417
C	08-GT36-1	7.57	0.370	0.991	7.50	1.03	0.381
C	09-GT36-1	7.50	0.305	0.991	7.43	1.03	0.314
C	17-GT36-1	7.55	0.264	0.991	7.48	1.03	0.272
D	10-GT36-2	9.60	0.435	0.991	9.51	1.03	0.448
D	11-GT36-2	9.75	0.460	0.991	9.66	1.03	0.474
D	12-GT36-2	9.75	0.460	0.991	9.66	1.03	0.474
D	18-GT36-2	9.45	0.485	0.991	9.36	1.03	0.500
E	13-GT36-3	13.7	0.480	0.991	13.6	1.03	0.494
E	14-GT36-3	15.5	0.525	0.991	15.4	1.03	0.541
E	15-GT36-3	15.0	0.505	0.991	14.9	1.03	0.520
E	16-GT36-3	15.3	0.370	0.991	15.2	1.03	0.381
F	21-GT36-1	0.79	0.470	0.991	6.74	1.03	0.484
F	22-GT36-1	7.13	0.400	0.991	7.07	1.03	0.412

*Geometric correction coefficients.

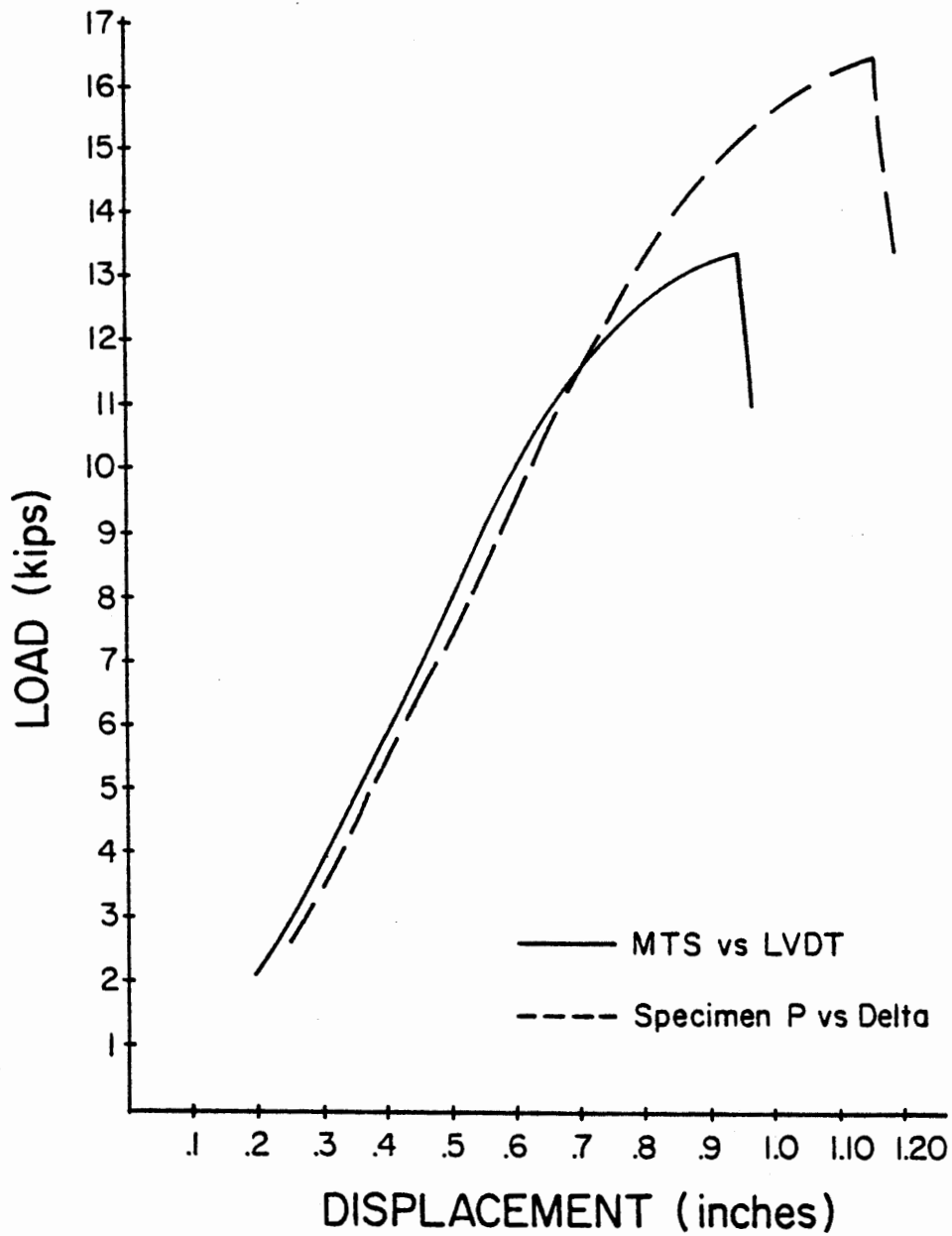


Figure 3. Load vs displacement plot for test specimen OI-GT48-OI

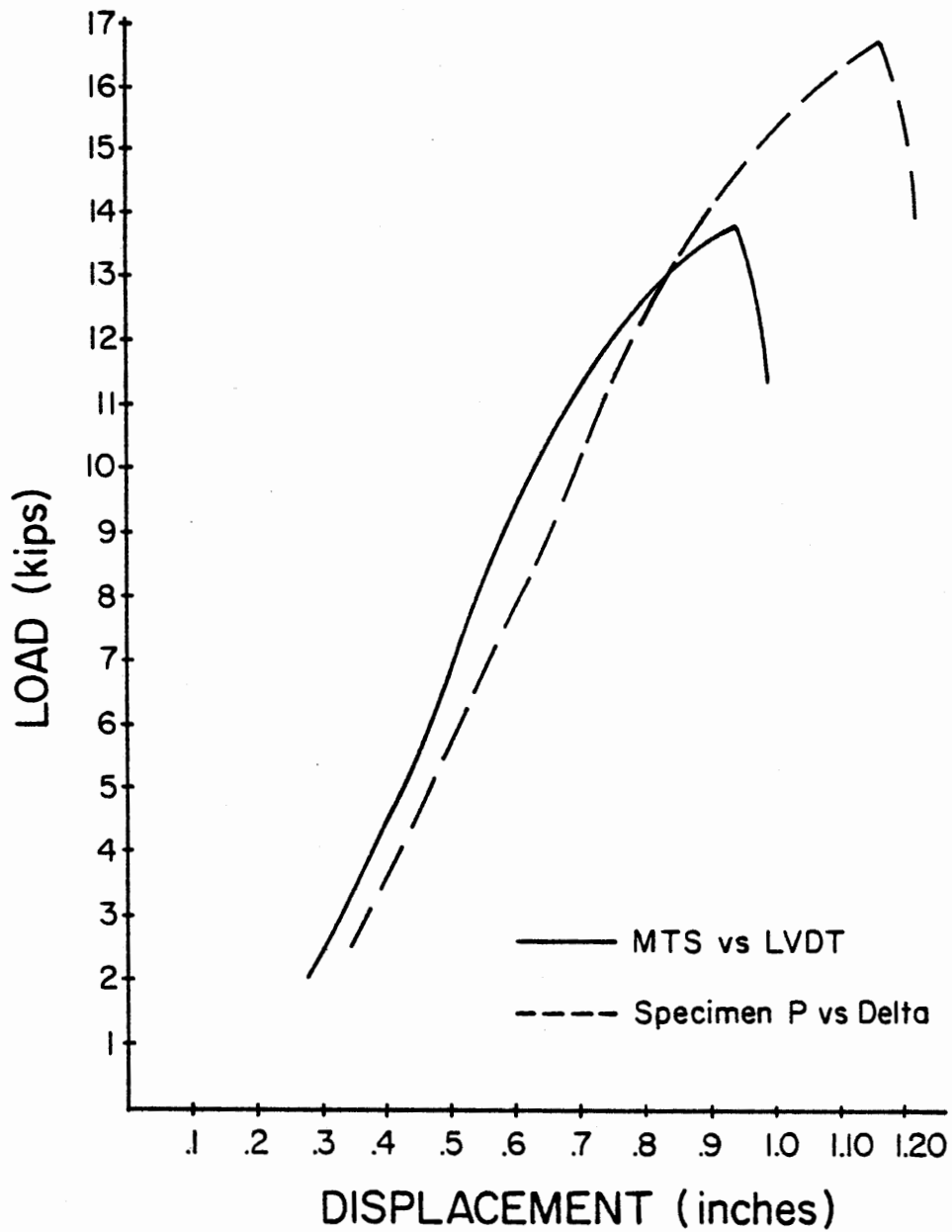


Figure 4. Load vs displacement plot for test specimen O2-GT48-01

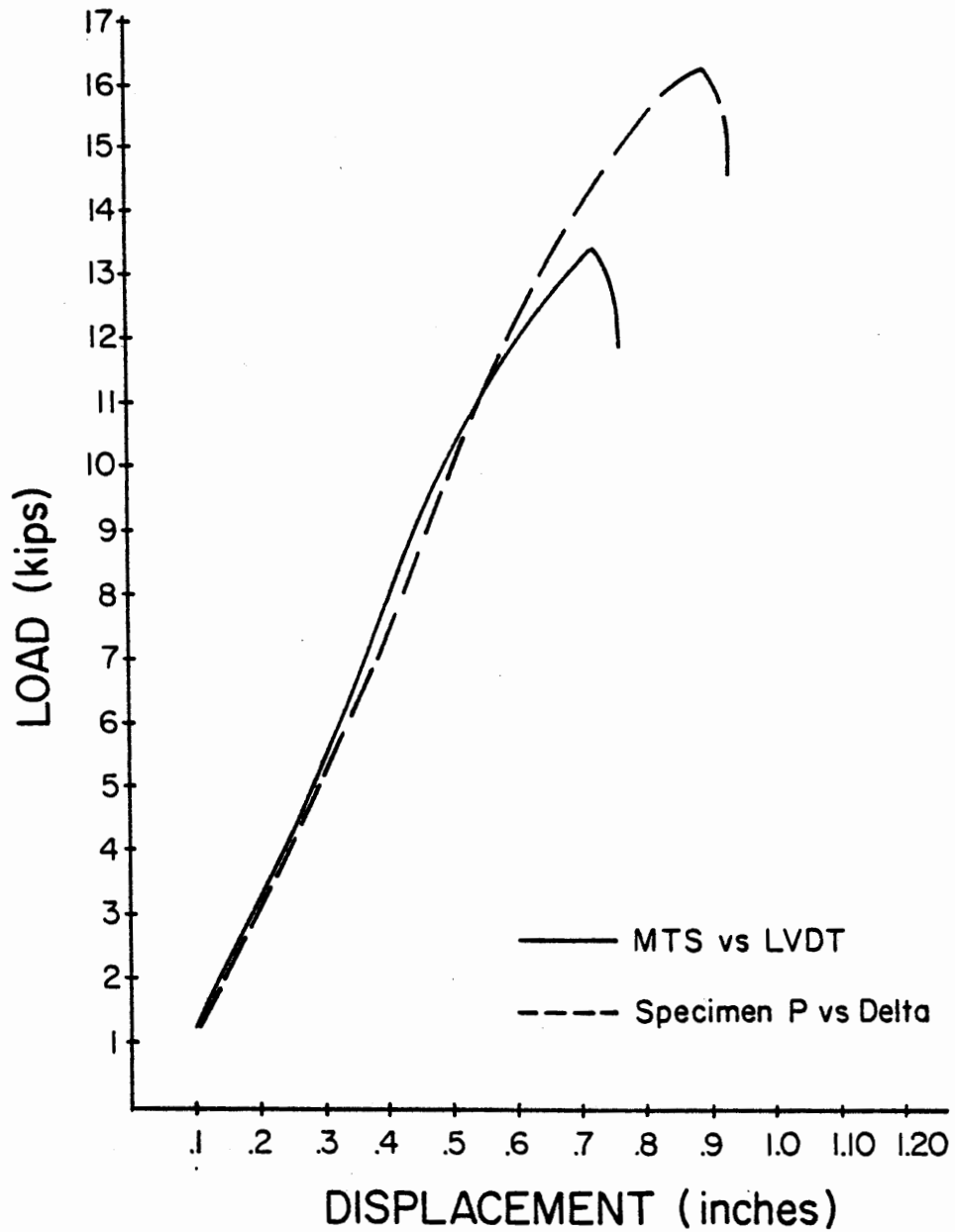


Figure 5. Load vs displacement plot for test specimen 03-GT48-01

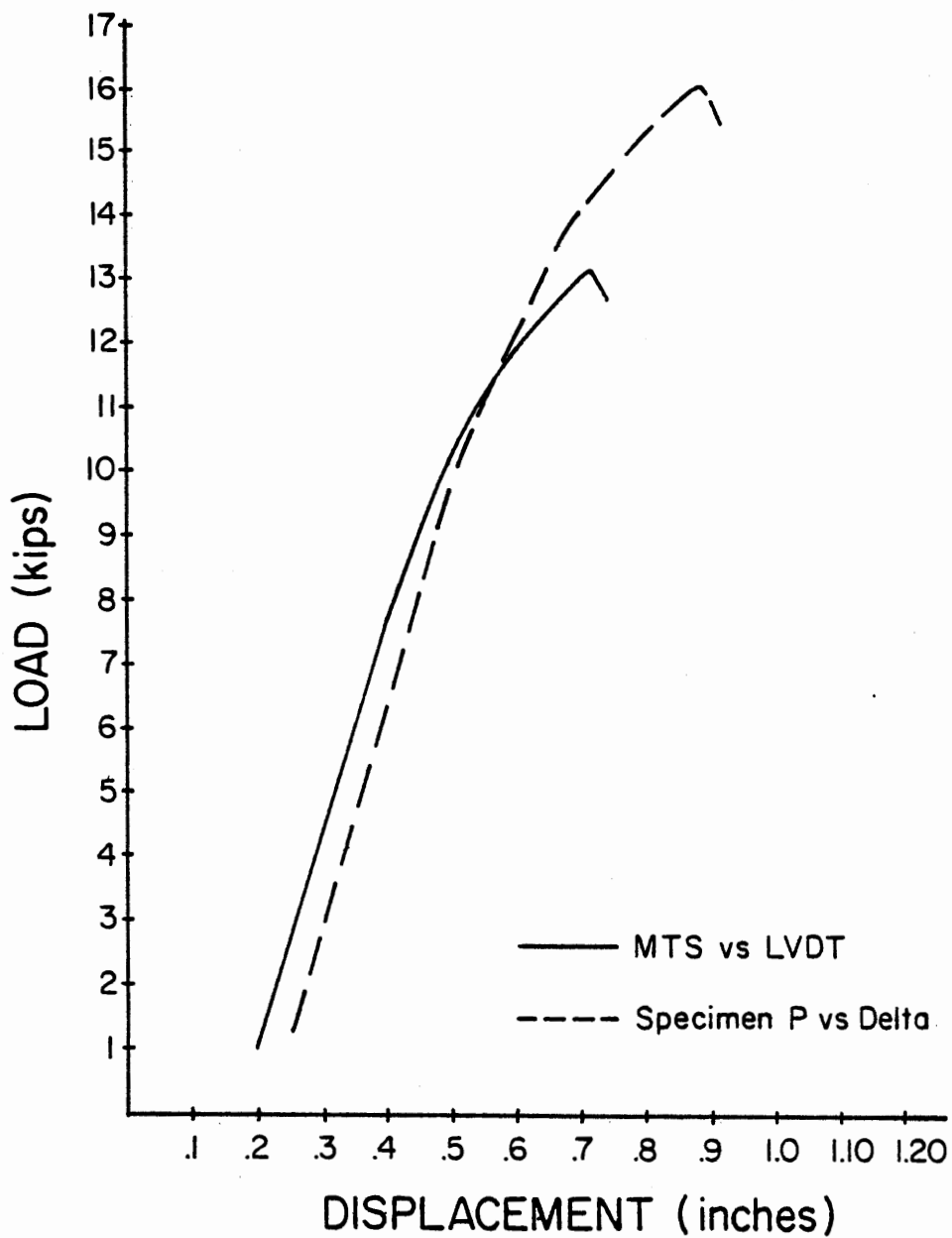


Figure 6. Load vs displacement plot for test specimen 20-GT48-01

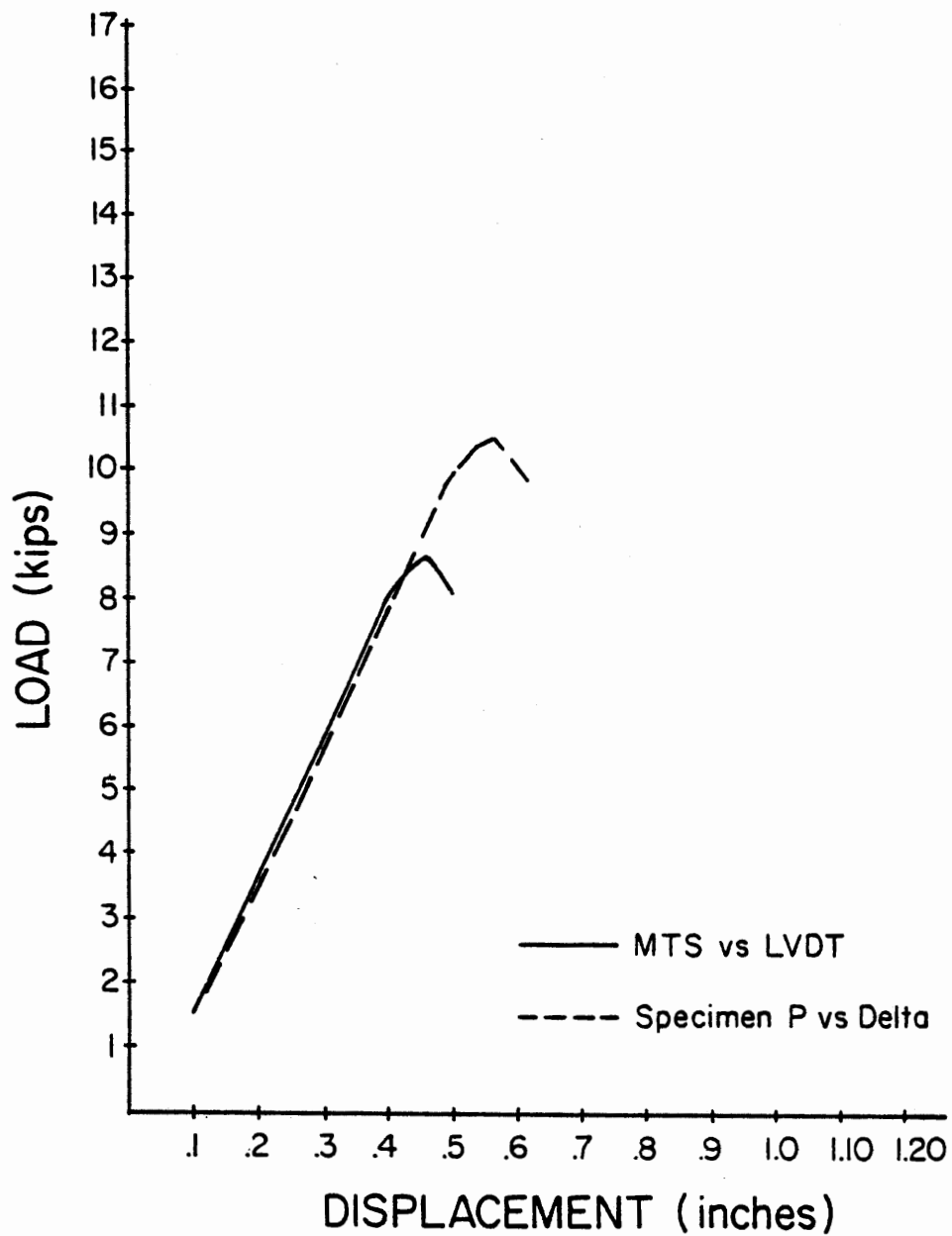


Figure 7. Load vs displacement plot for test specimen O4-GT48-02

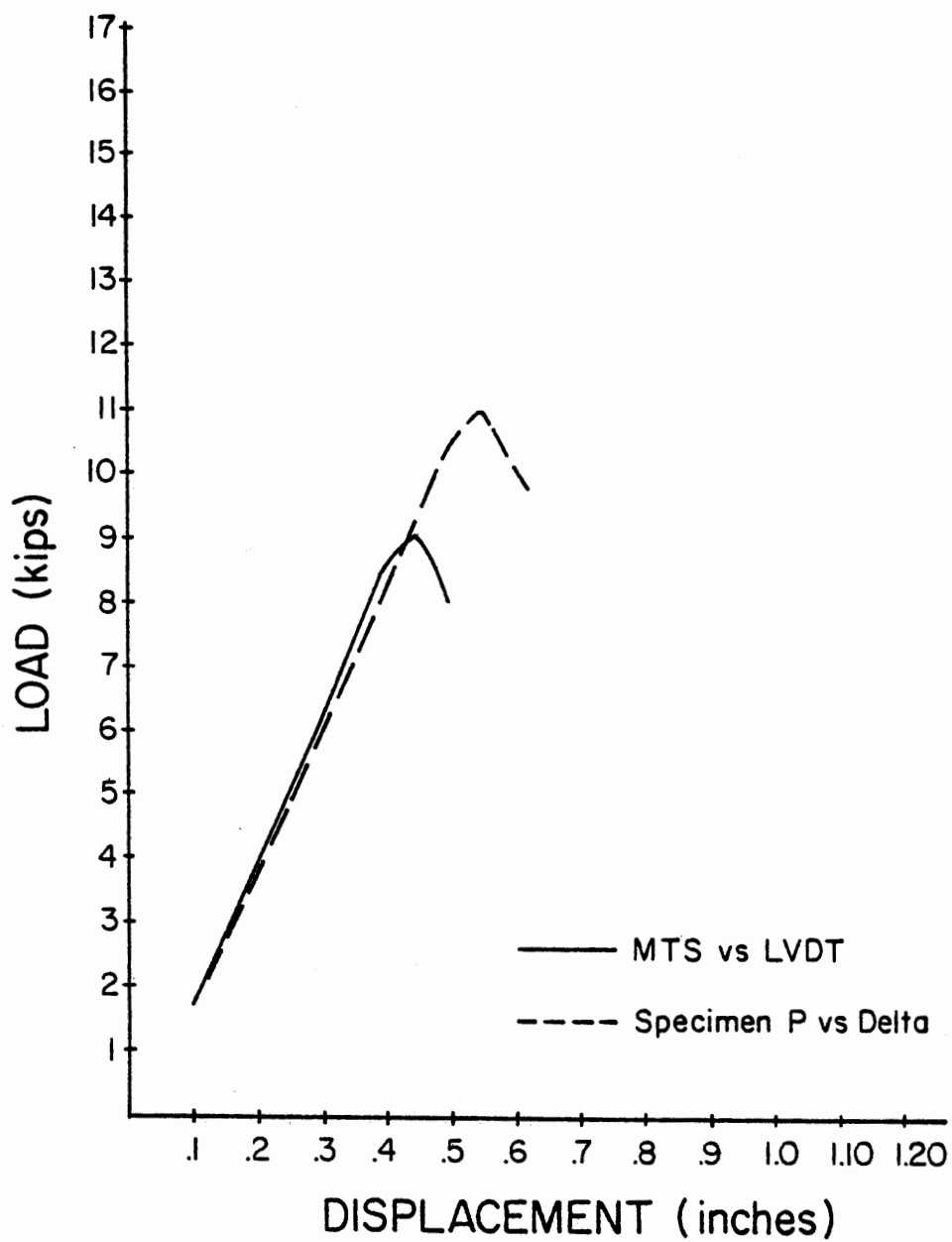


Figure 8. Load vs displacement plot for test specimen O5-GT48-02

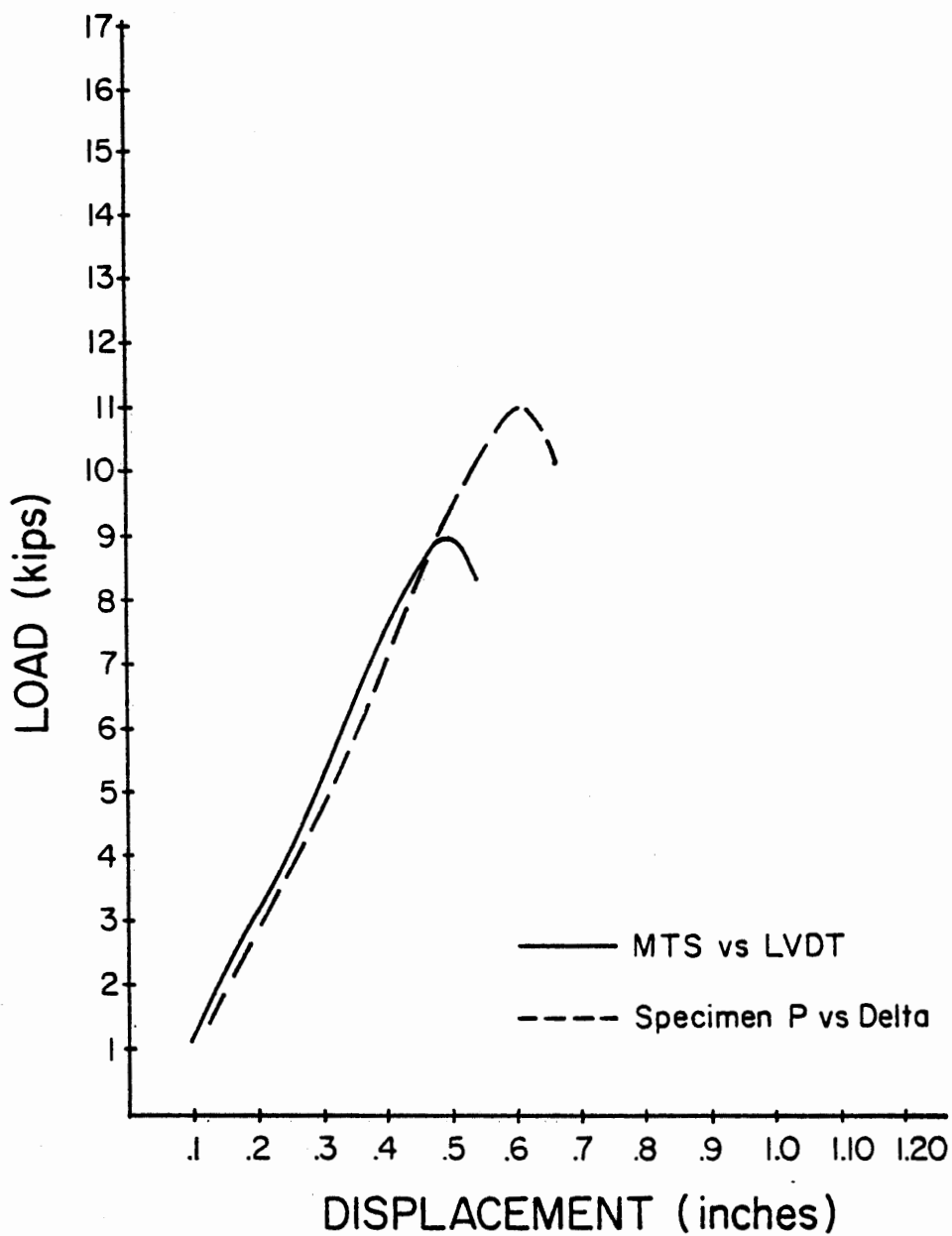


Figure 9. Load vs displacement plot for test specimen 06-GT48-02

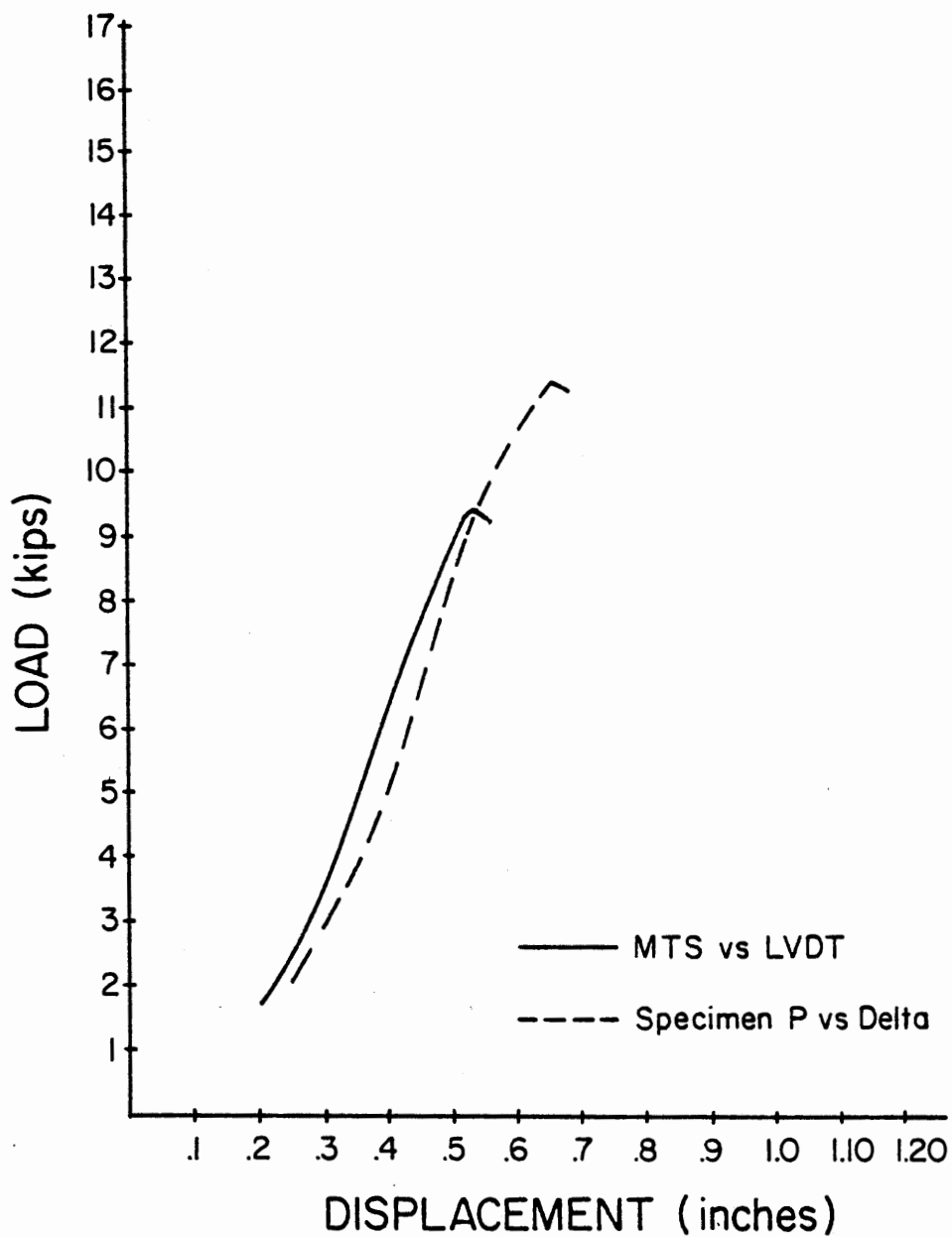


Figure 10. Load vs displacement plot for test specimen 19-GT48-02

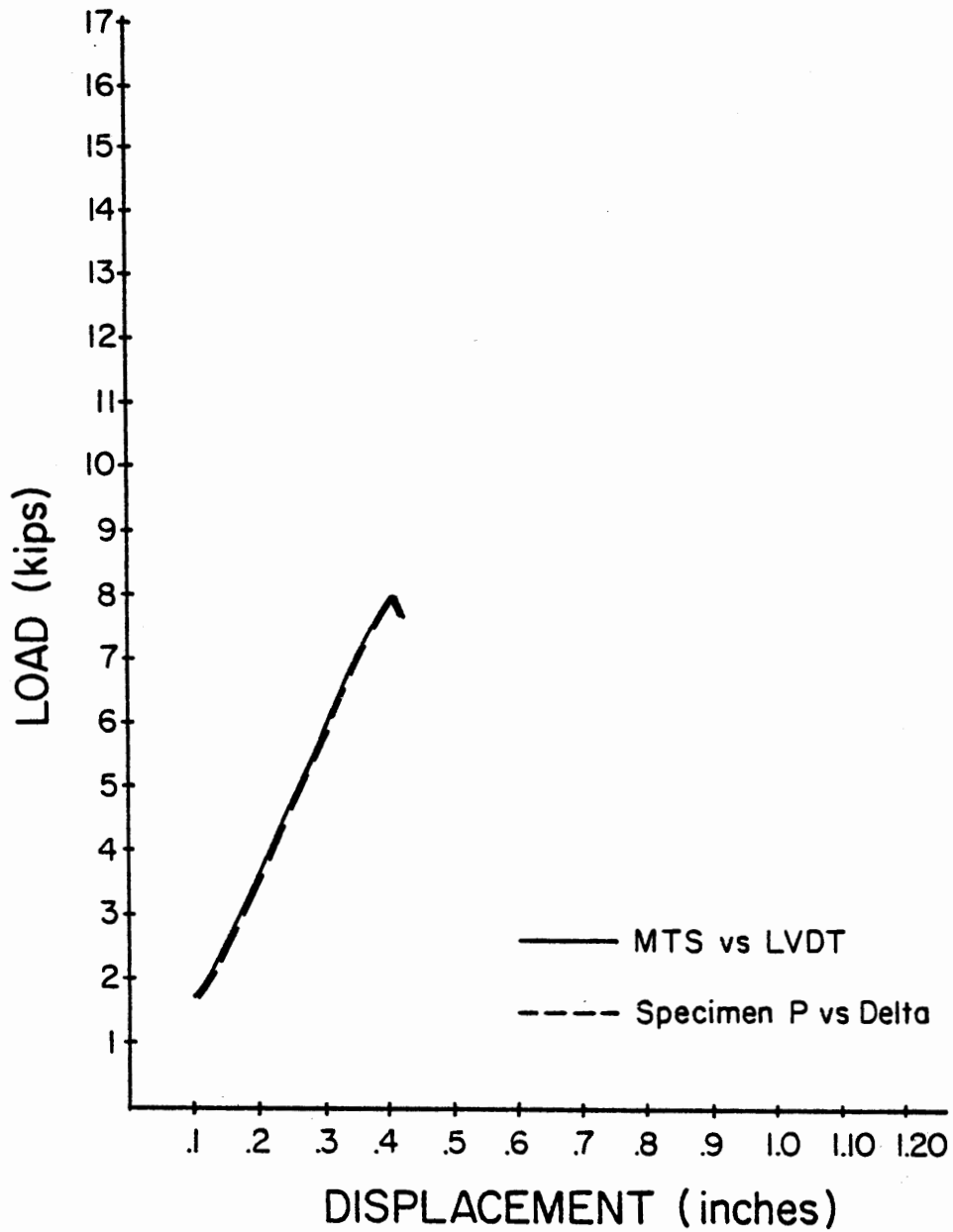


Figure II. Load vs displacement plot for test specimen 07-GT36-01

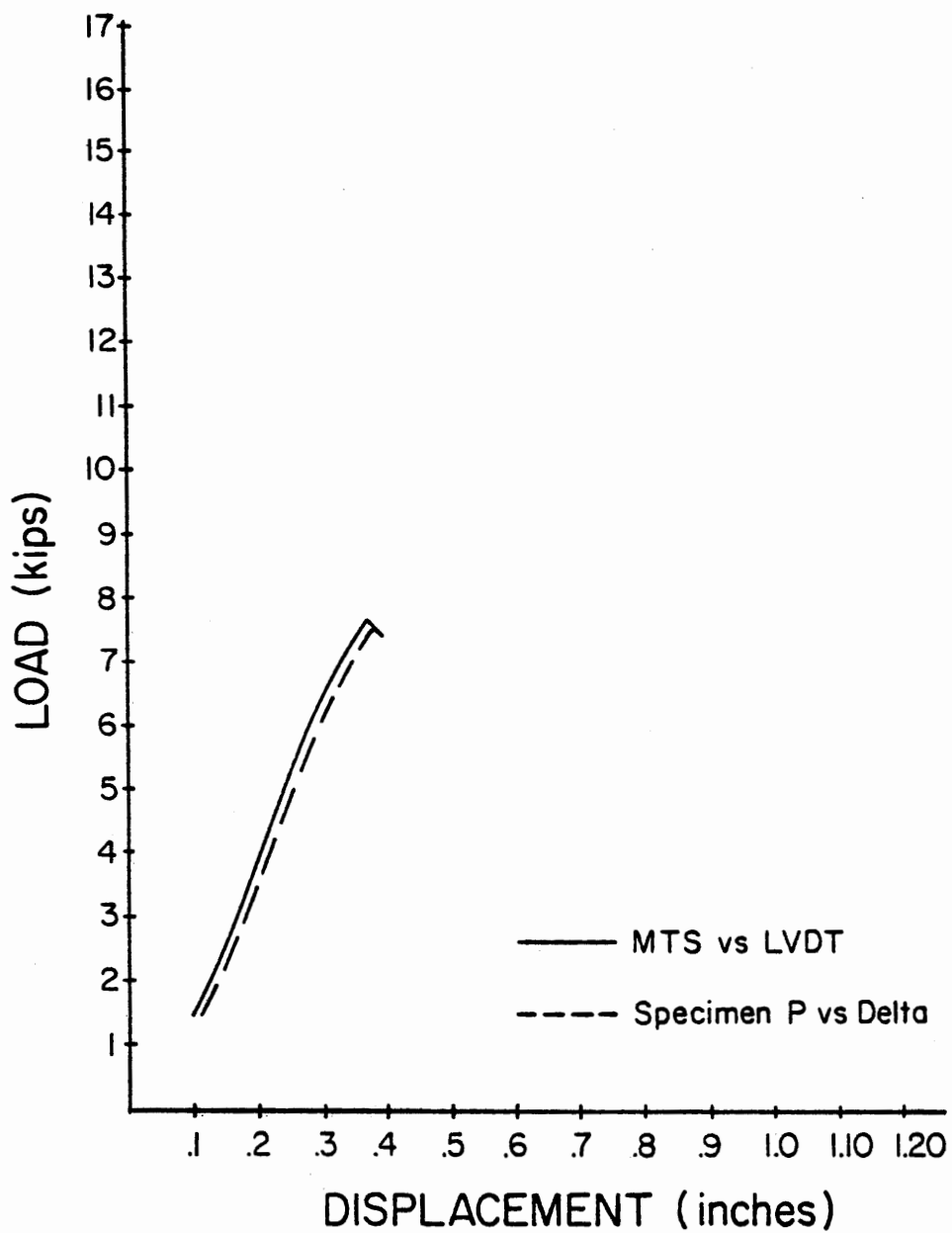


Figure 12. Load vs displacement plot for test specimen 08-GT36-01

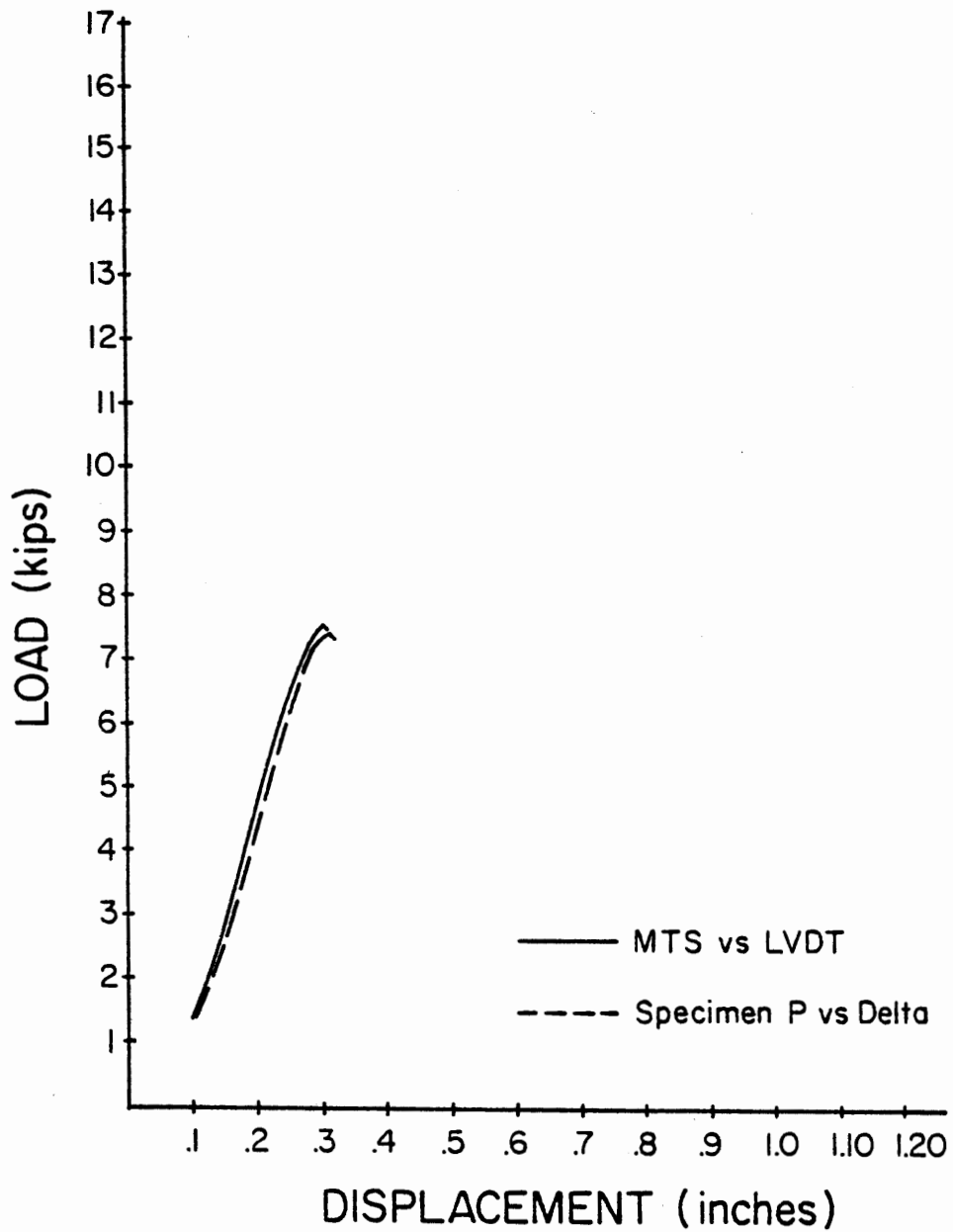


Figure 13. Load vs displacement plot for test specimen 09-GT36-01

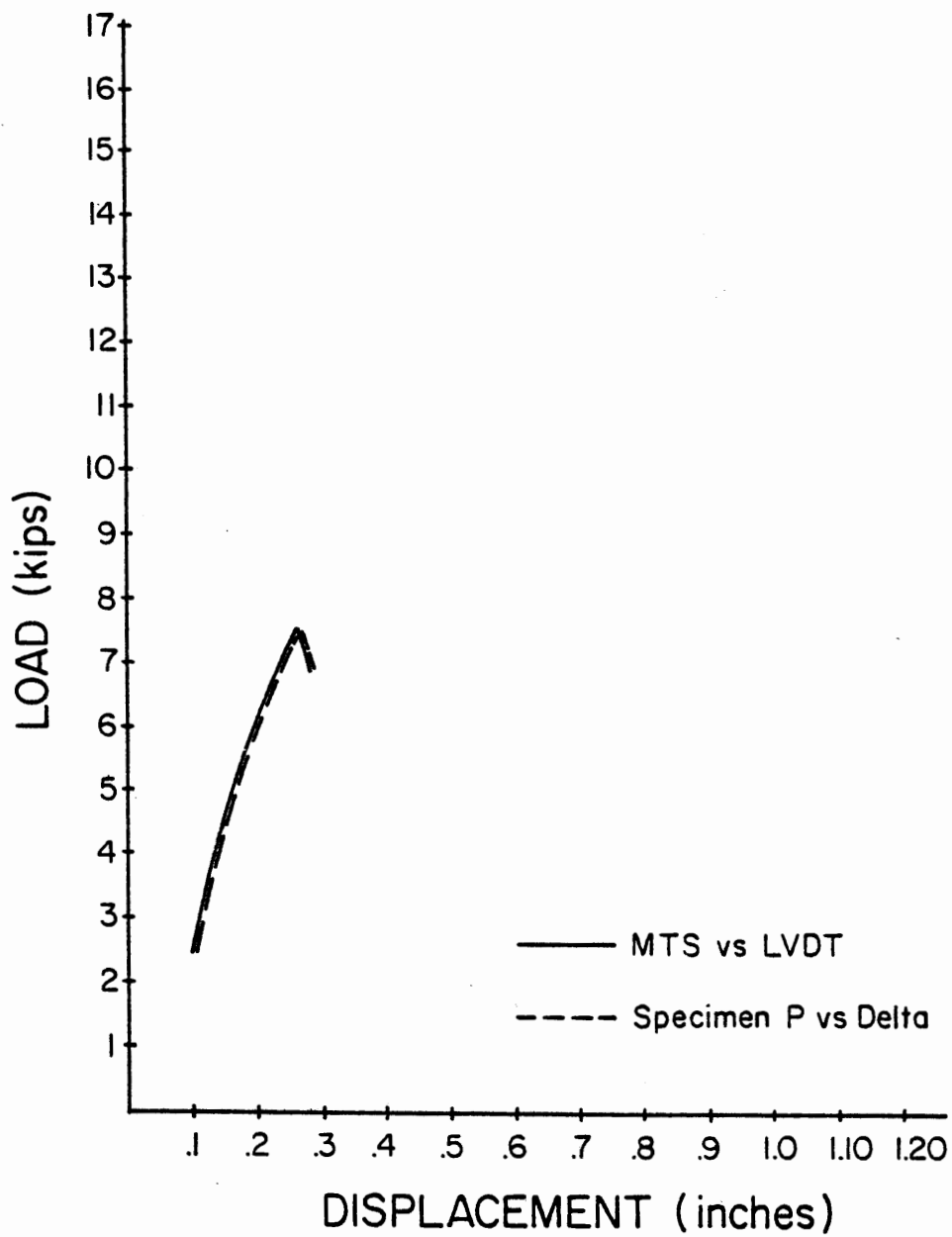


Figure 14. Load vs displacement plot for test specimen 17-GT36-01

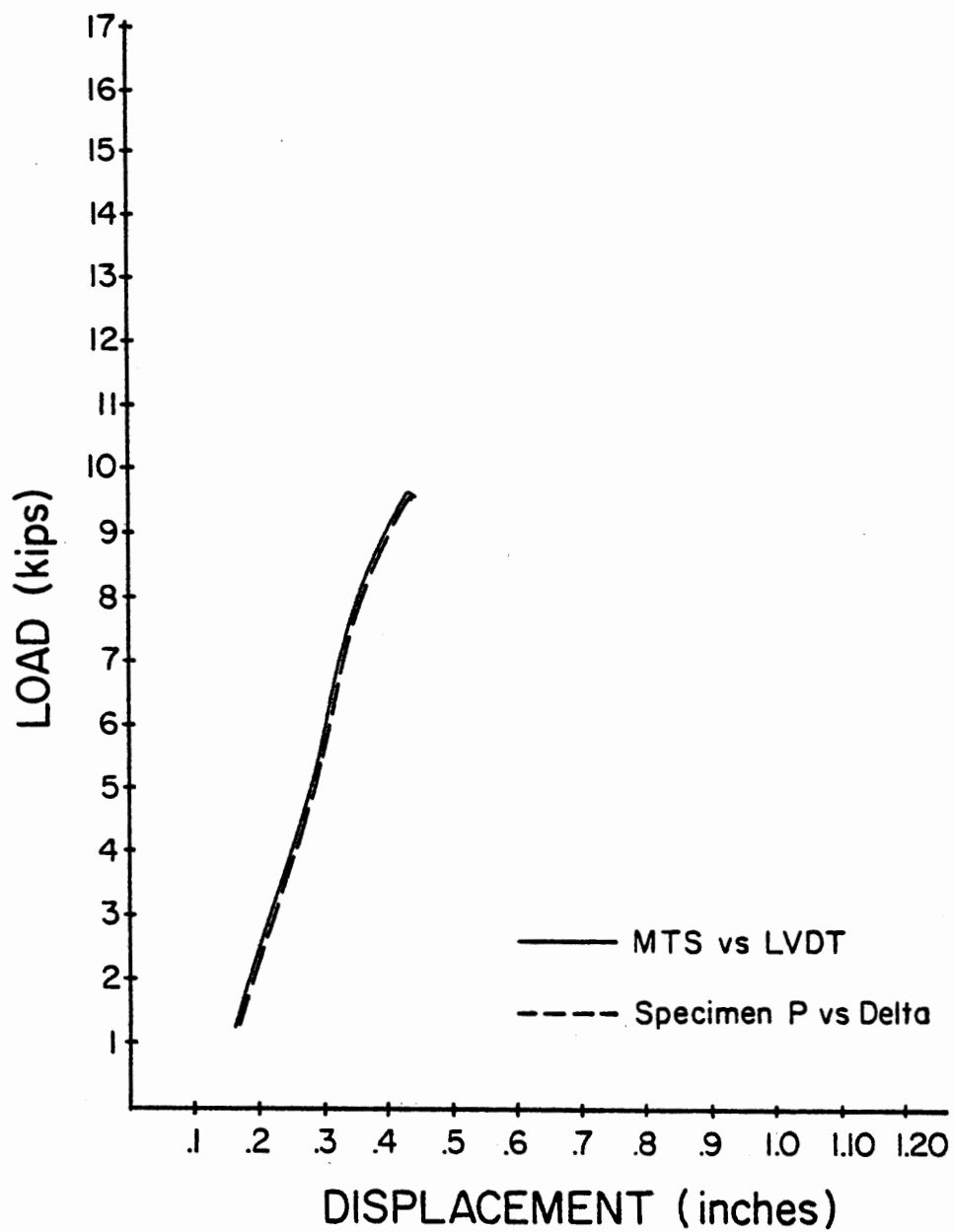


Figure 15 Load vs displacement plot for test specimen 10-GT36-02

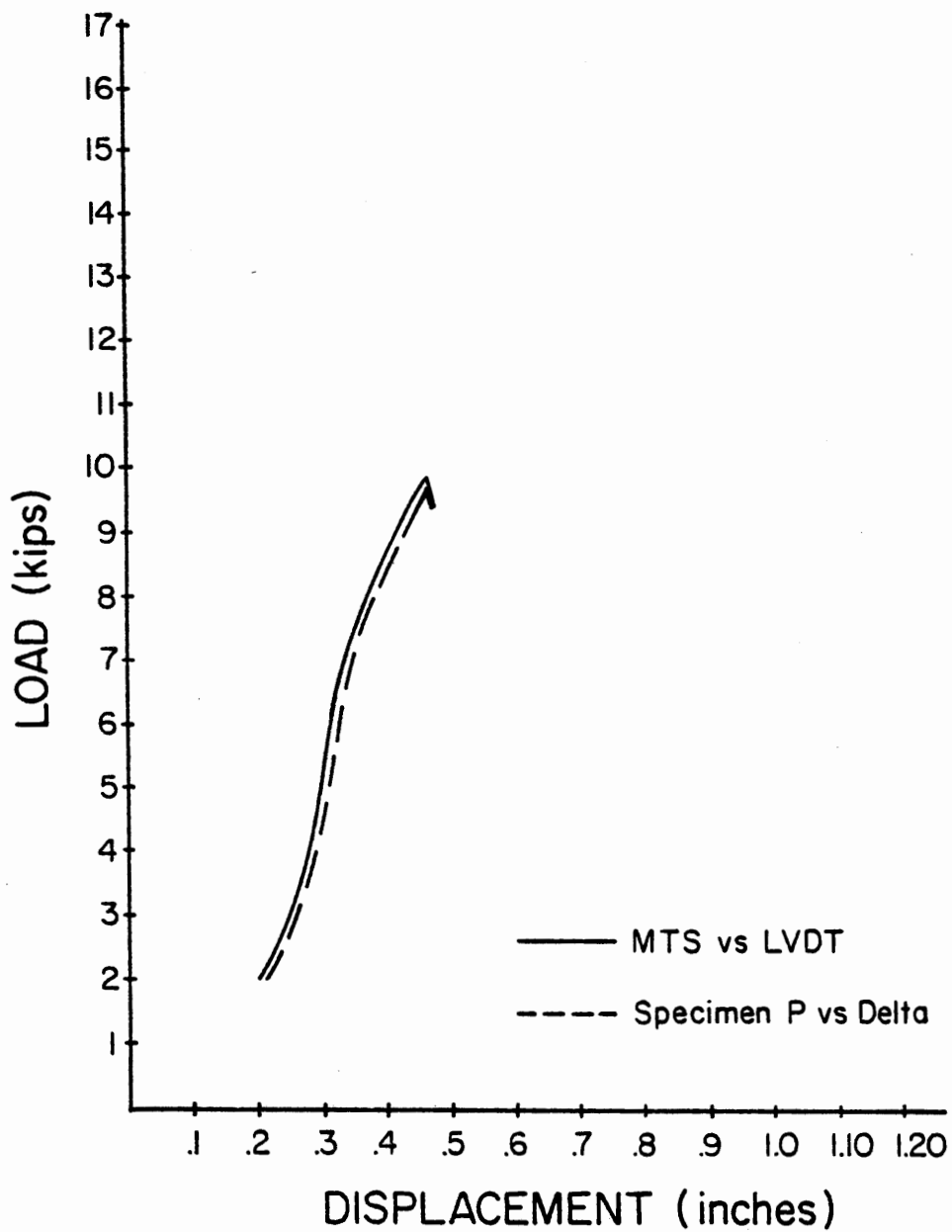


Figure 16. Load vs displacement plot for test specimen II-GT36-02

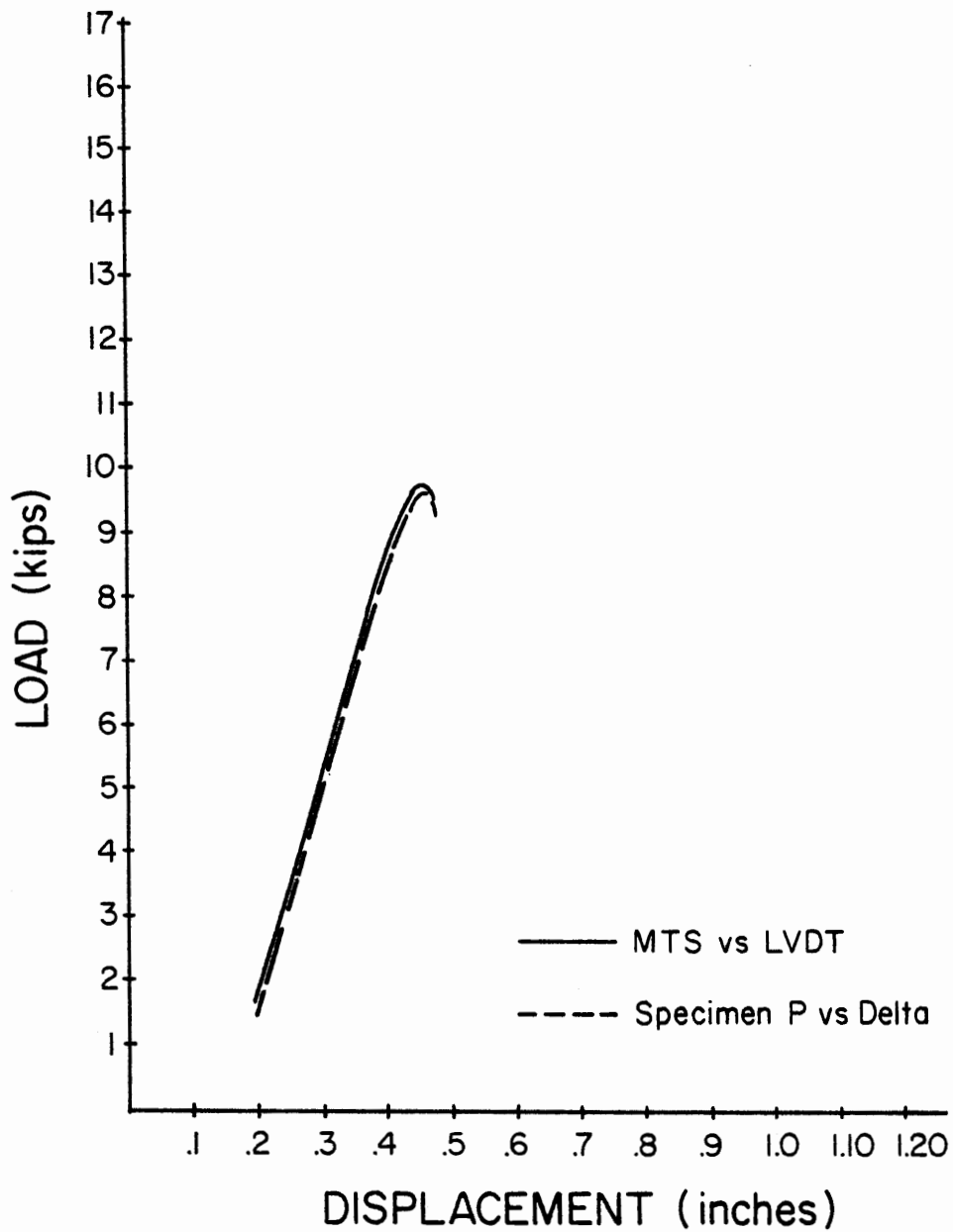


Figure 17. Load vs displacement plot for test specimen 12-GT36-02

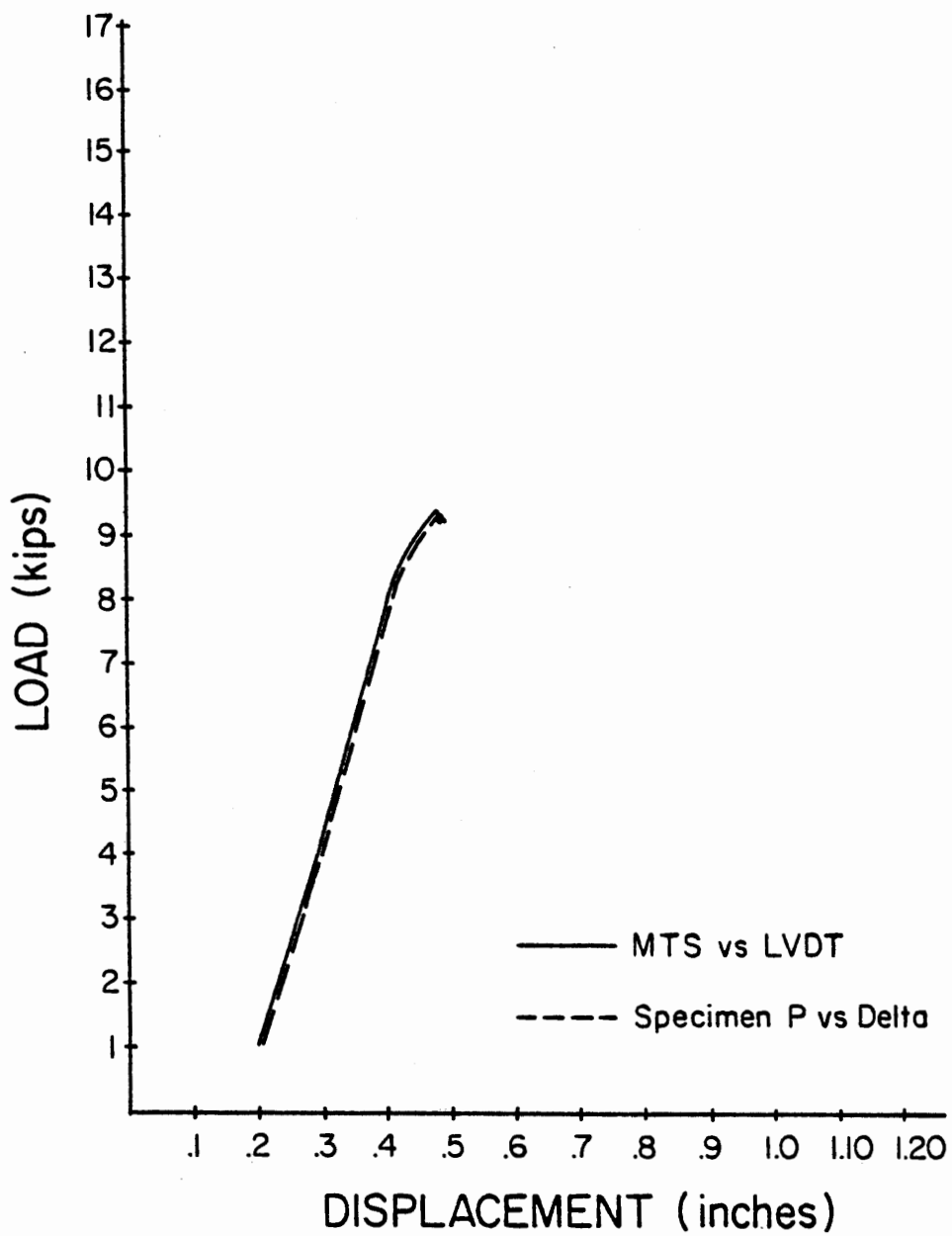


Figure 18. Load vs displacement plot for test specimen 18-GT36-02

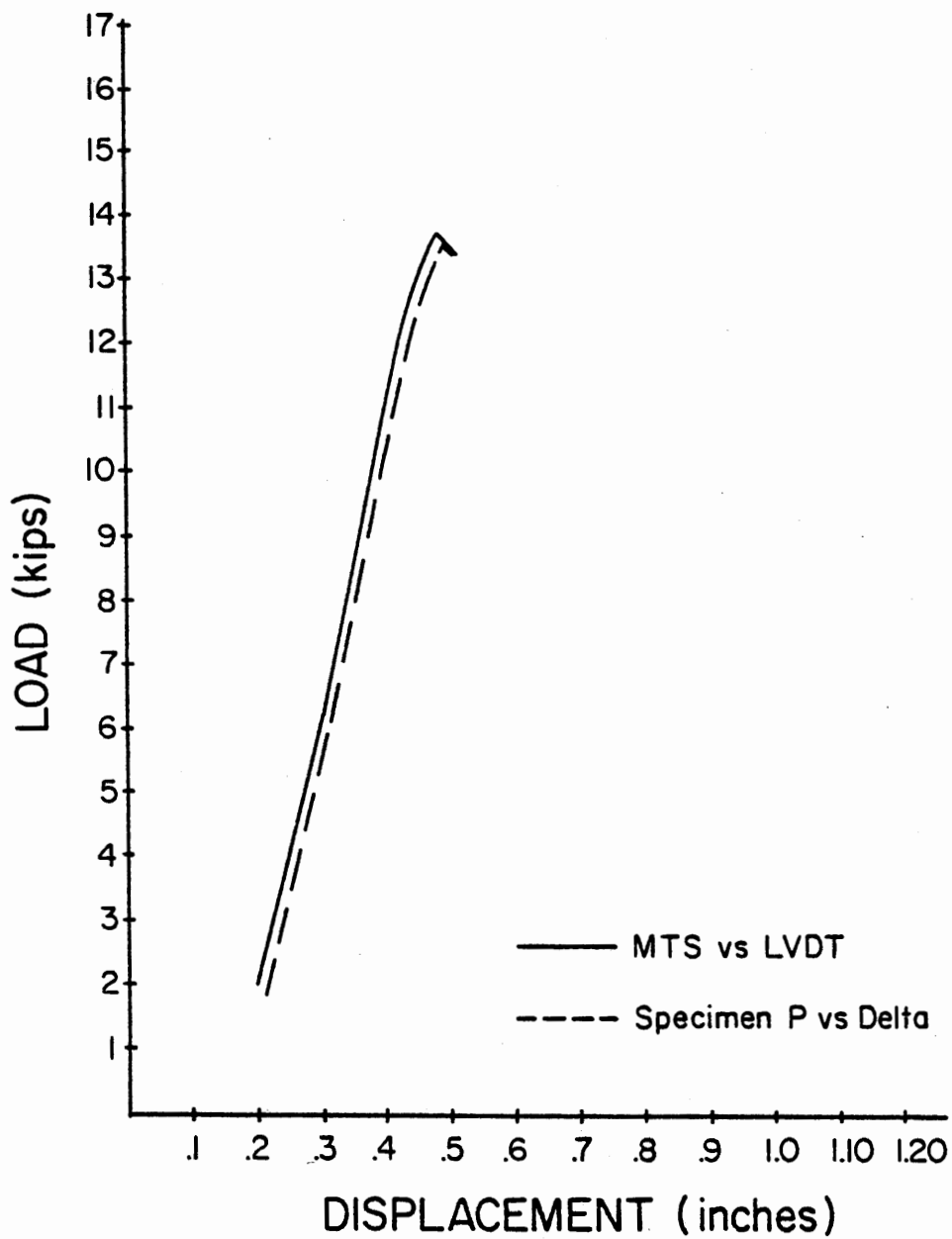


Figure 19. Load vs displacement plot for test specimen 13-GT36-03

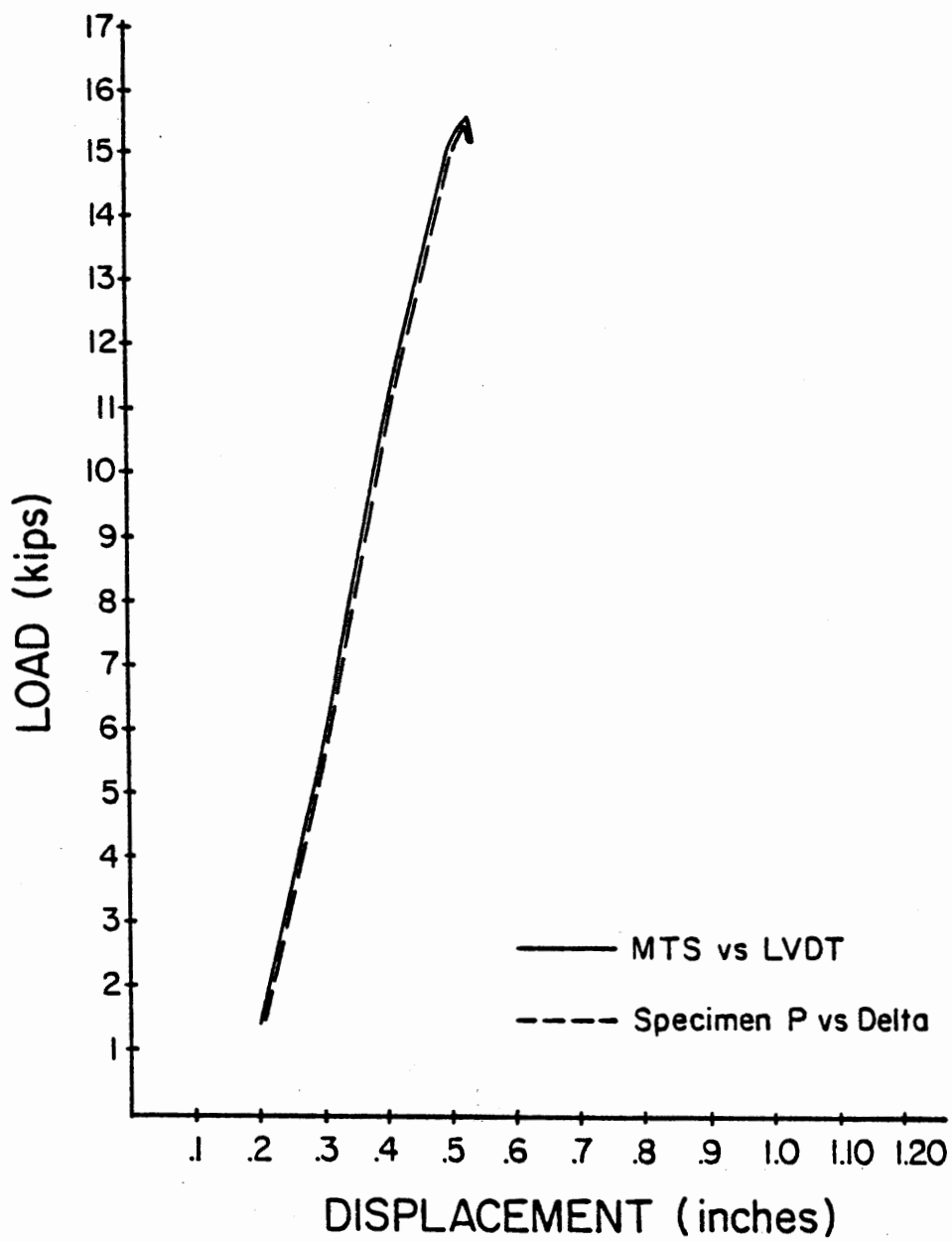


Figure 20. Load vs displacement plot for test specimen 14-GT36-03

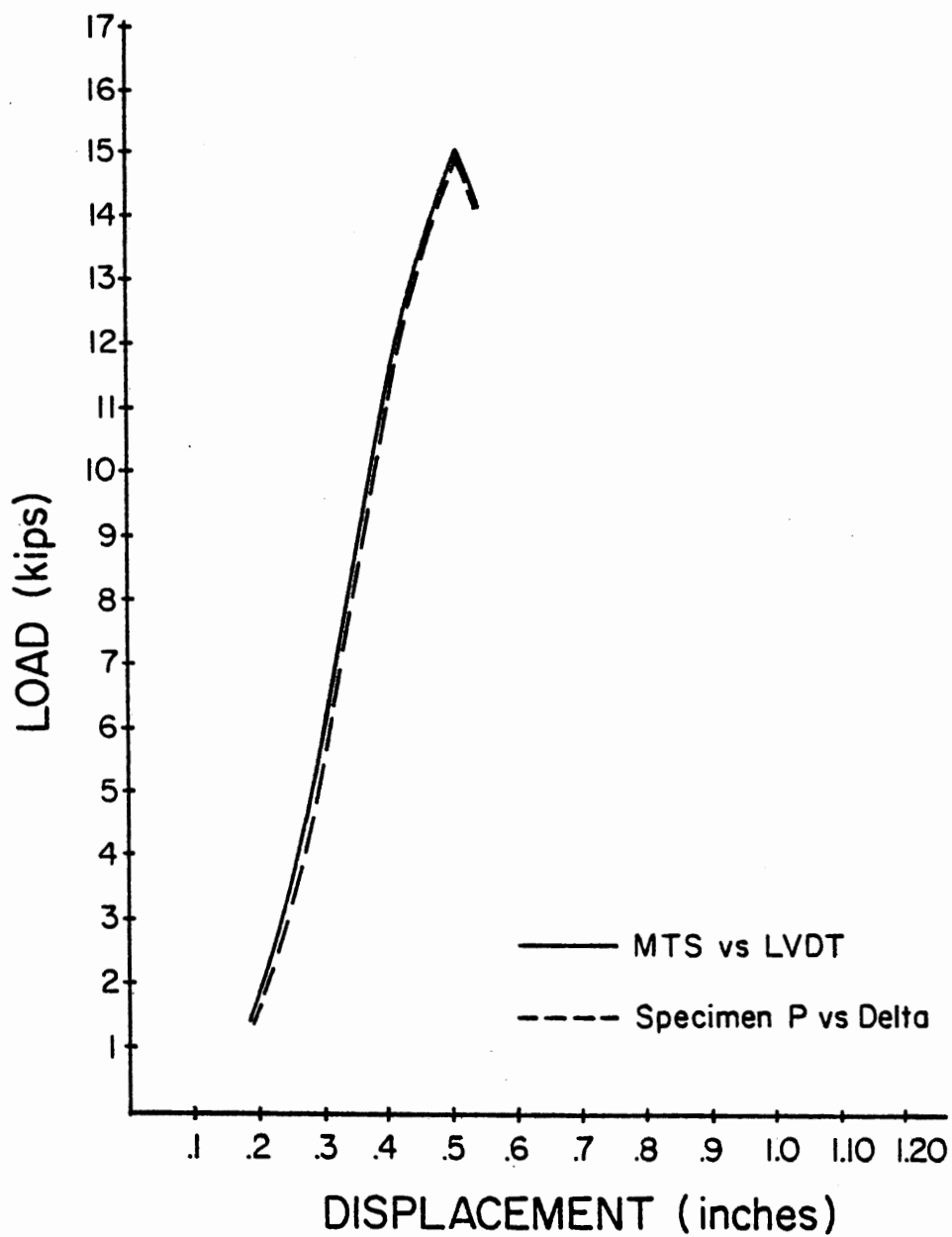


Figure 21. Load vs displacement plot for test specimen 15-GT36-03

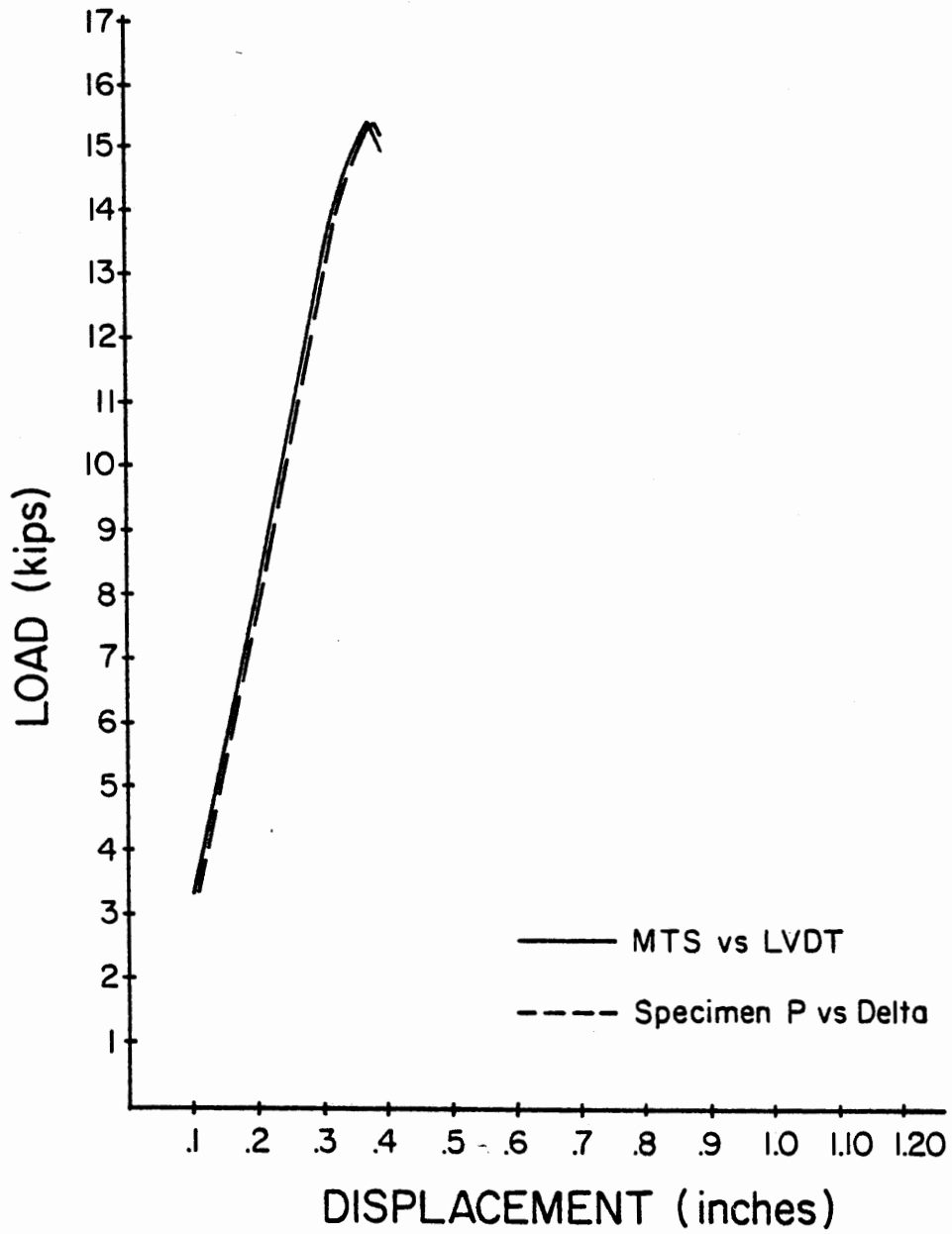


Figure 22. Load vs displacement plot for test specimen 16-GT36-03

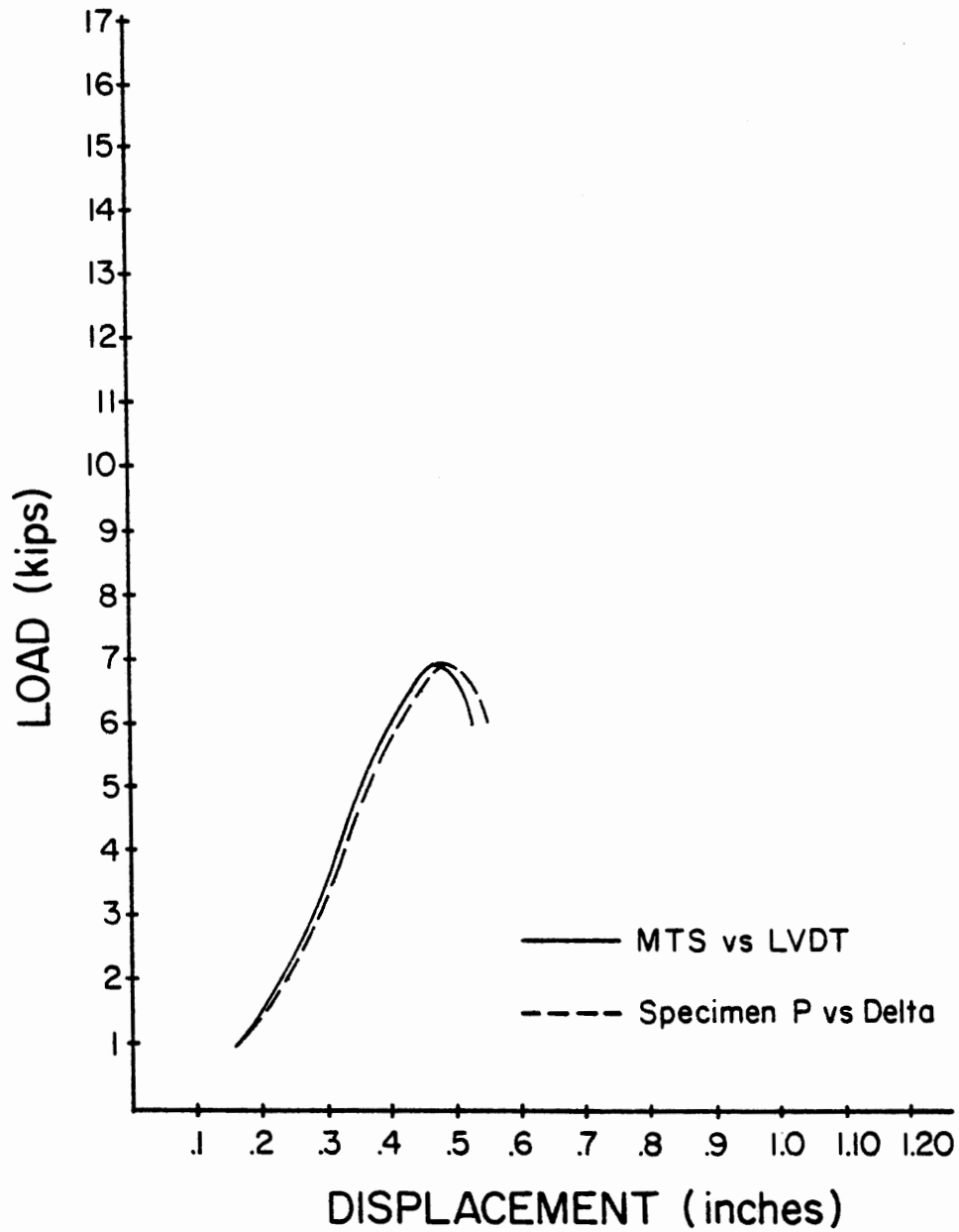


Figure 23. Load vs displacement plot for test specimen 21-GT36-01

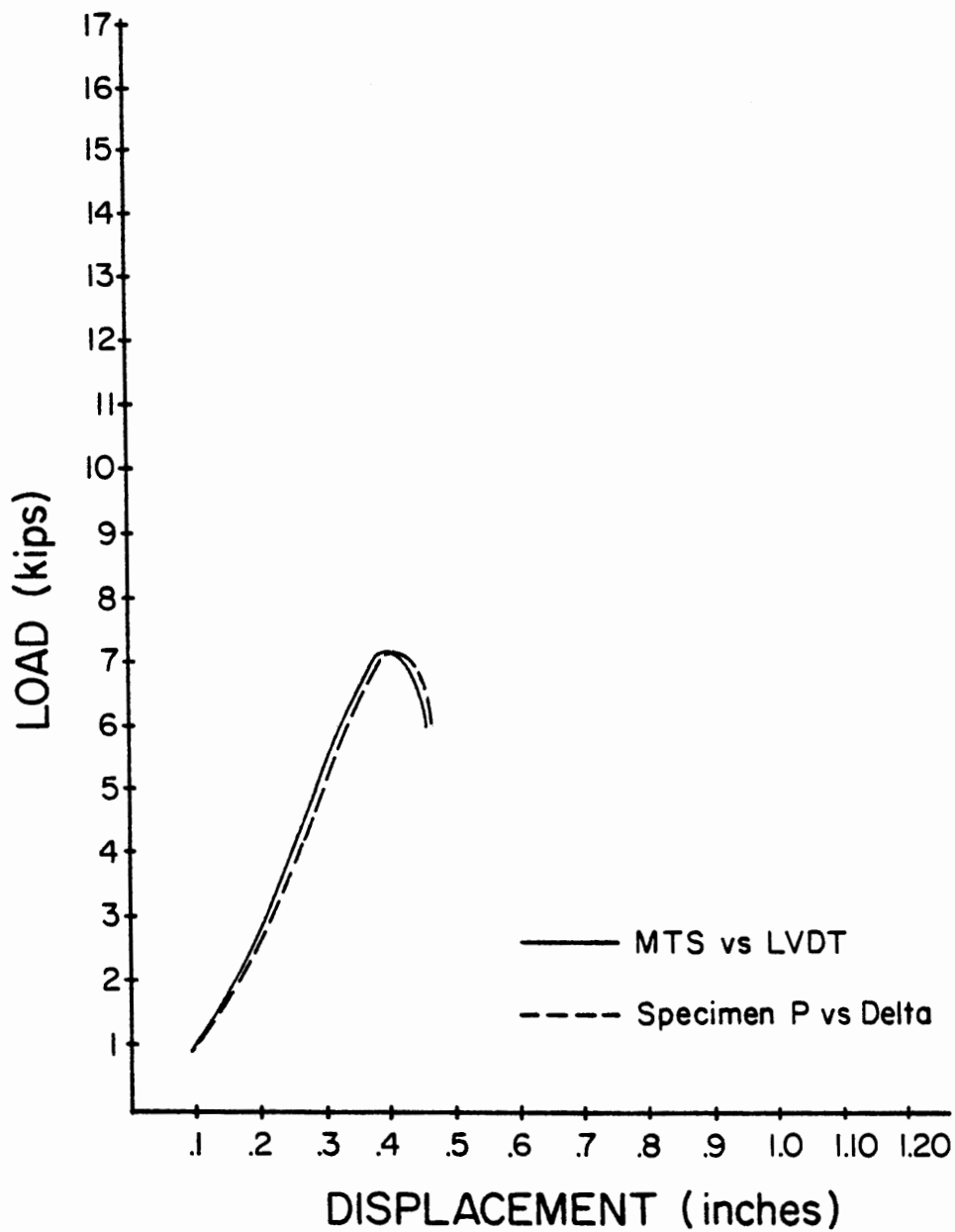


Figure 24. Load vs displacement plot for test specimen 22-GT36-02

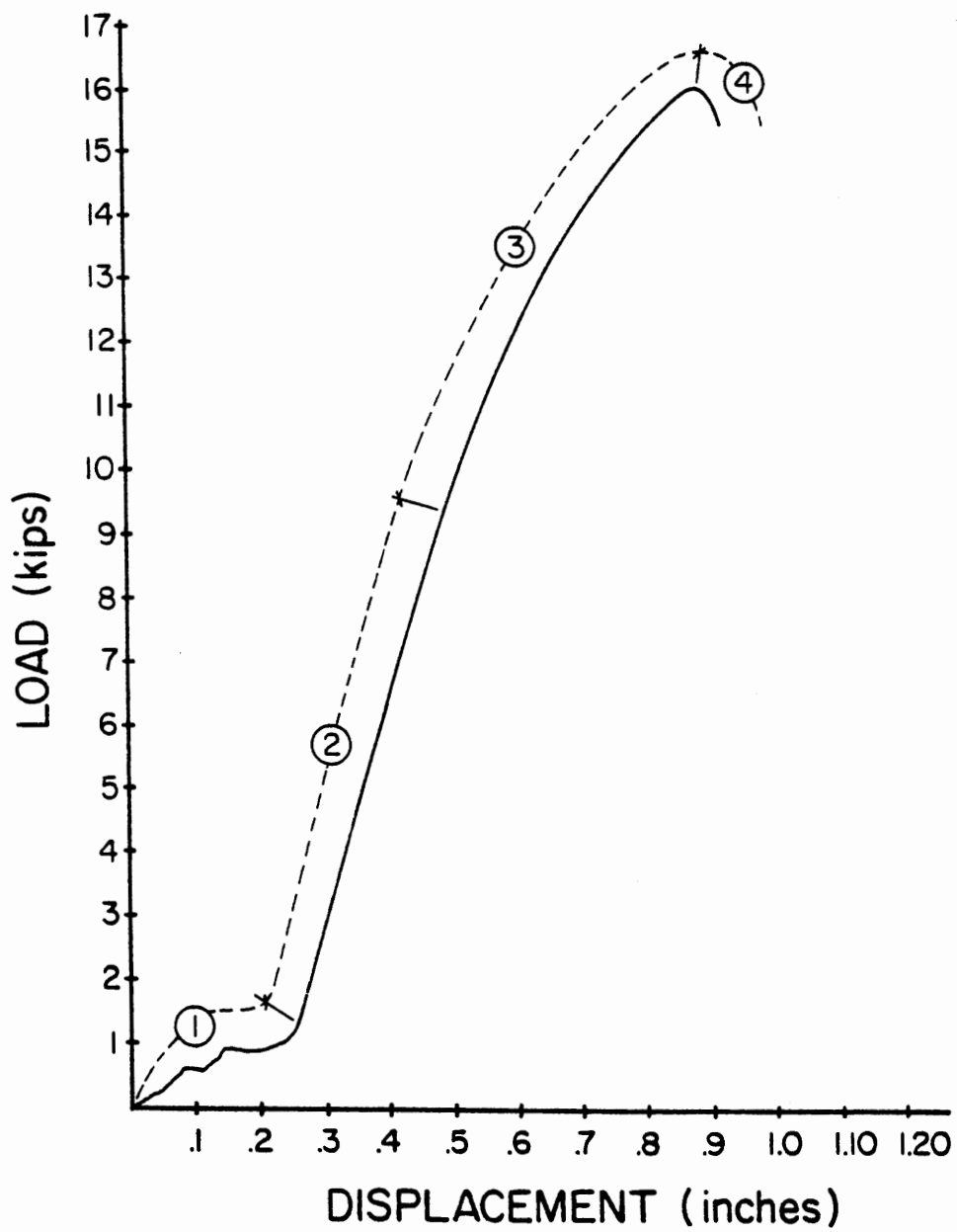


Figure 25. Typical load/displacement plot

eccentric end conditions and, secondly, the yielding in bearing of the member end connections and, third, the local and/or lateral torsional buckling of the compression leg.

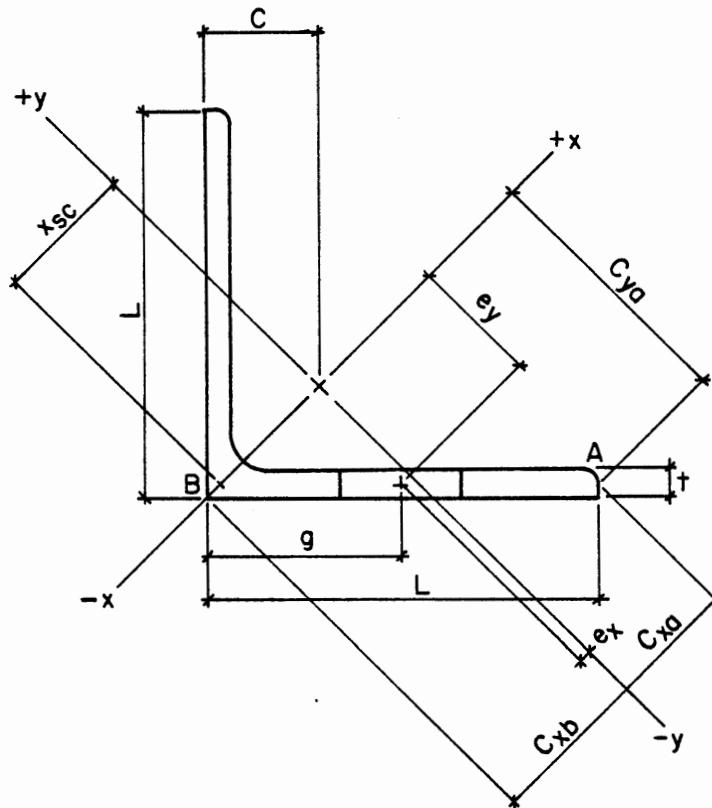
4. Curve segment DE represents the sudden decrease in member capacity upon buckling.

The relative magnitude of these four segments varied between test specimens. Factors contributing to the variances between curves were L/r ratio, member area, angle width-to-thickness ratio and end connection eccentricity.

The general mode of failure of the twenty-two specimens was by buckling about the yy axis as referenced in Figure 26. This figure also references the connection eccentricity relative to the member centroid. The e_x and e_y eccentricity varied with the member cross-section and are indicated in Table III.

Immediately upon the application of axial loading, all test specimens bowed upwards in the positive X direction. This was a result of the large e_y eccentricity and caused leg AB of the angle to develop compressive stresses due to both the axial load and the end moment induced curvature. Because the centroid of the cross-section, at the midpoint of the test specimen, translated relative to the end connection, the e_x and e_y eccentricities both increased in magnitude.

Upon application of higher axial load, the angle compression leg, AB, began to buckle at A causing the angle cross-section to rotate counterclockwise. The relative magnitude of the buckling of the



$$e_x = \left(g + \frac{t}{2}\right) \frac{1}{\sqrt{2}} - C\sqrt{2}$$

$$e_y = -\left(g - \frac{t}{2}\right) \frac{1}{\sqrt{2}}$$

$$x_{sc} = -\left(C - \frac{t}{2}\right) \sqrt{2}$$

Figure 26. Diagram of angle cross section and major axis

TABLE III

CONNECTION ECCENTRICITY AND LOCATION OF SHEAR CENTER

Group	C	gage	e_{xx}	e_{yy}	x_{cg}	C_w
A	0.694	1.25	-0.0313	0.818	-0.849	2.34×10^{-4}
B	0.569	1.00	-0.0313	0.641	-0.672	5.79×10^{-5}
C	0.484	1.00	+0.067	0.663	-0.596	2.45×10^{-6}
D	0.546	1.00	-0.0209	0.663	-0.684	5.61×10^{-6}
E	0.569	1.00	-0.0313	0.641	-0.672	5.79×10^{-5}
F	0.484	0.875	-0.022	0.575	-0.596	2.45×10^{-6}

compression leg varied between specimen groups and will be discussed in greater detail later. This rotation caused the curvature induced compressive stress at A to decrease, but continued to increase the compressive stresses at B. Also, because of the cross-section rotation at the member midpoint, the end connection eccentricity e_y decreased in magnitude while the e_x eccentricity increased in magnitude.

As the axial load was further increased, the cross-section continued to rotate. The compressive stress at point B continued to increase until the member ultimately buckled about the y axis.

Figure 27 shows the various stages of the typical angle cross-section during the test process.

For discussion purposes, the twenty-two test specimens may be put into six distinct groups. Within each of these groups, every specimen was identical in section type, length and bolt layout. The only variable, aside from normal fabrication tolerances, was the material yield strength. To make valid comparisons, it was necessary to determine the yield strength of each test specimen. To do this, a coupon was cut from each specimen. Each of these coupons was installed in the MTS test system and loaded in tension under strain control at a rate of 6.67 kips/min. A continuous load vs. elongation plot was taken and used to determine the material yield stress. Figures 28 thru 48 show the load vs. elongation curves of each specimen. Table IV summarizes the resulting yield stress calculations which will be discussed along with the compression test results.

It should be noted that the tension coupons were taken from the test specimens after completion of the compression tests. The coupons

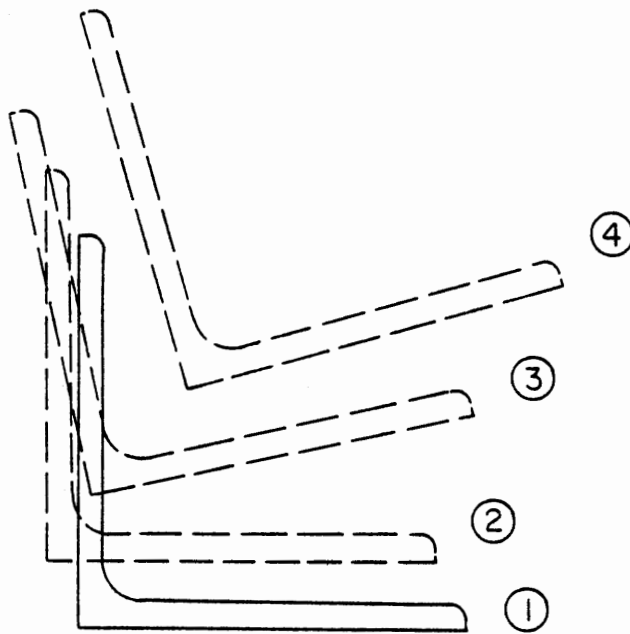


Figure 27. Typical midspan movement of test specimen cross-section

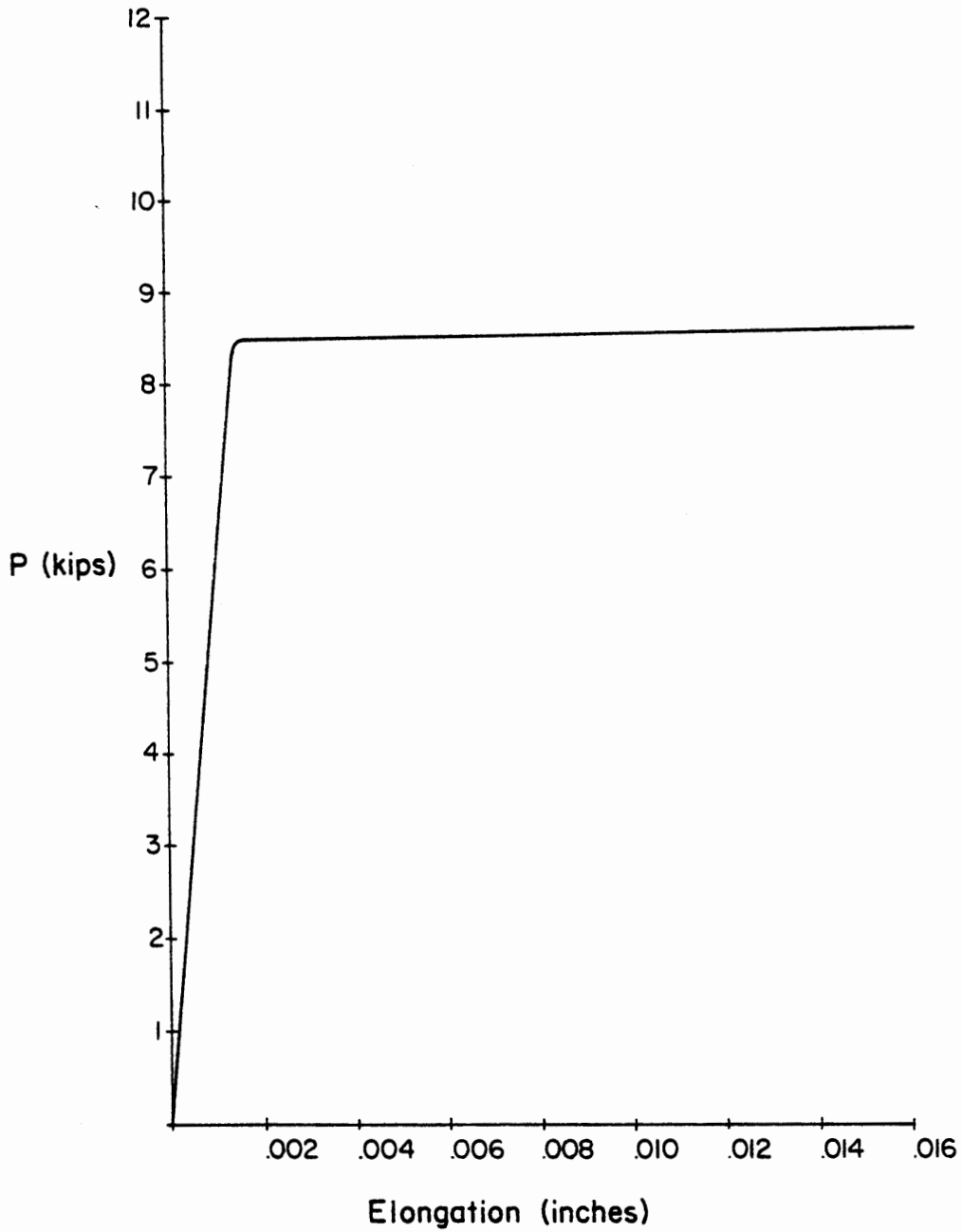


Figure 28. Yield stress determination, test specimen 01-GT48-01

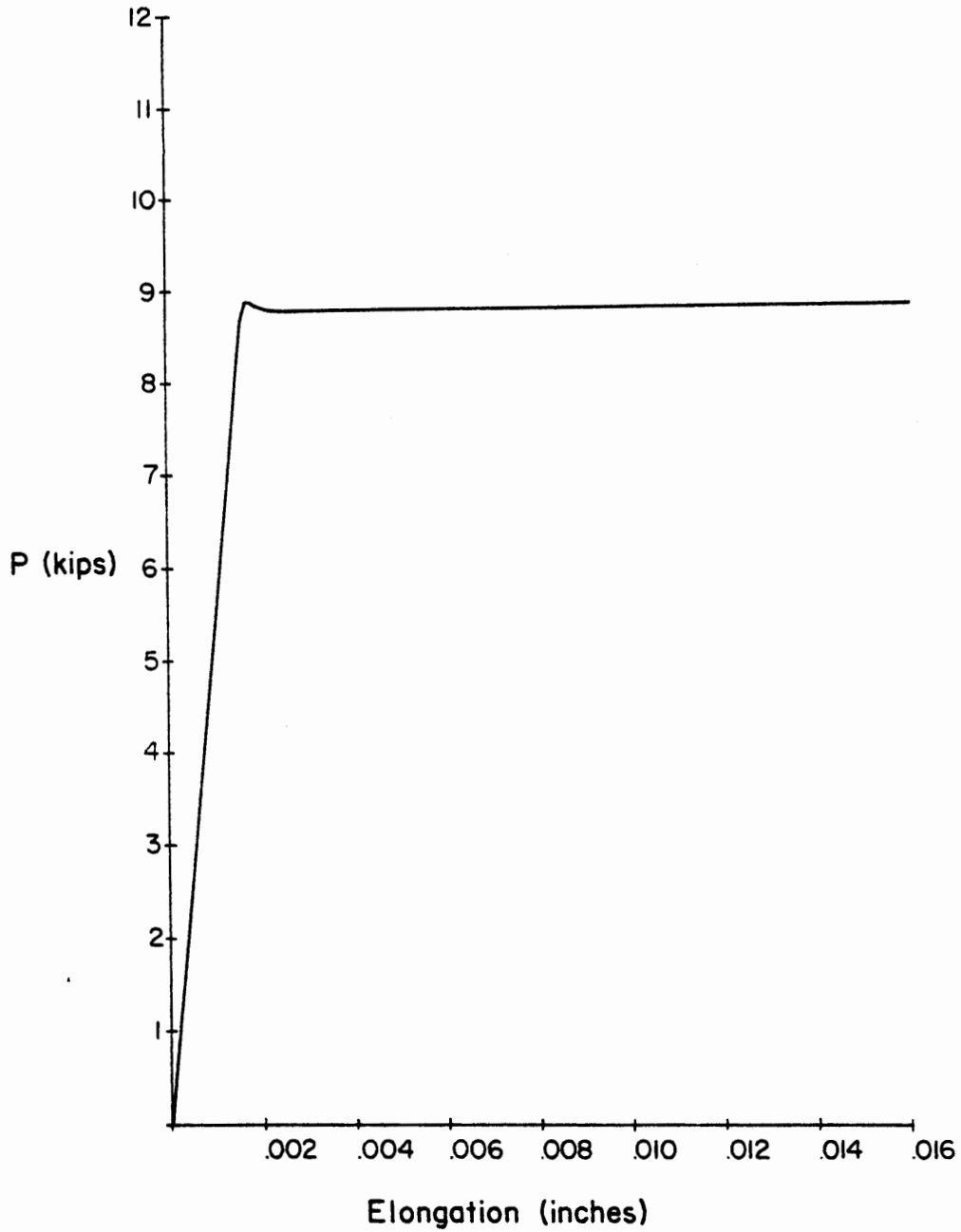


Figure 29. Yield stress determination, test specimen O2-GT48-01

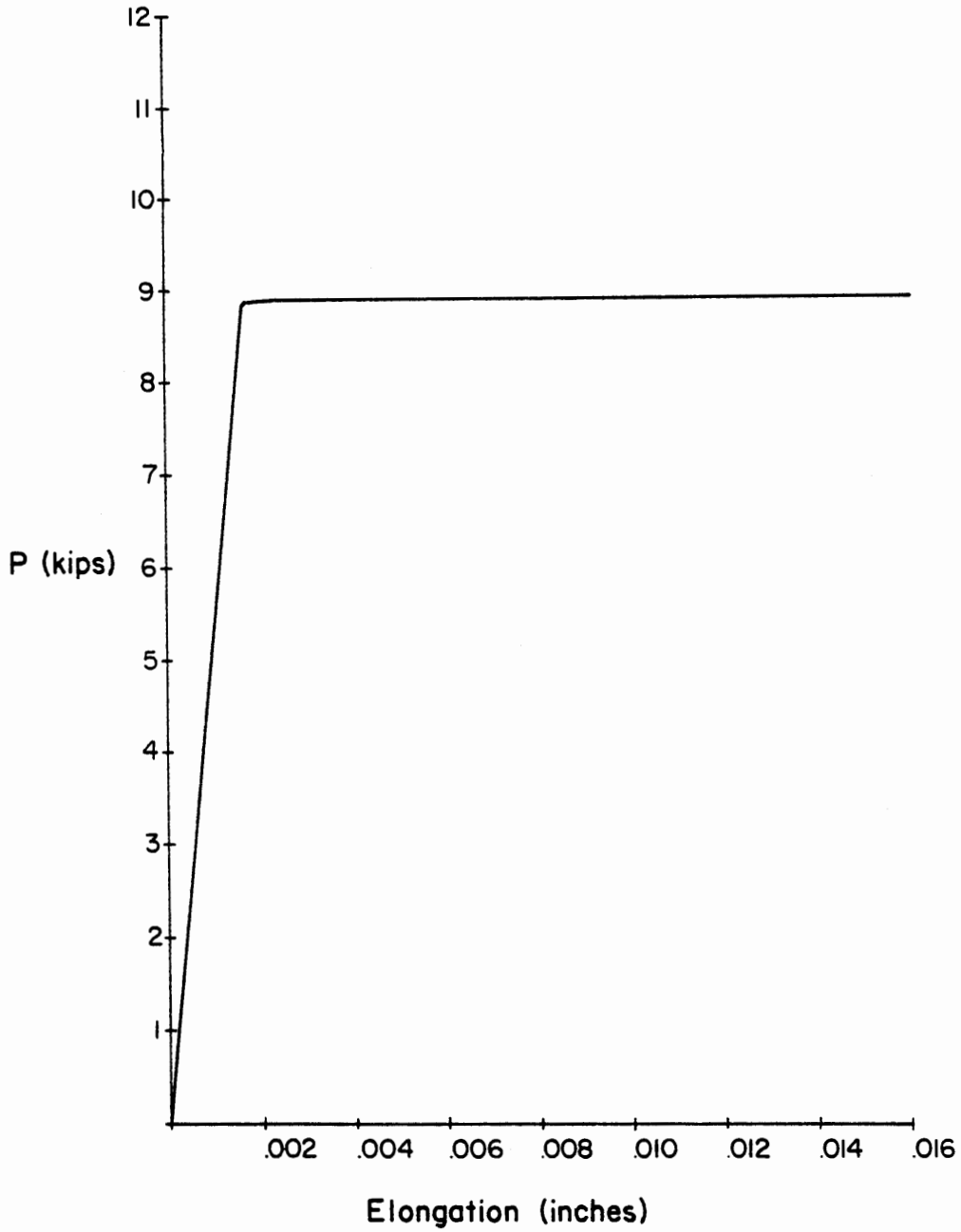


Figure 30. Yield stress determination, test specimen O3-GT48-01

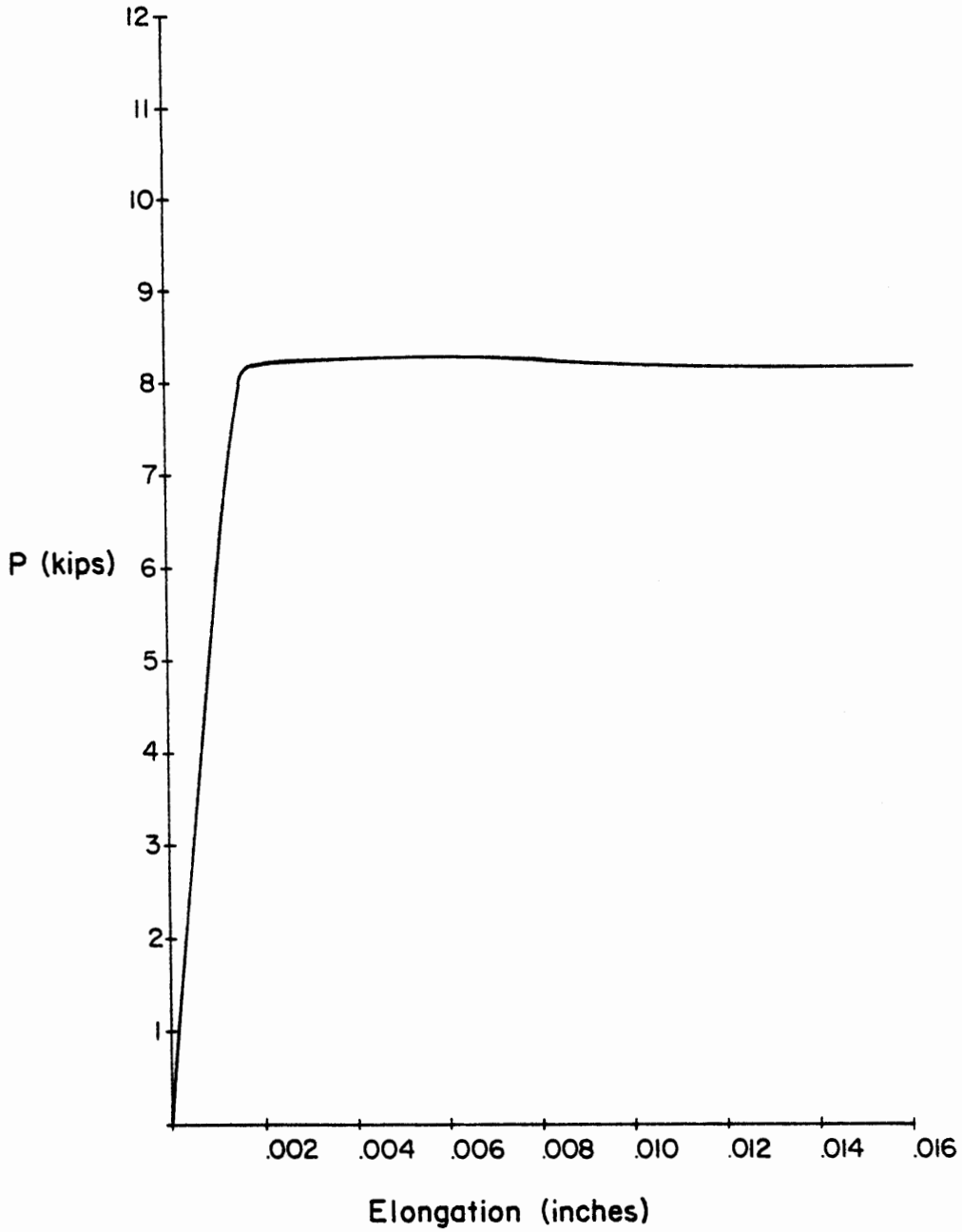


Figure 31. Yield stress determination, test specimen 20-GT48-01

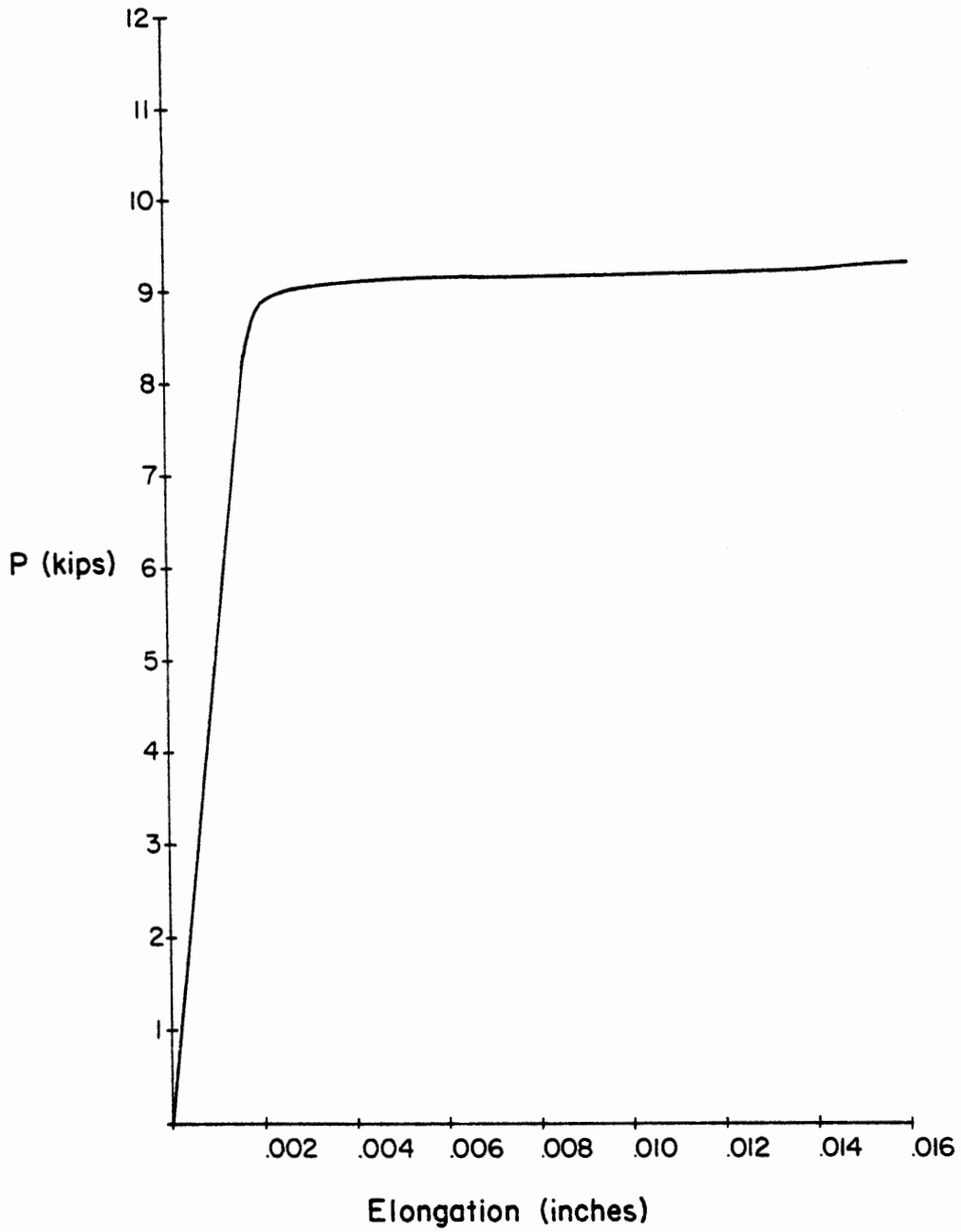


Figure 32. Yield stress determination, test specimen O4-GT48-02

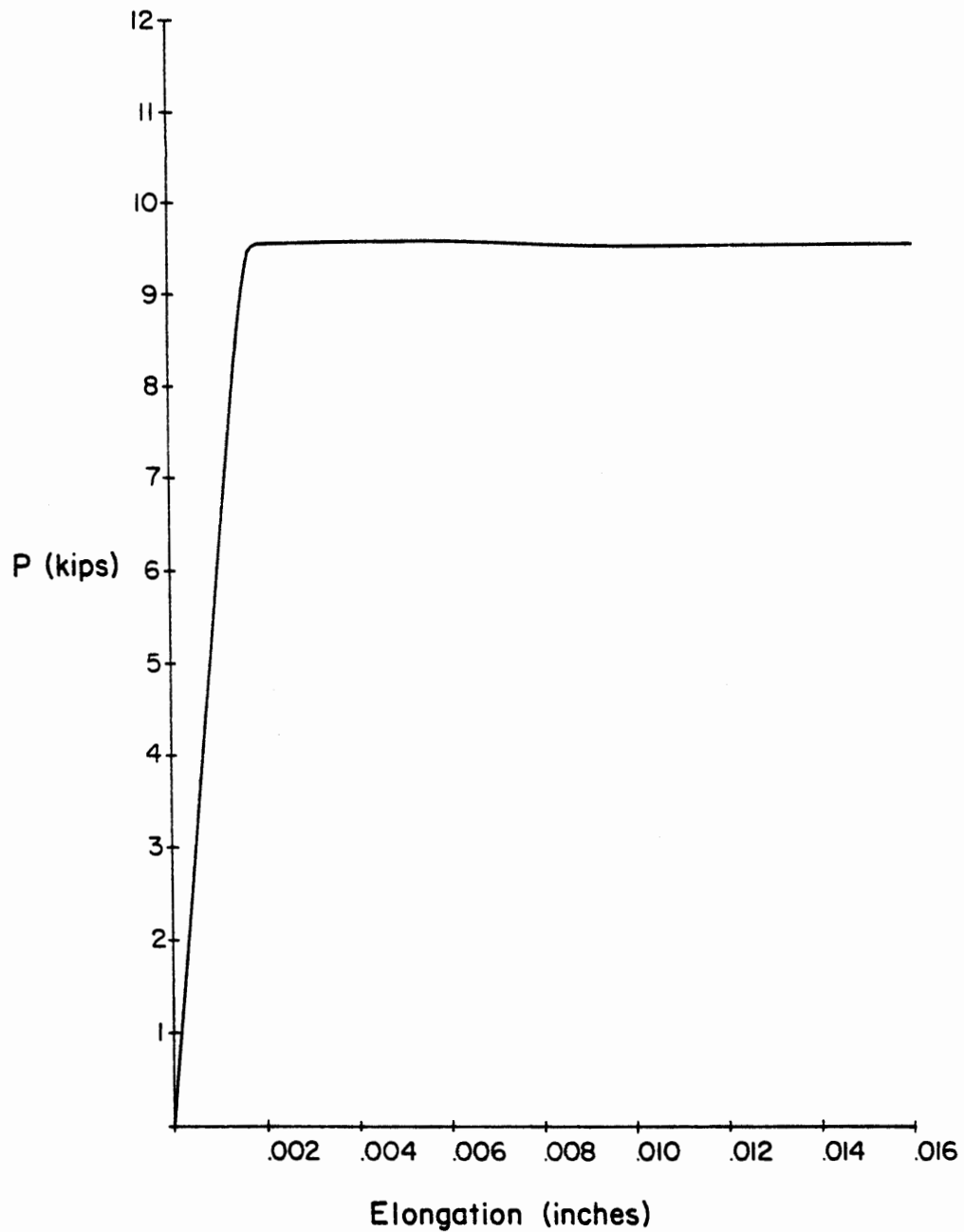


Figure 33. Yield stress determination, test specimen O5-GT48-02

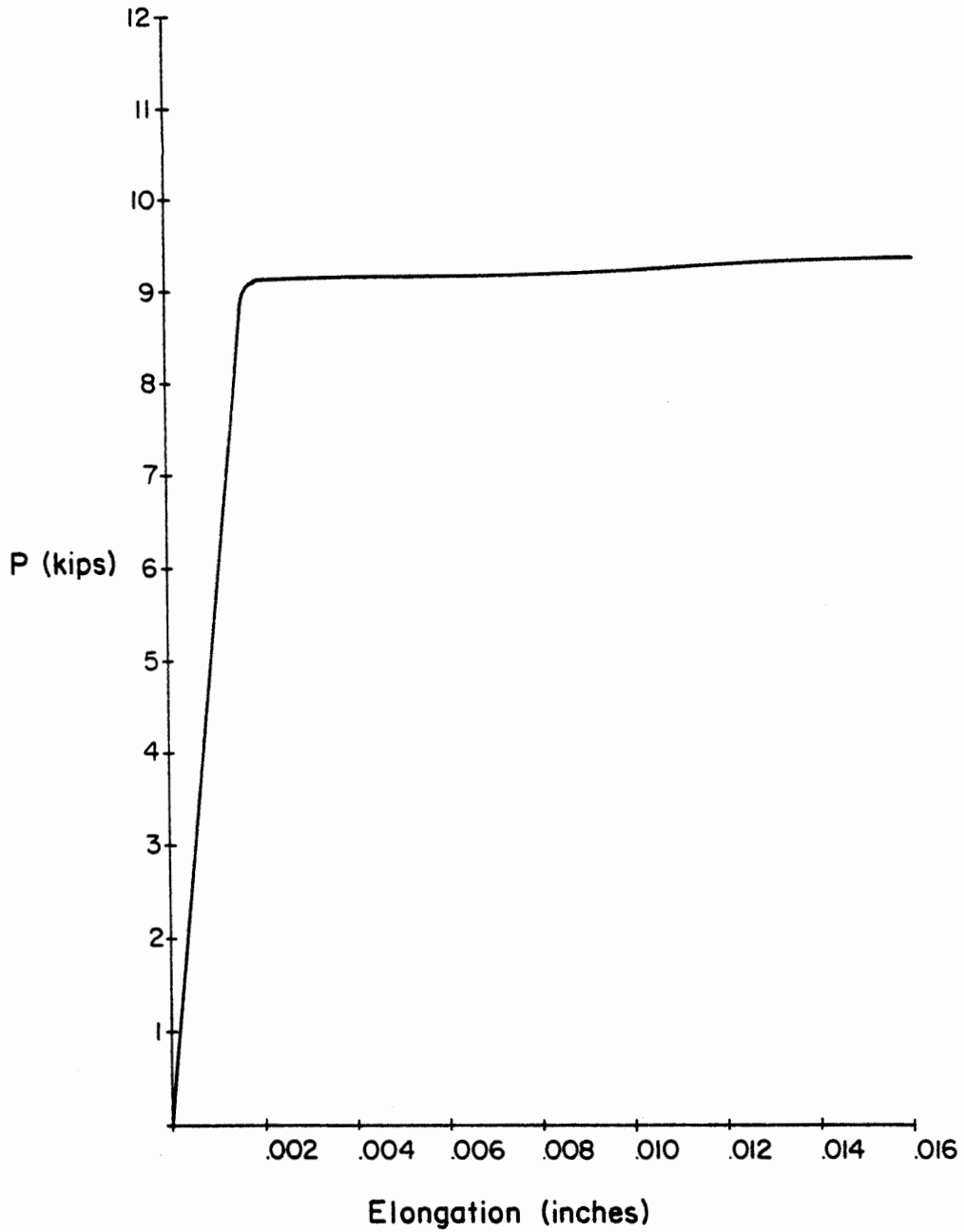


Figure 34. Yield stress determination, test specimen O6-GT48-02

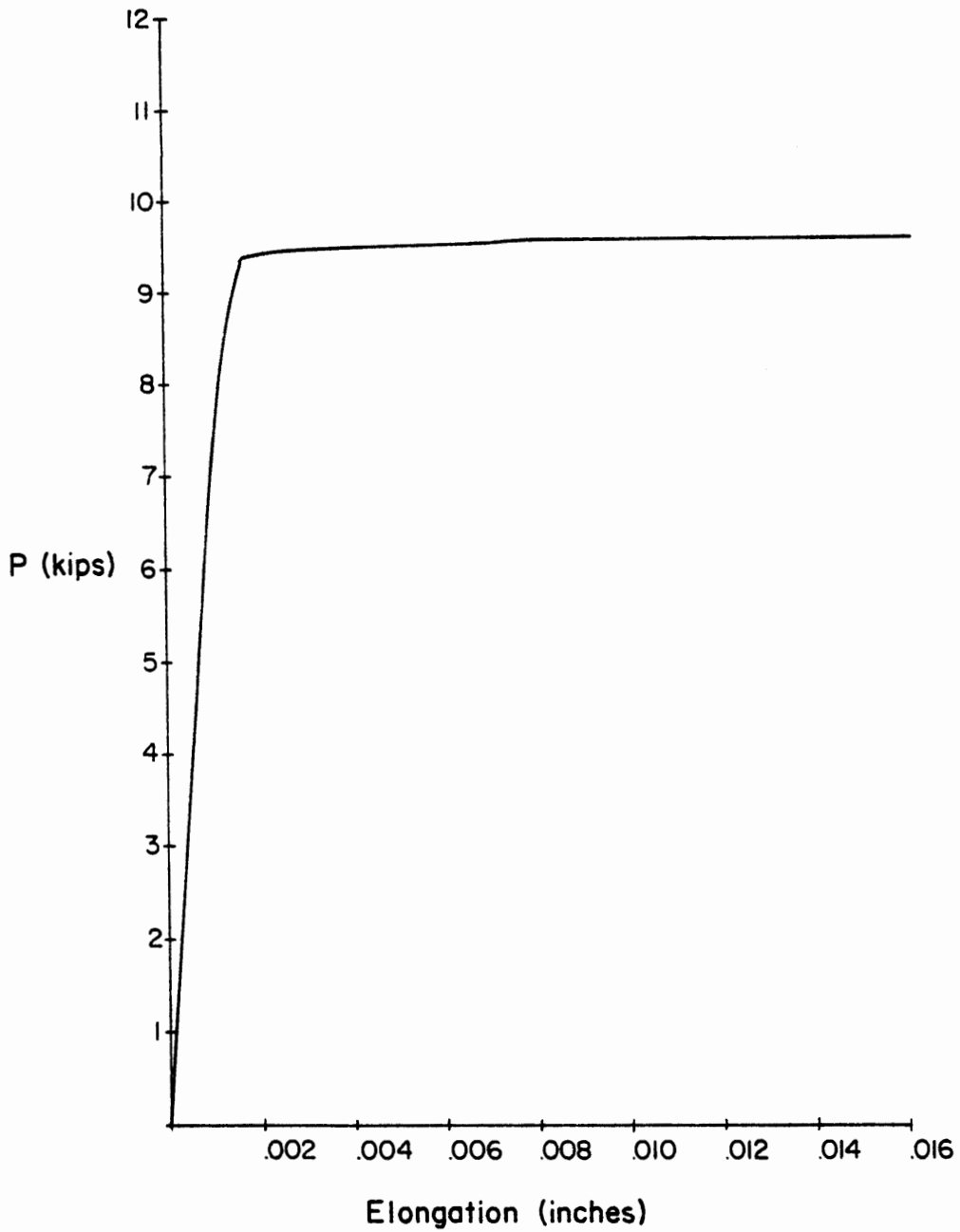


Figure 35. Yield stress determination, test specimen 19-GT48-02

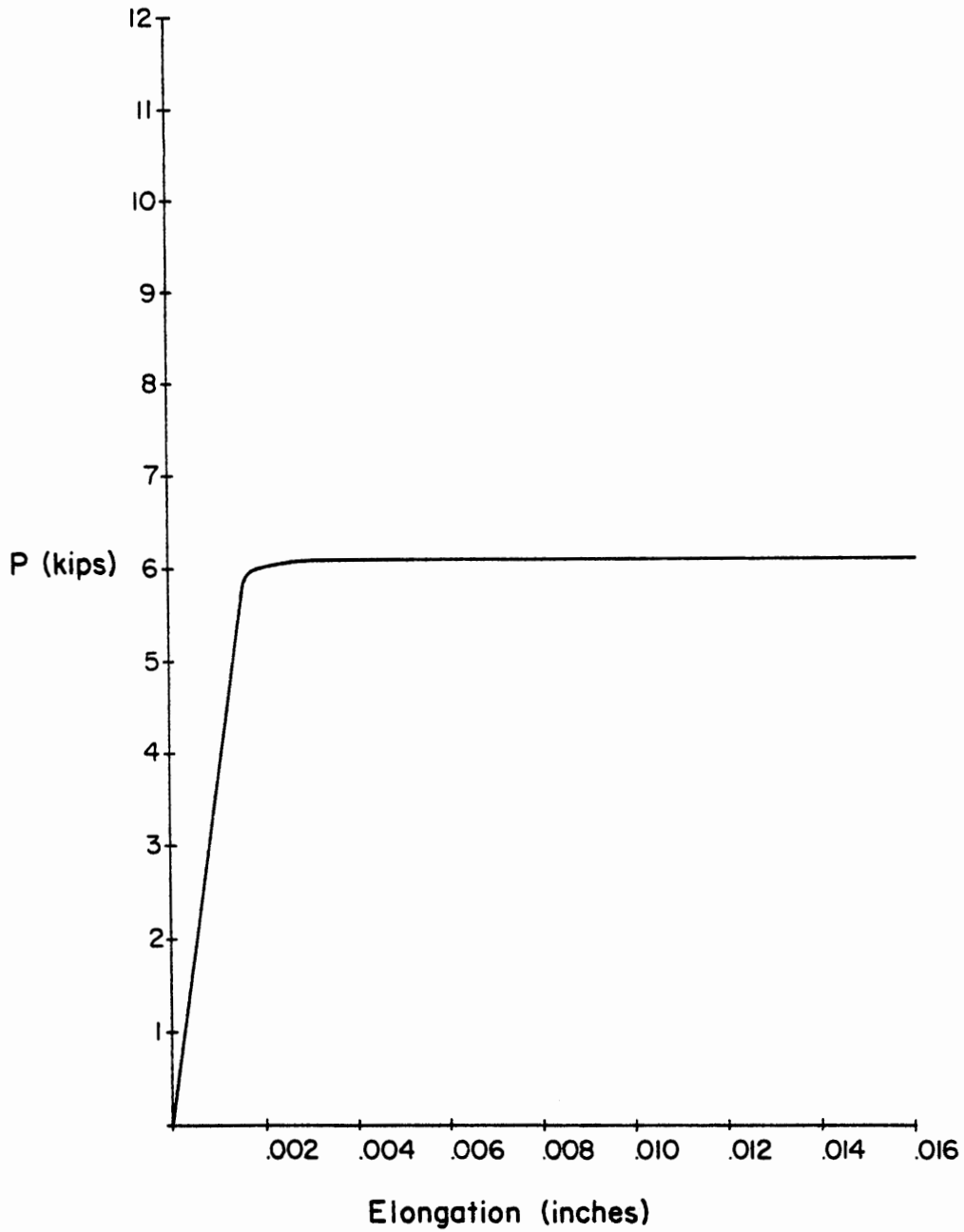


Figure 36. Yield stress determination, test specimen 07-GT36-01

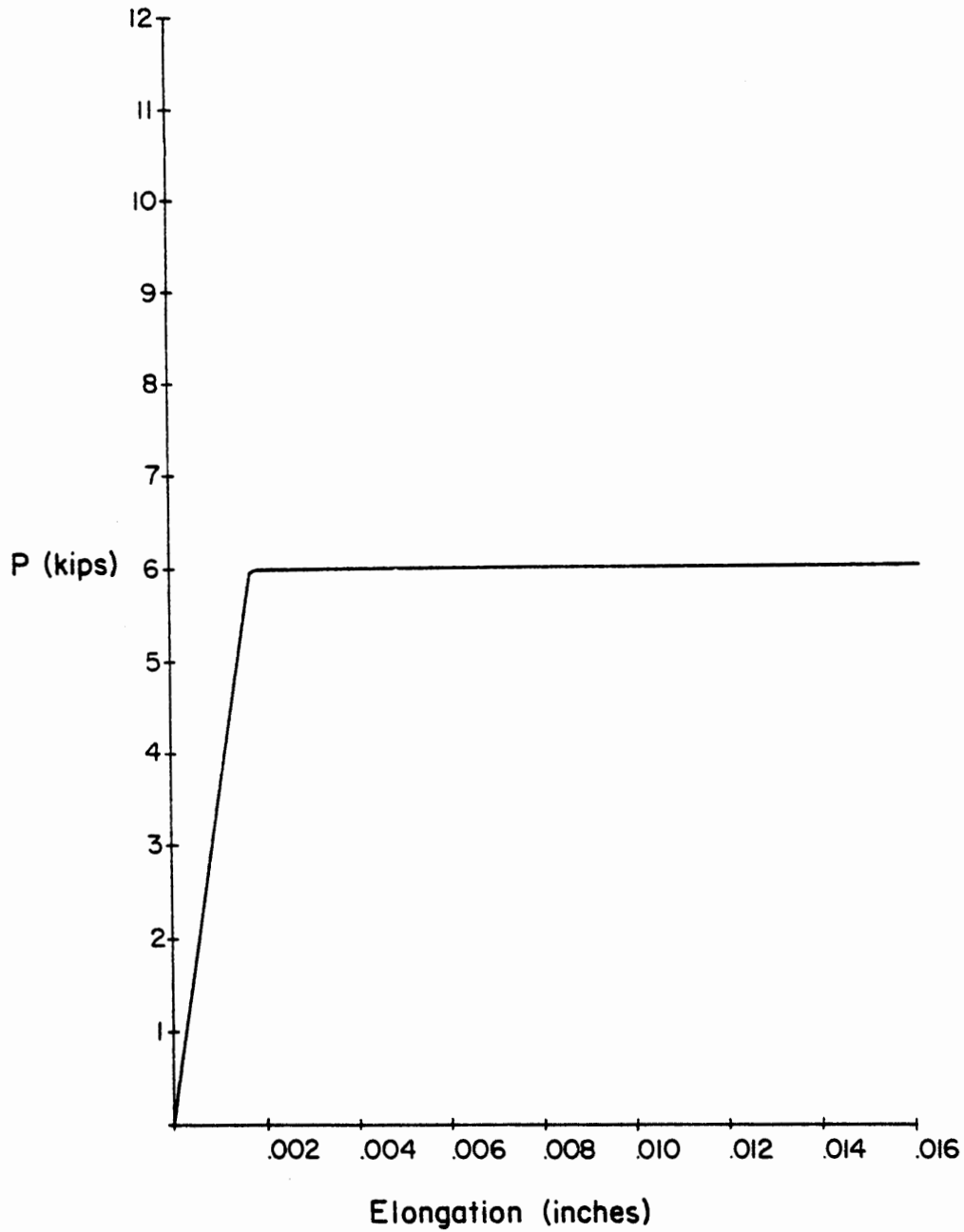


Figure 37. Yield stress determination, test specimen 08-GT36-01

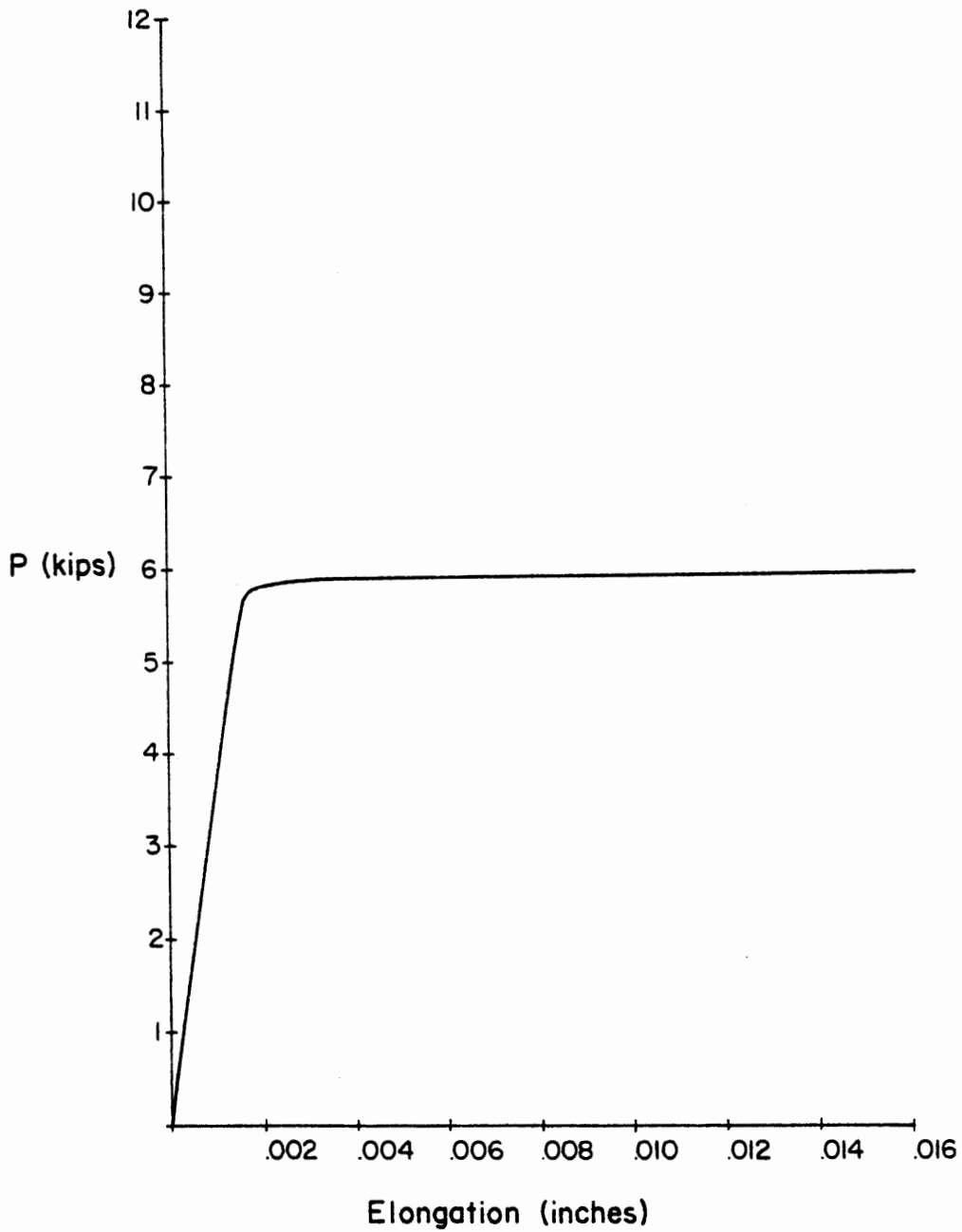


Figure 38. Yield stress determination, test specimen 09-GT36-01

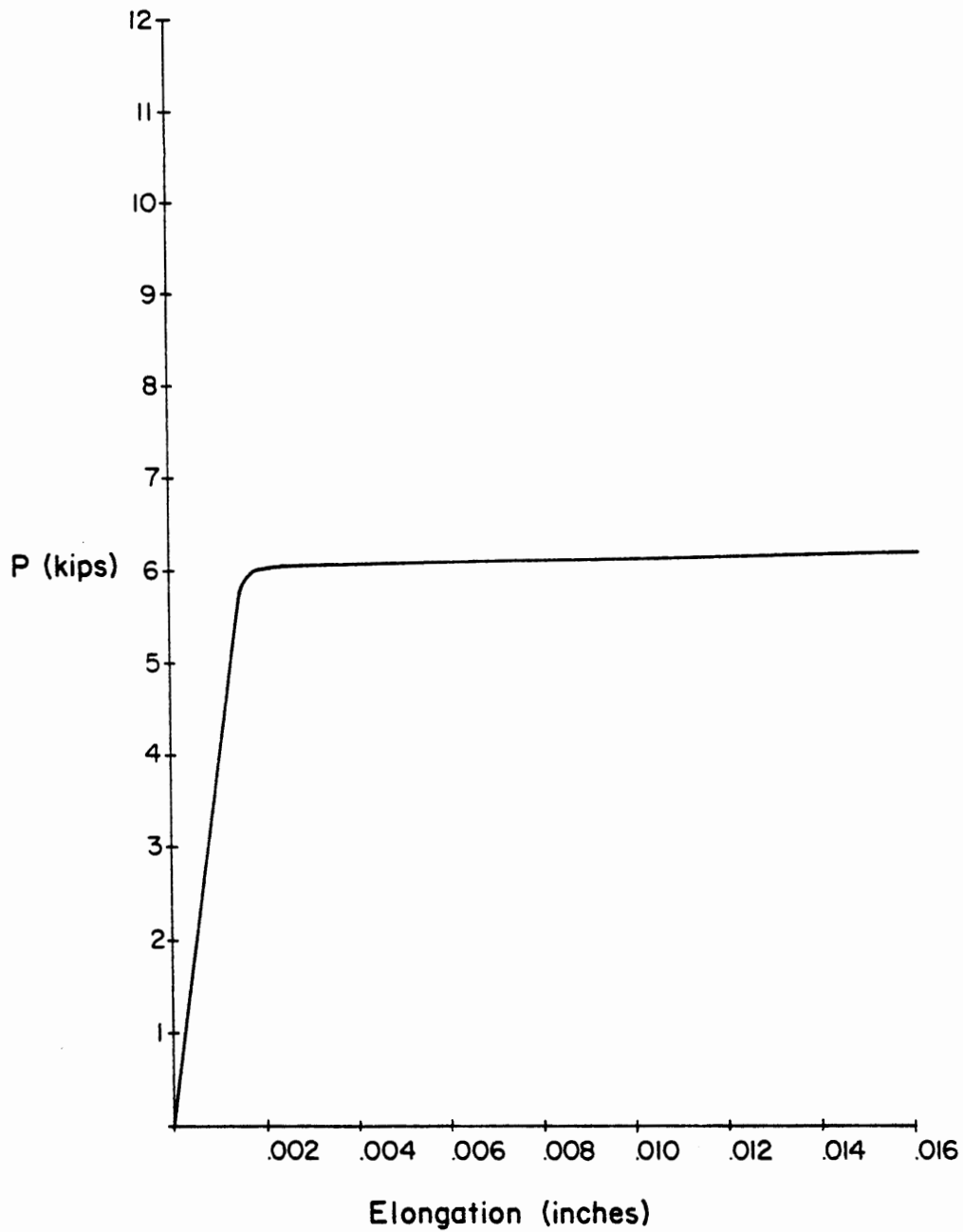


Figure 39. Yield stress determination, test specimen 17-GT36-01

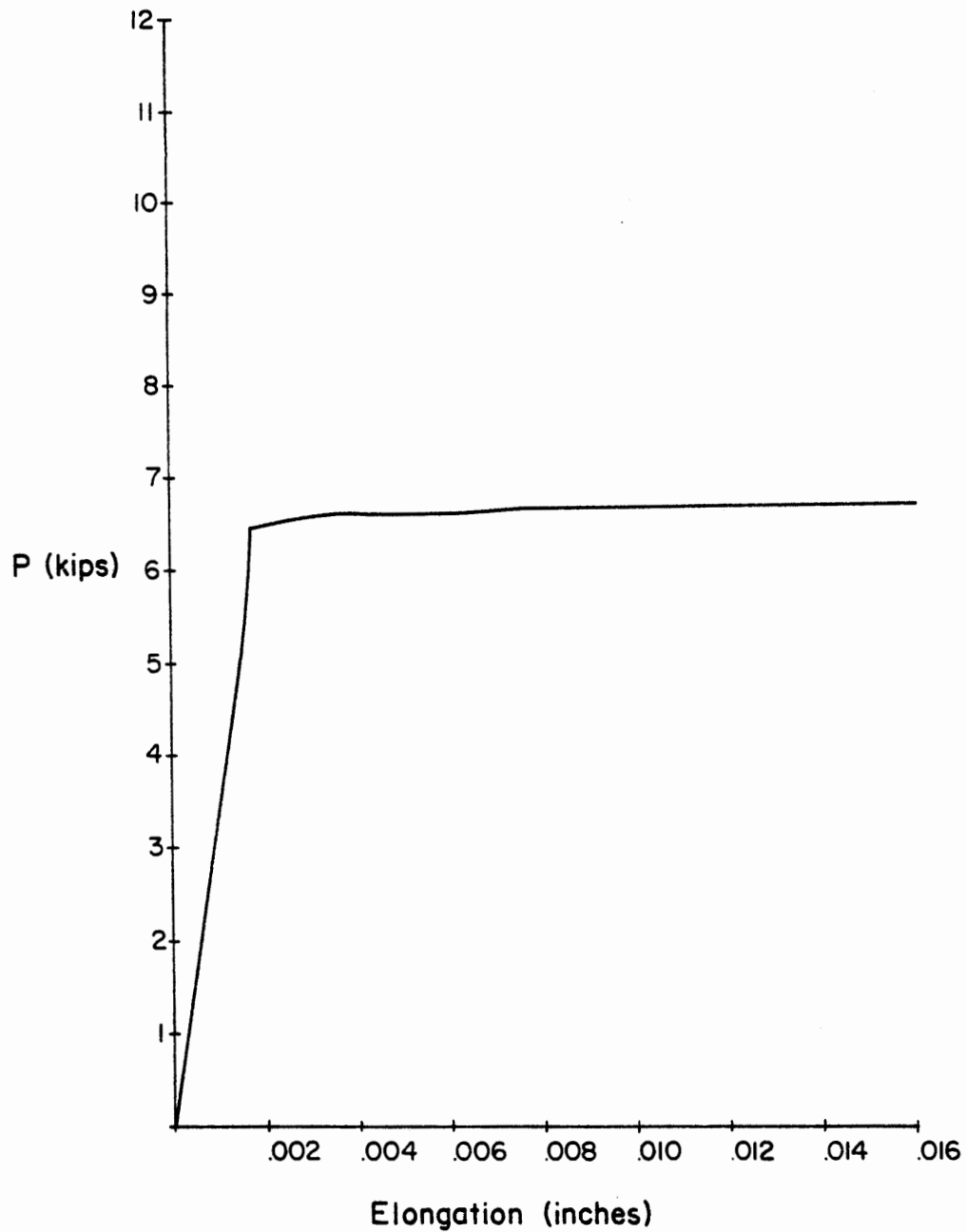


Figure 40. Yield stress determination, test specimen 10-GT36-02

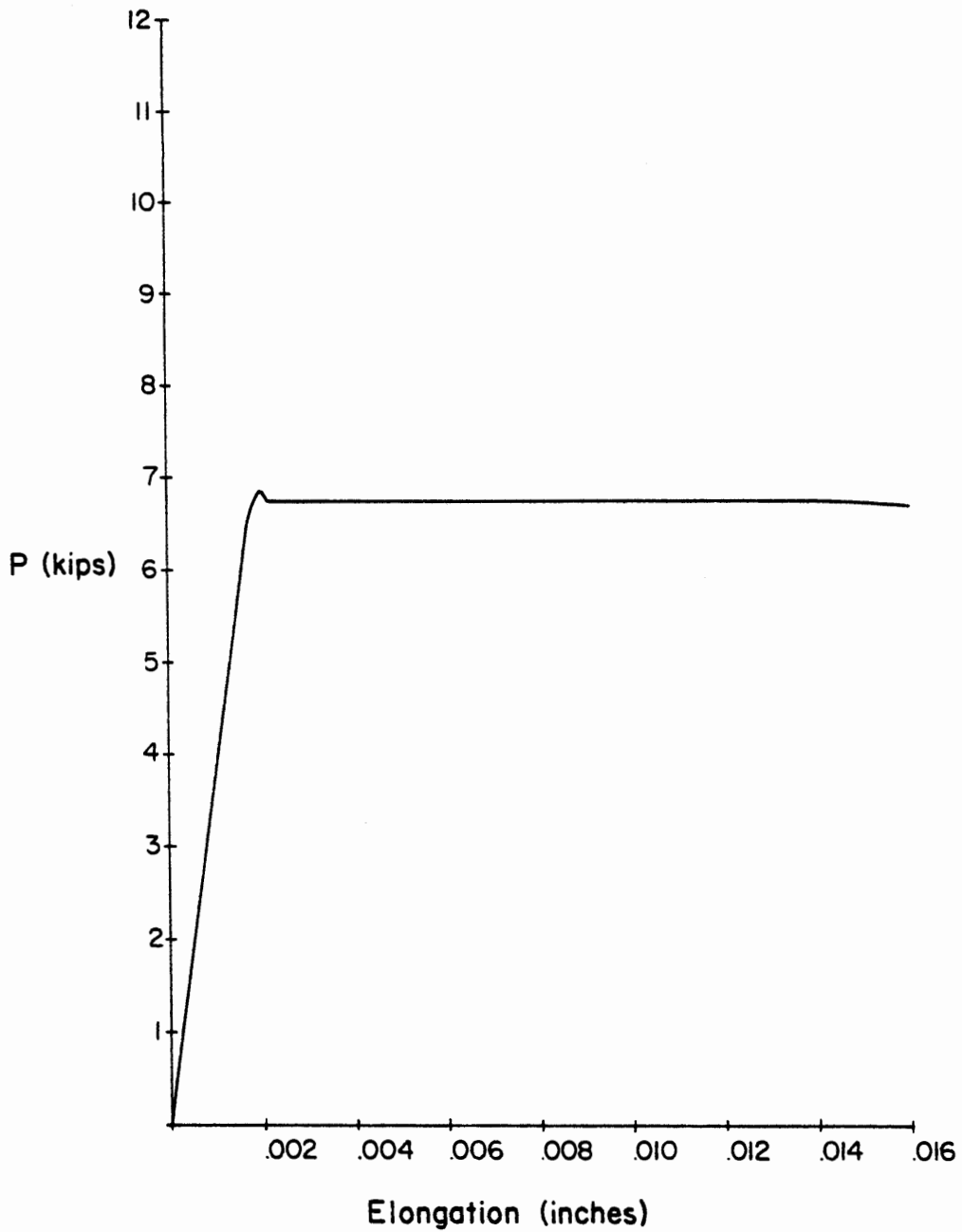


Figure 41. Yield stress determination, test specimen II-GT36-02

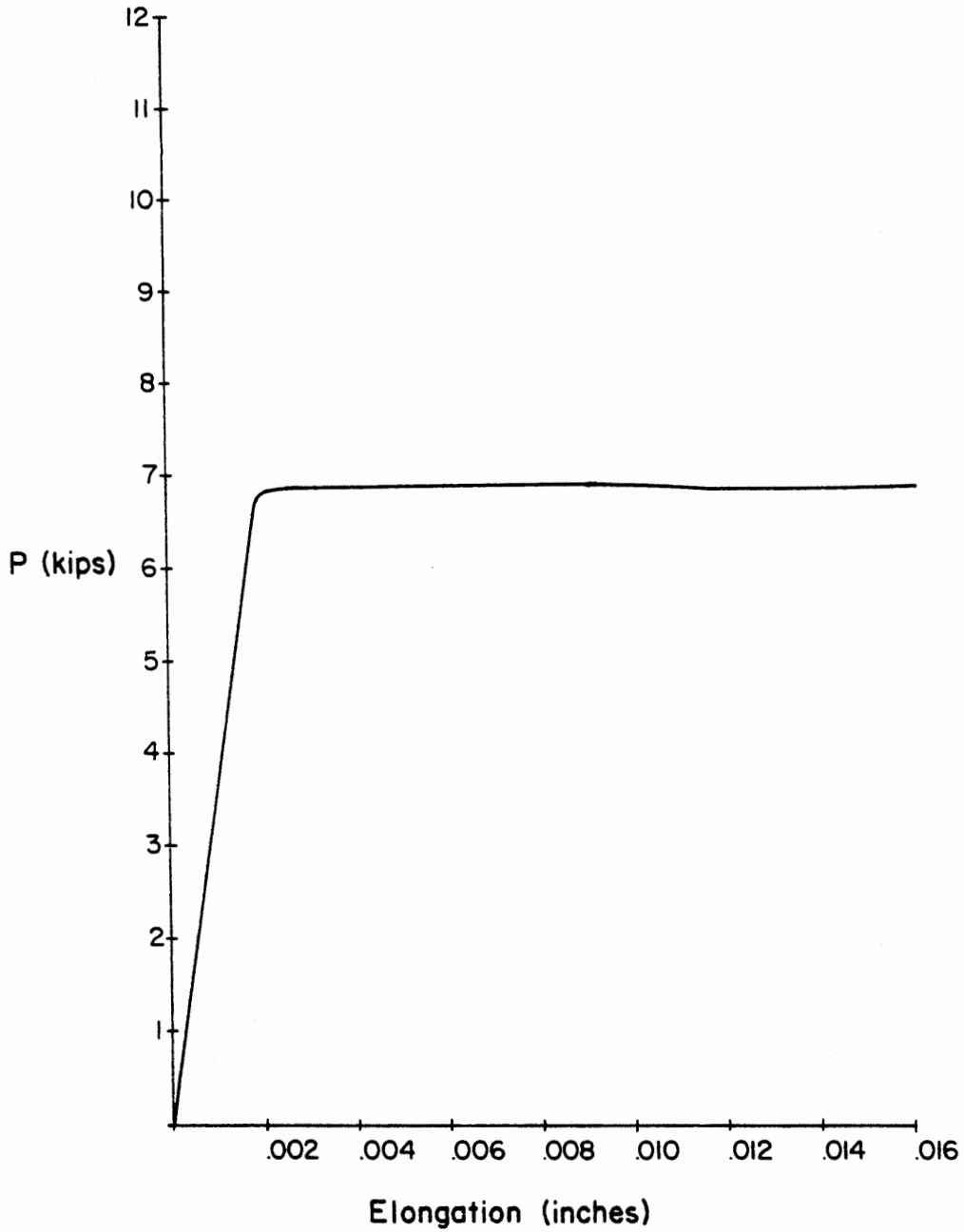


Figure 42. Yield stress determination, test specimen 12-GT36-02

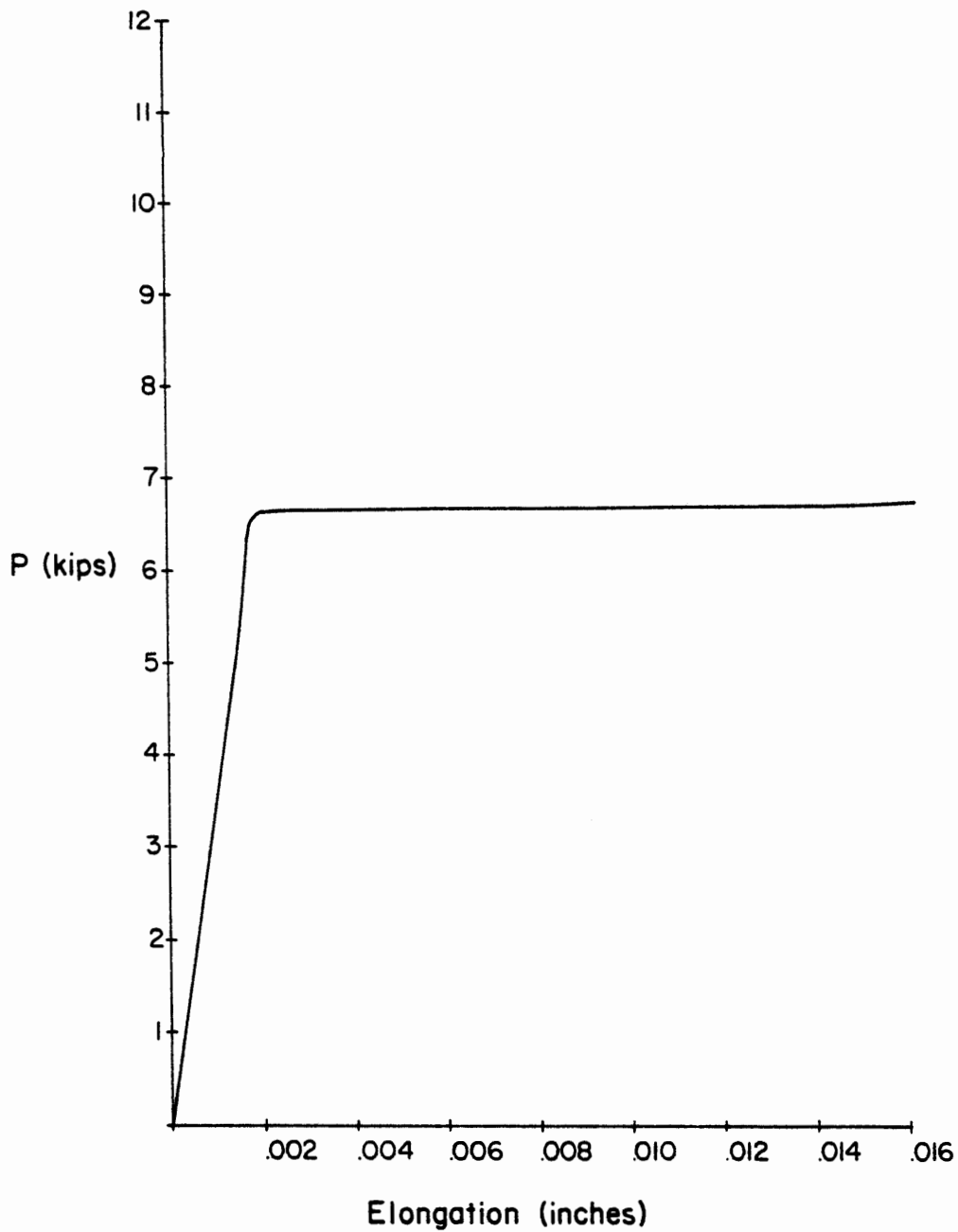


Figure 43. Yield stress determination, test specimen 18-GT36-02

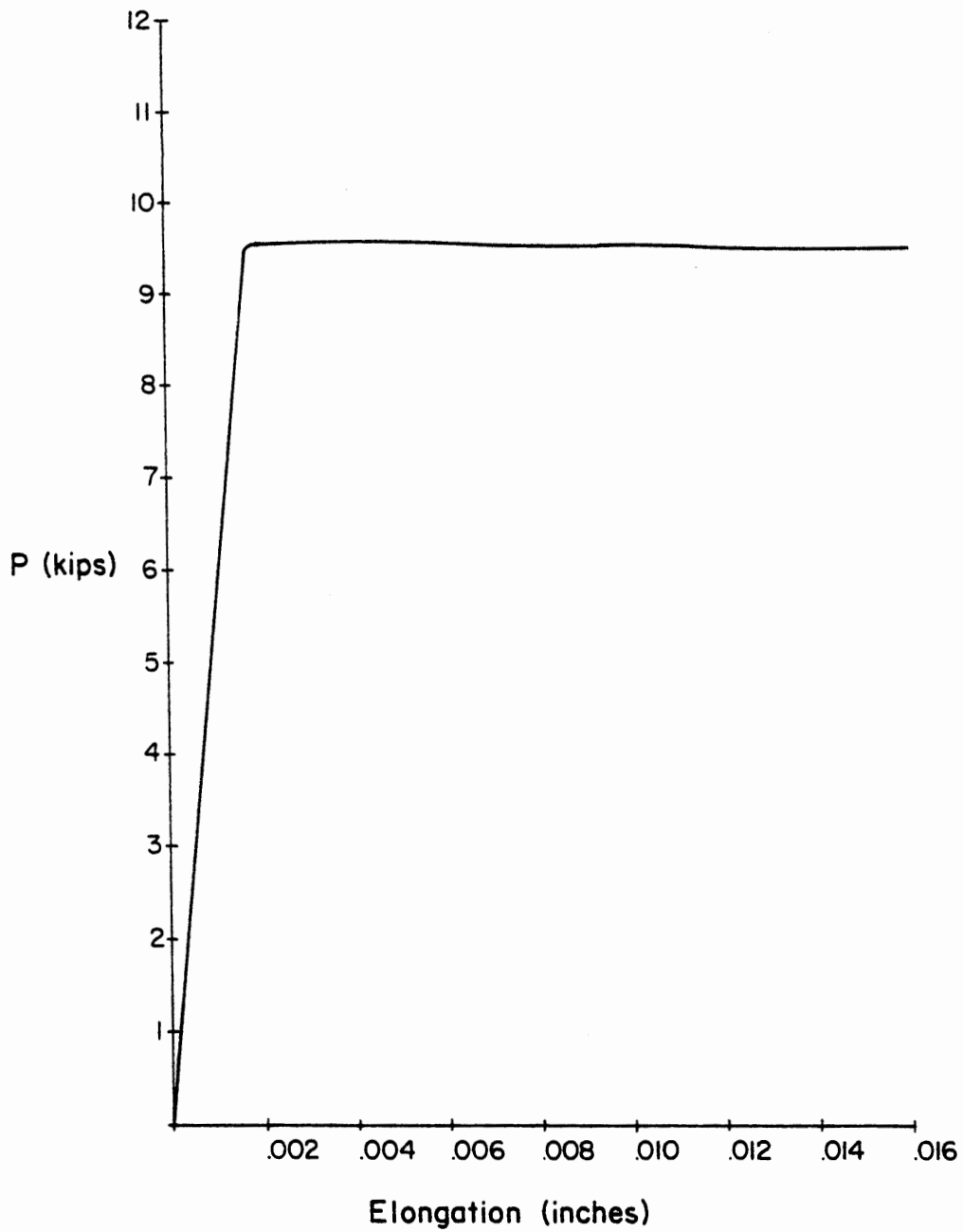


Figure 44. Yield stress determination, test specimen 13-GT36-03

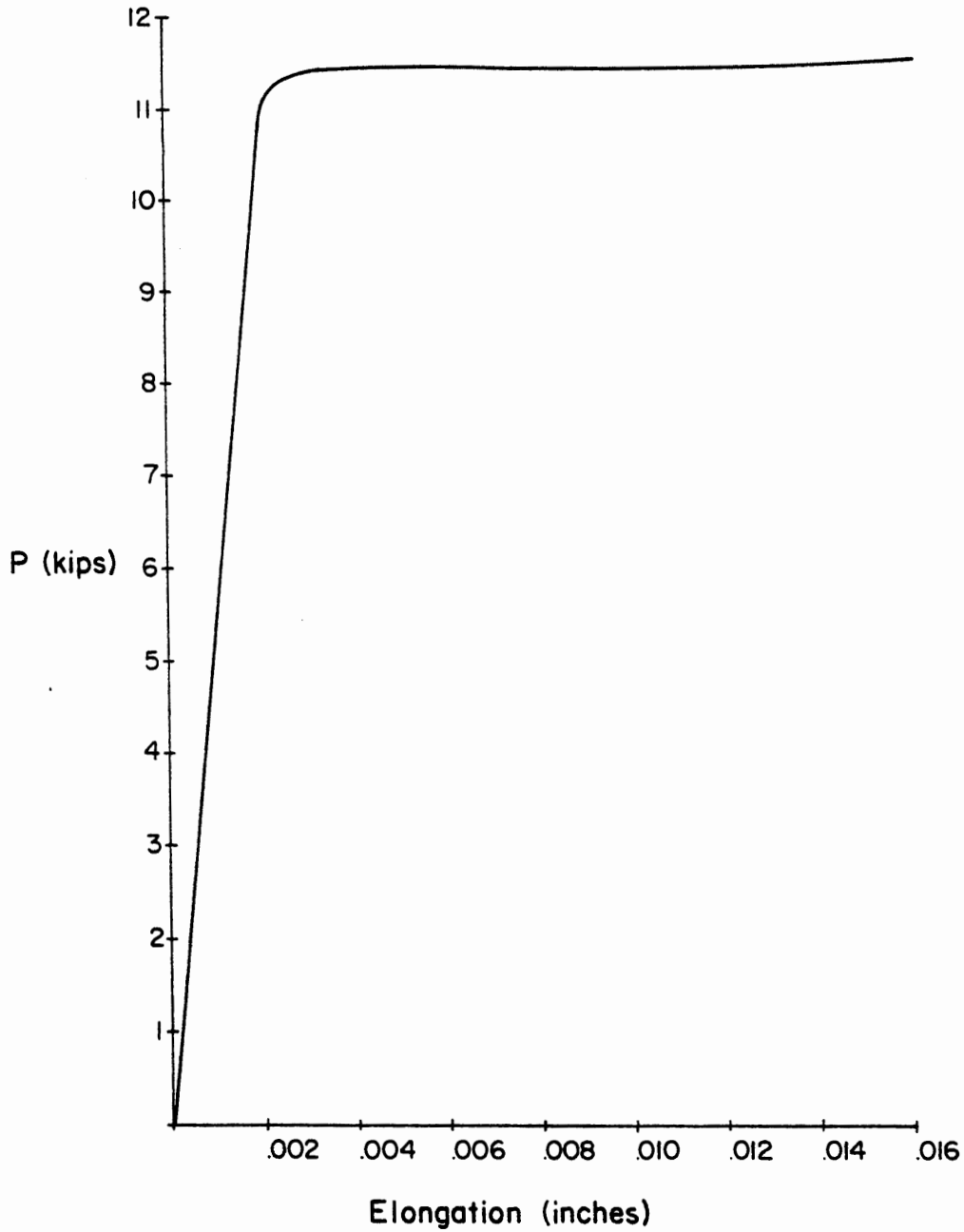


Figure 45. Yield stress determination, test specimen 14-GT36-03

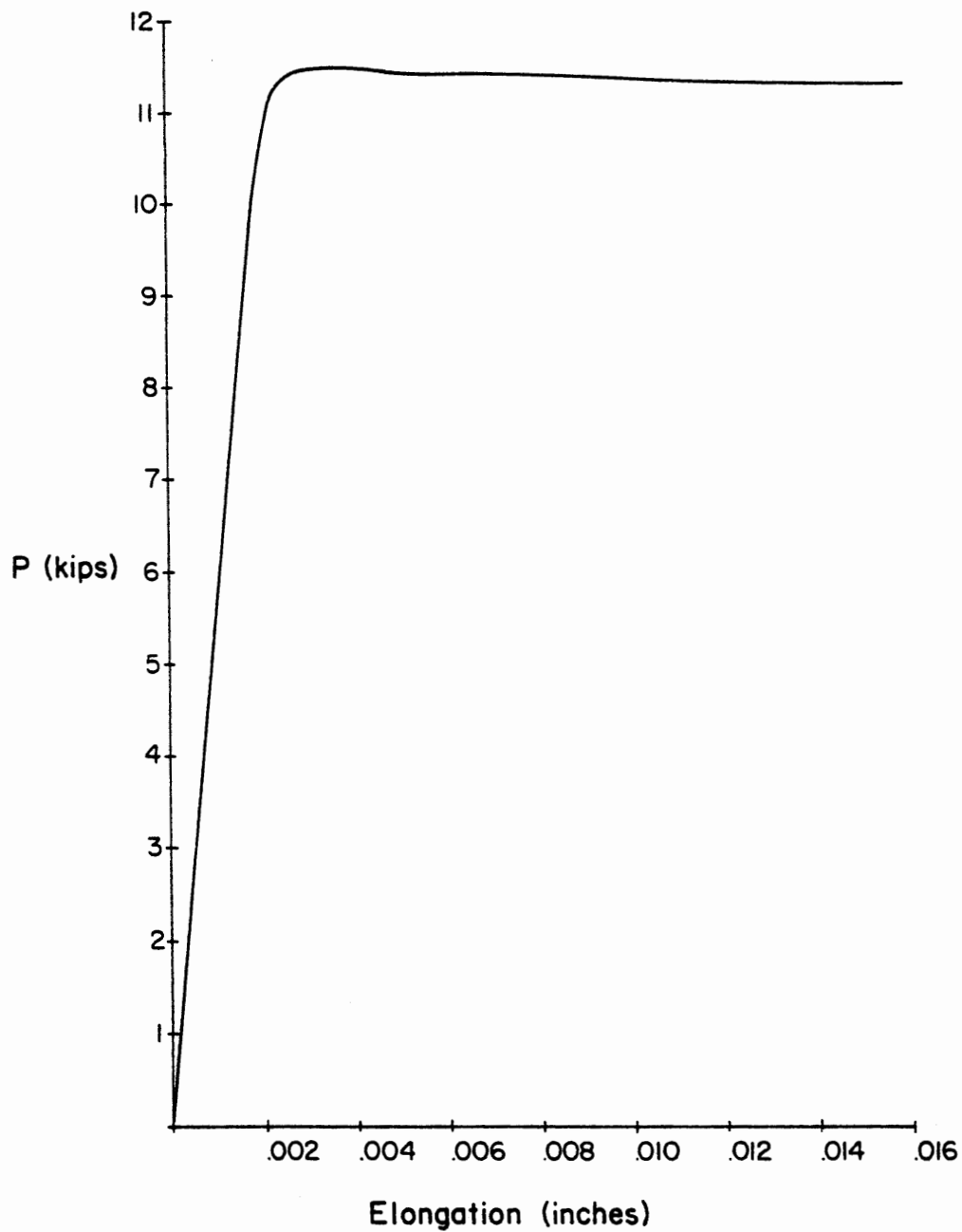


Figure 46. Yield stress determination, test specimen 15-GT36-03

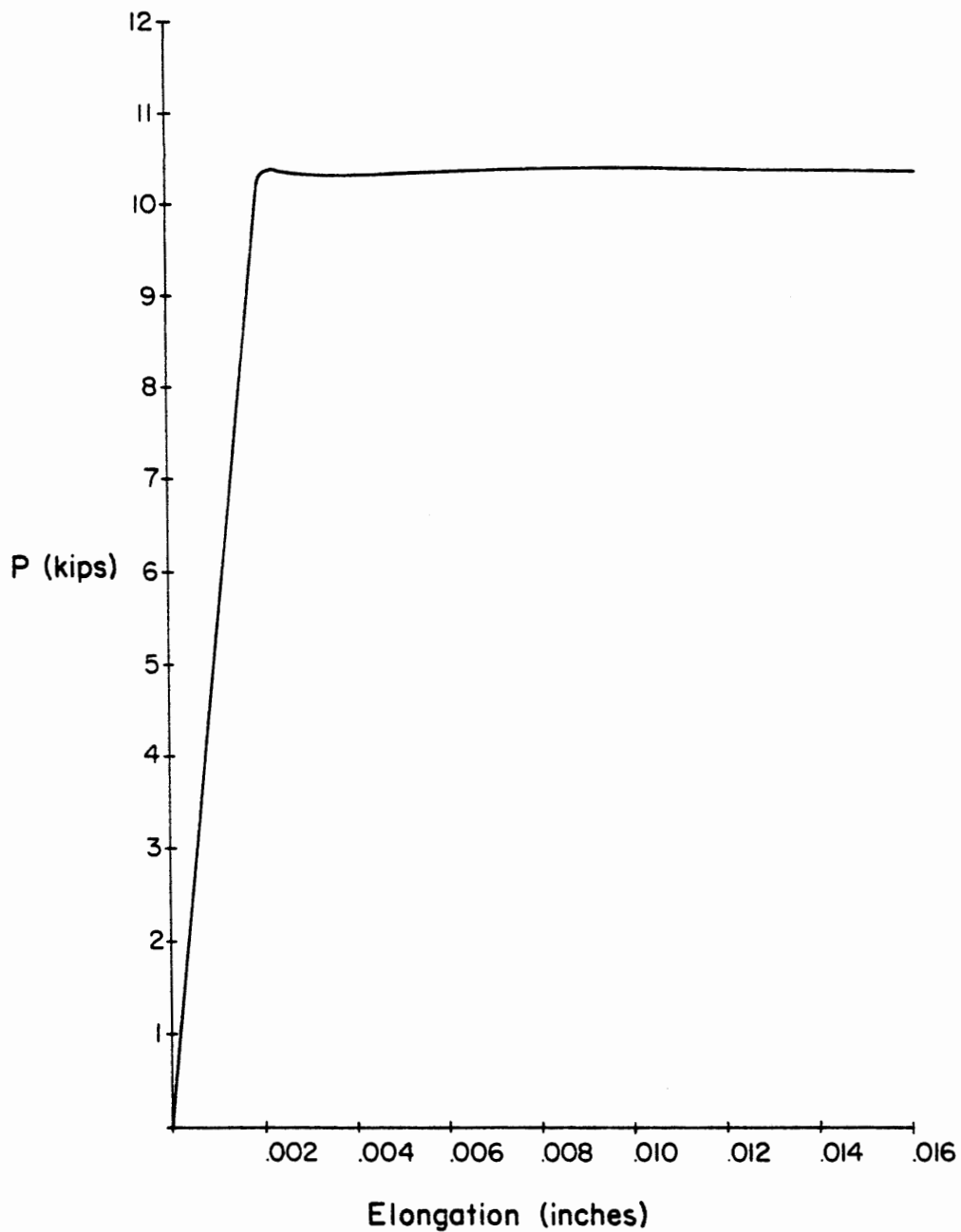


Figure 47. Yield stress determination, test specimen 16-GT36-03

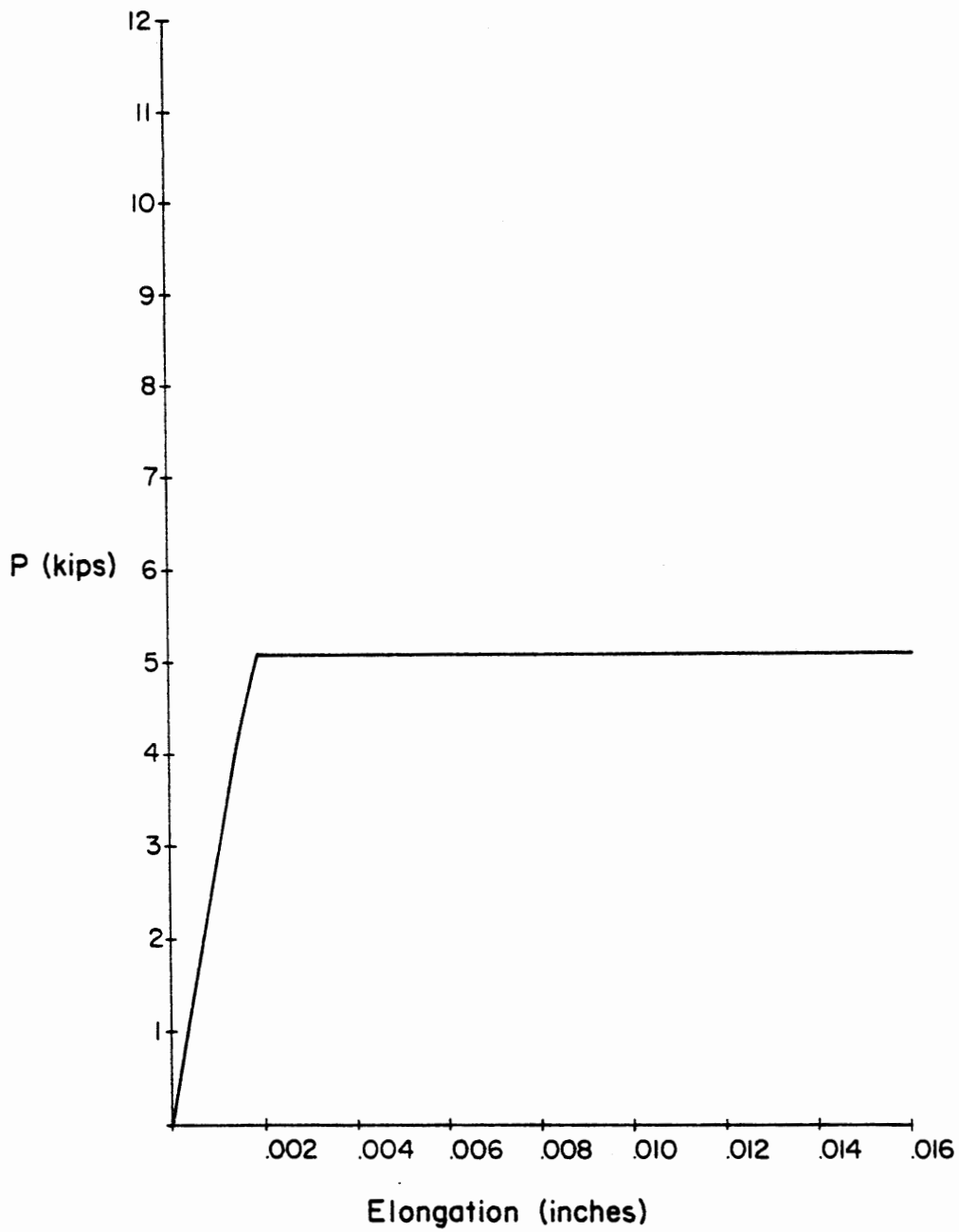


Figure 48. Yield stress determination, test specimen 21-GT36-01 and 22-GT36-01

TABLE IV

SUMMARY OF TEST SPECIMEN YIELD STRENGTH VALUES

Group	Specimen #	Area	P _{max} (k)	F _y (ksi)
A	01-GT48-1	0.1875	8.50	45.3
A	02-GT48-1	0.1875	8.80	46.9
A	03-GT48-1	0.1875	8.90	47.5
A	20-GT48-1	0.1875	8.18	43.6
B	04-GT48-2	0.1875	9.17	48.9
B	05-GT48-2	0.1875	9.55	50.9
B	06-GT48-2	0.1875	9.17	48.9
B	19-GT48-2	0.1875	9.56	51.0
C	07-GT36-1	0.125	6.07	48.6
C	08-GT36-1	0.125	6.00	48.0
C	09-GT36-1	0.125	6.07	48.6
C	17-GT36-1	0.125	5.90	47.2
D	10-GT36-2	0.125	6.64	53.1
D	11-GT36-2	0.125	6.72	53.8
D	12-GT36-2	0.125	6.87	55.0
D	18-GT36-2	0.125	6.64	53.1
E	13-GT36-3	0.1875	9.50	50.7
E	14-GT36-3	0.1875	11.42	60.9
E	15-GT36-3	0.1875	11.40	60.8
E	16-GT36-3	0.163	10.25	62.9
F	21-GT36-1	0.0975	5.08	52.1
F	22-GT36-1	0.0975	5.08	52.1

were cut from the outstanding leg of one end of each specimen. It was felt that this area of the specimen would have little or no residual stresses resulting from the actual member test. Residual stresses cause the stress/strain plot to become rounded at the proportional limit of the test specimen. Test specimens with no residual stress would exhibit a sharp transition between the elastic and plastic range of stresses. The greater the residual stress, the more rounded or gradual is the elastic/plastic transition. The resulting stress-strain curves, Figures 28 thru 48, verified this assumption showing only small traces of residual stress.

Test group A consisted of specimens 01-GT48-01, 02-GT48-01, 03-GT48-01 and 20-GT48-01. All four specimens exhibited similar characteristics. Immediately upon application of axial compression, the members bowed upwards. At failure, the specimens exhibited a midpoint bow of approximately 1 inch. Also at failure, there was noticeable torsional rotation of the cross section at the member midpoint.

Upon removal from the testing apparatus, all the members exhibited significant bolt hole elongation. This elongation, approximately 1/16 inch, was a result of the very high bolt bearing stresses. Table V summarizes the maximum bearing stresses for all 5 test groups. As Table V indicates, Test group A had an average maximum bolt bearing stress of 139 ksi. Significant connection yielding would be expected from such a large bearing stress.

Test Group B consisted of specimens 04-GT48-02, 05-GT48-02, 06-GT48-02 and 19-GT48-02. This group performed similarly to Group A. There was significant bowing about the horizontal axis upon application

TABLE V

CONNECTION AVERAGE MAXIMUM BEARING STRESSES

	Pave	t	b	A	f_{brg}	F_y
A	16.3	0.1875	0.625	0.117	139.	45.6
B	11.0	0.1875	0.625	0.117	93.9	49.9
C	7.56	0.125	0.625	0.0781	96.8	48.1
D	9.55	0.125	0.625	0.0781	122.	53.8
E	14.8	0.1875	0.625	0.117	126.	58.8

of axial load. At failure the members were beginning to rotate about their longitudinal axis and buckle in the y-y (weak) axis. Again, as the members were removed from the test frame, significant connection yielding was apparent. The stress strain curves for these specimens are shown in Figures 32 thru 35. As can be seen, there were little residual stresses in the test members. The yield stresses for this group showed little variation.

Test Group C consisted of specimens 07-GT36-01, 08-GT36-01, 09-GT36-01 and 17-GT36-01. These members were shorter than the members of test groups A and B and therefore necessitated the changing of the link between the test frame and the MTS actuator.

As expected, the members of group C performed similarly to the previous groups. The members began to arch vertically immediately upon application of axial load as had the previous test groups. The torsional rotation of the members of this group was apparent much sooner than for the previous test groups. This can be accounted for by looking at the connection eccentricity. For Group C, the e_x eccentricity, as indicated in Table III, was positive, whereas it was negative for all other test groups. Because of this positive eccentricity, point A, Figure 26, received compressive bending stresses from both the e_x and e_y eccentricities, whereas for test groups A, B, D and E, point B received compressive bending stresses from the e_y eccentricity and tensile bending stresses from the e_x eccentricity. The load-displacement tests for the members of group C showed very little variation and again the apparent residual stresses were small.

Test group D, consisted of specimens 10-GT36-02, 11-GT36-02, 12-GT36-02 and 18-GT36-02. The results from this test group were very consistent. All four members exhibited noticeable bowing about the horizontal axis immediately upon application of axial compression. At approximately 35% of the failure load, torional rotation was evident in all group C specimens. With a width-to-thickness ratio of 16.0, these members were expected to exhibit early buckling of the compression flange. The load-displacement curves for the members of test group D are shown in Figures 15 thru 18. Figures 40 thru 43 provide the load-elongation curves for the yield stress evaluation of the specimens of test group D. As can be seen, little residual stresses were evident.

Group E consisted of specimens 13-GT36-03, 14-GT36-03, 15-GT36-03 and 16-GT36-03. The performance of this group was consistent with the prior groups except there was little torsional rotation of specimen cross-section. Of the 5 test groups, Group E should have been the least susceptible to lateral torsional buckling because of their shorter length and low width-to-thickness ratio. One initial inconsistency was apparent in test Group E. Specimen 13-GT36-03 had a failure approximately 11% lower than the 3 other members of Group E. This apparent discrepancy was resolved upon completion of the yield strength determination. The yield strength of specimen 13-GT36-03, Figure 44, was significantly less than the other members of group E, Figures 45, 46 and 47. Therefore, the ratio of member axial stress at failure to material yield stress was found to be consistent within the group.

Group F consisted of specimens 21-GT36-01 and 22-GT36-02. These specimens were identical to Group C except for the gage line dimension

of the bolt holes. For this group, the 1 inch gage line of Group C was reduced to 7/8 inch. This change was made to help verify a conclusion made in interpreting the results of test groups A thru E. This conclusion will be discussed in more detail later.

For group F, only one tension coupon was made since it was known that both specimens were cut from the same piece of raw material. The results of this tension coupon test are shown on Figure 48.

Summary of Test Results

The values resulting from the test program were very consistent. As described previously in Chapter III, all the test members failed in a similar mode. This mode of failure was expected and predictable because of the design of the member end connections.

The significant difference between the results of test member group C and F was, however, unexpected. The members of test group C were fabricated with the bolt holes on a 1 inch gage and those of group F having a 7/8 inch gage (see Table I). This small but subtle difference resulted in an e_{xx} eccentricity, Table III and Figure 26, of +0.067 inches for test group C and -0.022 inches for test group F. Because the two values of e_{xx} were of opposite sign the resulting bending moments, induced by the eccentricity of the axial load, were also of opposite sign. For the members of test group C, this bending moment initially created a tensile stress at the heel of the angle, point B figure 26, rather than the compressive stress of the other test groups. As the axial load for the group C members gradually increased, and the members continued to arch upwards, the value of the e_{xx} eccentricity ultimately switched from a positive value to a negative

value and the bending stress at point B switched to compression as in all the other test member groups.

By having the e_{xx} eccentricity initially positive, the members of test group C were effectively prestressed against their eventual mode of failure. This prestressing effectively allowed the members of test group C to sustain higher relative axial loads.

The members of test groups D and E should have exhibited very similar results because their KL/r ratios were effectively equal. The results indicated that the members of test group E failed at a lower relative stress level than those of test group D. This was not expected because the members of test group E were of a larger cross-section. The differing results can again be attributed to the e_{xx} eccentricity. For the members of test group D, e_{xx} was -0.0209 inches, while for the members of test group E e_{xx} was -0.0313 inches. This is a 50% increase in eccentricity compared with a 43% increase in bending stiffness.

All the test specimens failed because of buckling. This can be determined by looking at figures 3 through 24. All the figures indicate a sharp decrease in load carrying capacity upon reaching their critical load. If there had been excessive yielding or inelastic buckling of the test specimens more of a transition or smoothing of the load/displacement plots at or near the failure load would have been observed.

All test members immediately bowed vertically upon application of axial load but ultimately twisted and buckled about their weak axis. None of the members exhibited any tendency to rotate about the end connection even though there was only a single bolt at each end. This

fact implies that there was significant end restraint to buckling about the weak axis.

The sensitivity to weak axis eccentricity and lack of sensitivity to the strong axis eccentricity of these tests was consistent with the previous results of Mueller and Erzurumlu (7).

CHAPTER IV

ANALYTICAL METHODS

To analytically predict the behavior of an imperfect or "real" column the investigator must attempt to develop a model whose behavior approaches that of the real column's. This can be done quite accurately for long columns with small eccentricities. When these columns are sufficiently short, so that portions of the member cross section begin to yield, the analytical models begin to get extremely complex.

The members used in this test program have significant end connection eccentricity, and are short enough to expect some yielding of the cross-section. They also exhibit a certain amount of connection fixity.

Because of these complexities, the development of a specific analytical model to predict the behavior of the test members was beyond the scope of this project. Instead, an attempt was made to utilize existing methods and compare the calculated results to the actual test results.

Two significantly different models were chosen. The first is a classical elastic combined stress method and the second a numerical inelastic computer method. The following discussion covers the elastic method, the inelastic computer method, and concludes with a discussion of the results of the two methods and how they compare with the test results.

Elastic Method

A column with eccentric end connections can be treated as having its cross section in a state of combined stress. The member would have a uniform axial compressive stress combined with a constant bending stress. For ease of analysis these two dependent stresses can be assumed to act independently and then modified through the use of coefficients to account for their mutual interaction.

Reference 4 provides an excellent derivation of the elastic method used in this report. The combined stress equation takes the following form:

$$\frac{f_a}{F_a} + \frac{C_{mx} f_{bx}}{\left(1 - \frac{f_a}{F'_{ex}}\right) F_{bx}} + \frac{C_{my} f_{by}}{\left(1 - \frac{f_a}{F'_{ex}}\right) F_{by}} = 1 \quad (1)$$

- Where:
- f_a = axial compressive stress
 - F_a = maximum compressive stress
 - C_{mx} = modification factor dependent upon bending mode about the x axis.
 - F_{bx} = bending stress in x-x axis
 - F'_{ex} = Euler stress based upon L_x/r_x
 - F_{bx} = maximum allowable bending stress about x-x axis
 - C_{my} = modification factor dependent upon bending mode about the y axis
 - f_{by} = bending stress in y-y axis
 - F'_{ey} = Euler stress based upon L_y/r_y
 - F_{by} = maximum allowable bending stress about y-y axis

The allowable compressive stress term, F_a , has two possible values depending upon the magnitude of the effective length-to-radius of gyration or KL/r ratio. After removal of the factors-of-safety utilized for design purposes (5) the value of F_a can be expressed as follows:

$$\text{for } \frac{KL}{r} \leq C_c$$

$$F_a = \left(1 - \frac{(KL/r)^2}{2C_c^2} \right) F_y$$

$$\text{for } \frac{KL}{r} > C_c$$

$$F_a = \frac{\pi^2 E}{\left(\frac{KL}{r} \right)^2}$$

$$\text{where } C_c = \sqrt{\frac{2 \pi^2 E}{F_y}}$$

The term C_c is the transition point between inelastic and elastic buckling.

For the members and connection configuration of this test program the coefficients C_{mx} and C_{my} are both equal to 1.0. These coefficients provide for a reduction in bending stresses if the bending moment at the midpoint of the member is less than that at the ends of the member. Because all the test members exhibited single curvature and the end moments were equal in magnitude, no reduction in bending stresses should be expected.

The term $1 - f_a/F'_e$ in the denominator of the second and third terms of the combined stress equation is an amplification factor which accounts for the inherent P-delta effect of a beam-column.

The allowable bending stress terms F_{bx} , and F_{by} can be based on either the actual allowable working stresses (5) or the actual material

yield stresses. For purposes of comparison with the test results, the calculations have been based upon the material yield strengths.

These bending stress terms f_{bx} and f_{by} can be expressed in terms of the applied axial load and the corresponding moment of inertia as follows:

$$f_{bx} = \frac{P e_x C_x}{I_{yy}} \quad (2a)$$

$$f_{by} = \frac{P e_y C_y}{I_{xx}} \quad (2b)$$

Where: P = applied axial load
 e_x, e_y = eccentricity of applied load about the x and y axis respectively
 C_x, C_y = distance to extreme fiber in the x and y axis respectively
 I_{xx}, I_{yy} = moments of inertia about x and y axis respectively

Likewise the axial compressive stress can be expressed as a function of the applied compressive load, P, and the member cross-sectional area, A.

Combining all the above, equation (1) develops into the following form:

$$\frac{P}{F_a A} + \frac{P e_y C_y}{F_y I_{xx} \left(1 - \frac{P}{A F'_{ey}}\right)} + \frac{P e_x C_x}{F_y I_{yy} \left(1 - \frac{P}{A F'_{ex}}\right)} = 1 \quad (3)$$

for KL/r ratios greater than C_c .

Two different approaches were taken to solve equation (3). The first was a general numerical solution and the second was an exact solution assuming a particular failure mode.

The general numerical solution is based upon an iterative procedure (8) wherein a value for the axial compression P is assumed and, using this value, equation (3) is solved. If the resulting value of the left side terms are equal to 1 ± 0.001 the solution was assumed to be sufficiently accurate and the current value of P is the maximum compressive load. If not, the current value of P is incremented and the procedure is repeated.

This particular solution method was implemented on an APPLE II microcomputer and a listing of the resulting program is given in Figure 49.

The exact solution assumes point B, the heel of the angle section as referenced in Figure 26, was the point of maximum compressive stress. This assumption was based upon the test results wherein every test member failed by buckling about the weak axis.

With this assumption, the second term of equation (3), the stress at B due to bending about x-x axis is zero allowing the resulting equation to be easily solved for P as a function of the remaining terms.

Again the solution was implemented on an APPLE II microcomputer and the program listing is shown in Figure 50.

Table VI summarizes all the necessary input parameters for both solution techniques. Table VII indicates the results of the calculations which, as should be expected, were identical in both solution techniques. These results were expected to be identical because the two solution techniques were solving the same equation.

An interesting result of the solution of equation (3) arose for Test Group C. Neither solution technique produced a valid result for

```

10 REM PROGRAM 'THESIS'
20 REM JRC 22 JANUARY 1983
30 REM
40 TEXT : HOME
50 PI = 3.14159
60 E = 29000
70 INPUT "L. IN?";L
80 INPUT "AREA. IN^2?":AREA
90 INPUT "IXX. IN^4?":IXX
100 RXX = SQR (IXX / AREA)
110 INPUT "IYY. IN^4?":IYY
120 RYY = SQR (IYY / AREA)
130 R = RYY
140 REM R = MINIMUM OF RXX & RYY
150 IF R > RXX THEN R = RXX
160 INPUT "EX. IN?":EX
170 INPUT "EY. IN?":EY
180 INPUT "F(Y). KSI?":YP
190 INPUT "CXA. IN?":XA
200 INPUT "CXB. IN?":XB
210 INPUT "CYA. IN?":YA
220 INPUT "CYB. IN?":YB
230 INPUT "K-FACTOR?":K
240 INPUT "CHECK @ A OR B?":A$
250 IF A$ = "A" THEN 280
260 X = XB:Y = YB
270 GOTO 290
280 X = XA:Y = YA
290 VTAB 17
300 FOR I = 1 TO 5
310 PRINT "
320 NEXT I
330 VTAB 15
340 FXE = PI * PI * E / (K * L / RXX) ^ 2
350 FYE = PI * PI * E / (K * L / RYY) ^ 2
360 CC = SQR (2 * PI * PI * E / YP)
370 P = 1:INC = 1
380 T1 = 0:T2 = 0:T3 = 0:T4 = 0
390 FA = P / AREA
400 IF (K * L / R) > CC THEN 440
410 PRINT " INELASTIC BUCKLING"
420 T1 = FA / YP / (1 - (K * L / R) ^ 2 / 2 / CC / CC)
430 GOTO 440
440 PRINT " ELASTIC BUCKLING "
450 T1 = FA / PI / PI / E * (K * L / R) ^ 2
460 REM BENDING ABOUT Y-Y AXIS
470 T2 = P * EX * X / IYY / (1 - FA / FYE) / YP
480 REM BENDING ABOUT X-X AXIS
490 T3 = P * EY * Y / IXX / (1 - FA / FXE) / YP
500 T4 = T1 + T2 + T3
510 VTAB 15
520 PRINT T4.A$
530 IF INT ((1.0 - T4) * 1000) = 0.0 THEN 600
540 IF T4 < 1.0 THEN 580
550 INC = INC / 2
560 P = P - INC
570 GOTO 380
580 P = P + INC
590 GOTO 380
600 PRINT
610 PRINT T1
620 PRINT T2
630 PRINT T3
640 VTAB 21
650 PRINT "ULTIMATE LOAD = "P" KIPS"
660 VTAB 1
670 GOTO 70
680 END

```

Figure 49. Computer listing of numerical combined stress solution.


```

10  REM      PROGRAM 'THESIS-EXACT'
20  REM      JRC 22 JANUARY 1983
30  REM
40  TEXT : HOME
50  PI = 3.14159
60  E = 29000
70  INPUT "L, IN?":L
80  INPUT "AREA, IN^2?":AREA
90  INPUT "IYY, IN^4?":IYY
100 RY = SQR (IYY / AREA)
110 INPUT "EX, IN?":EX
120 INPUT "F(Y), KSI?":YP
130 INPUT "CXB, IN?":CXB
140 INPUT "K-FACTOR?":K
150 PE = PI * PI * E * AREA / (K * L / RY) ^ 2
160 CC = SQR (2 * PI * PI * E / YP)
170 IF (K * L / RY) > CC THEN 210
180 PRINT : PRINT "INELASTIC BUCKLING"
190 F = (1 - (K * L / RY) ^ 2 / 2 / CC / CC) * YP * AREA
200 GOTO 230
210 PRINT : PRINT "ELASTIC BUCKLING  "
220 F = PE
230 G = EX * CXB / IYY / YP
240 R = G * F * PE + F + PE
250 Q = R * R - 4 * PE * F
260 IF Q < 0 AND B < ) PE * 2 THEN 370
270 Q = SQR (Q)
280 P1 = (R + Q) / 2
290 P2 = (R - Q) / 2
300 PRINT
310 VTAB 13
320 PRINT "ULTIMATE LOAD = "P1" KIPS"
330 PRINT " OR           = "P2" KIPS"
340 VTAB 1
350 GOTO 70
360 END
370 VTAB 13
380 PRINT "NO SOLUTION-- IMAGINARY ROOTS"
390 PRINT "
400 VTAB 1
410 GOTO 70

```

Figure 50. Computer listing of exact combined stress solution

TABLE VI
 INPUT VALUES FOR ELASTIC SOLUTION

Group	L	A	I _{xx}	I _{yy}	e _x *	e _y *	F _y	C _{xA} *	C _{xB} *	C _{yA} *	C _{yB} *
A	58.82	0.902	0.873	0.221	-0.0313	-0.818	45.8	0.853	-0.981	-1.70	0.00
B	58.82	0.715	0.434	0.110	-0.0313	-0.641	49.9	0.676	-0.805	-1.35	0.00
C	49.52	0.422	0.201	0.051	+0.067	-0.663	48.1	0.597	-0.684	-1.19	0.00
D	49.52	0.484	0.303	0.077	-0.0209	-0.663	53.8	0.686	-0.772	-1.37	0.00
E	49.52	0.715	0.434	0.110	-0.0313	-0.641	58.8	0.676	-0.805	-1.35	0.00
F	49.52	0.422	0.201	0.051	-0.022	-0.575	52.1	0.597	-0.684	-1.19	0.00

Units: Kips, inches, square inches.

*See Figure 26.

TABLE VII

RESULTS OF COMBINED STRESS SOLUTION

Test Group	K=1	K=0.9	K=0.8	K=0.65
A	14.45k	17.33k	20.53k	25.50k
B	7.42k	8.95k	11.02k	15.54k
C	No solution - imaginary roots, see text			
D	7.45k	9.02k	11.09k	14.70k
E	10.27k	12.37k	15.18k	20.62k
F	4.95k	5.99k	7.39k	10.39k

the maximum compression load. The numerical technique solution would not converge and the exact solution, which requires the solution of a quadratic equation, gave imaginary solutions.

Test Group C was the only test group which had a positive value for the e_x eccentricity. The results can be explained by studying Figure 26. When the e_x eccentricity is numerically positive, the resulting bending moment, $P e_x$, causes the heel of the angle to be in tension rather compression.

The numerical technique, because it was iterative showed that the equation results initially began to converge but then suddenly began to diverge. This can be explained by looking at the P-delta amplification factor in the bending stress term of equation (3). As P increases, the amplification factor decreases in magnitude which, in turn, increases the bending stresses. For Group C, because of the positive e_x values, these increased bending stresses result in increased tensile stresses at B. These tensile forces begin to balance the axial compressive stresses and ultimately dominate such that point B ends up in tension rather than compression.

These results, while mathematically correct, are from an analytic model which does not fully represent the actual member condition.

Various end conditions were tried in an effort to match the results of the test program. Figure 51 shows a plot of all the results tabulated in Table VII.

To eliminate the effects of the varying material yield stresses, the calculated maximum compressive loads, listed in Figure VII, were normalized to a relative percent of yield stress. This was done by

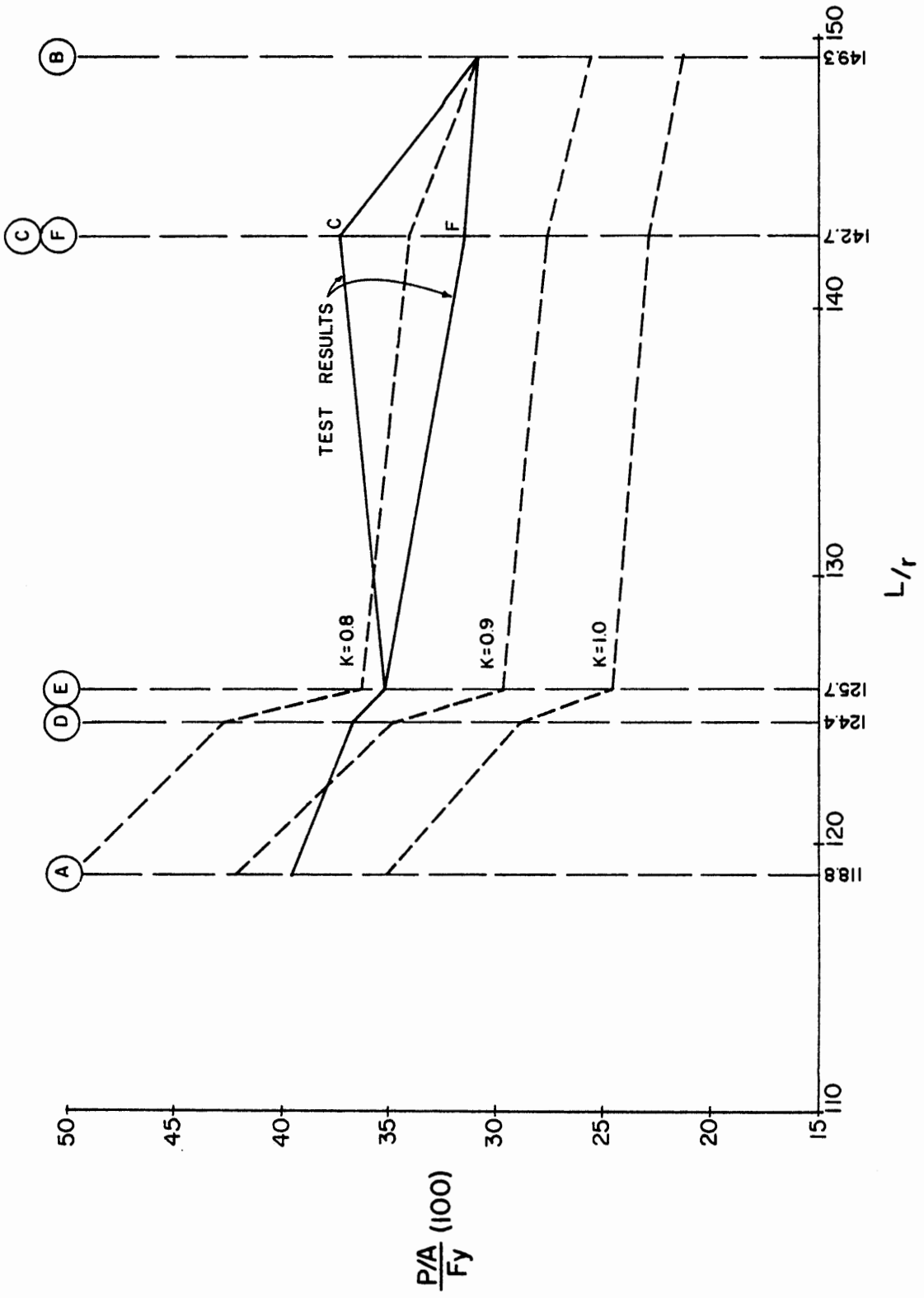


Figure 51. Plot of combined stress solution results.

dividing the calculated loads by their respective cross-sectional area and by their yield stress and multiplying by 100.

Inelastic Method

This technique was developed by Mueller and Erzurumlu (7). It is an iterative method based upon a finite difference solution of the differential equations describing the deflected shape of a beam column.

The technique assumes 3 degrees of freedom, X translation, Y translation and rotation about the Z (member) axis. For the solution, the member is divided into segments and for each segment a set of coefficients is developed which relate the member properties and loads to the displacements of the adjacent four segments. This results in a diagonally banded stiffness matrix which can be solved for the unknown displacements. Based upon these displacements the bending moment and curvature at each segment of the beam-column can be calculated.

Based upon these values of moment and curvature, a stiffness at each segment can be calculated. Within the elastic range of the members performance, this calculated stiffness should be identical to the member's actual stiffness. When the calculated stiffness is less than the actual stiffness the member is performing in the inelastic range. This is simply another way to state that the cross-section of the member is experiencing stresses high enough to cause a portion of the cross-section to exceed the yield strength of the material.

Once this condition is reached, the stiffness of the member cross-section is decreased and the entire process is repeated. This iteration process continues until an artificial stiffness is found which is consistent with the calculated moment and curvature.

The entire process described above is repeated with increasing values of P until the stiffness of the member cross-section becomes zero implying that the entire cross-section has reached a yielding condition. The value of P at this condition is the ultimate compressive load.

The computer program developed by Mueller and Erzurumlu (7) utilizes the aforementioned procedure. The technique has the ability to model both pinned and fixed end conditions.

Table VIII shows the necessary input parameters for the inelastic computer program. Computer calculations were made for both pinned-pinned and fixed-fixed end conditions. These computer runs were made on the Portland State University Honeywell computer. The results are listed in Table IX and plotted, along with the test results on Figure 52.

Summary of Analytical Methods

For KL/r values greater than 125, both analytical models gave results which paralleled the test results. For KL/r values less than 125, the inelastic method gave results similar to the tests results, but the elastic solution gave increasing unconservative results with lower KL/r ratios.

For a K value of 1.0, which is equivalent to a pinned end condition both analytical methods predicted conservative results. For test specimen groups B, E and F, the elastic solution gave results which were 33%, 30% and 28% respectively, below the test results. The inelastic solution gave results which were conservative by 31%, 25% and 24% respectively.

TABLE VIII

INPUT VALUES FOR INELASTIC SOLUTION

Test Group	Leg	t	h	ex	ey	EI _x	EI _y	A	GJ	X _{sc}	Y _{sc}
A	2.5	0.1875	1.96	-0.0313	-0.818	25317.	6409.	0.902	127.6	-0.848	0
B	2.0	0.1875	1.96	-0.0313	-0.641	12586.	3190.	0.715	102.0	-0.818	0
C	1.75	0.125	1.65	+0.067	-0.663	5829.	1479.	0.422	26.45	-0.684	0
D	2.00	0.125	1.65	-0.0209	-0.663	8787.	2233.	0.484	30.16	-0.596	0
E	2.00	0.1875	1.65	-0.0313	-0.641	12586.	3190.	0.715	102.0	-0.818	0
F	1.75	0.125	1.65	-0.022	-0.575	5829.	1479.	0.422	26.45	-0.684	0

TABLE IX

RESULTS OF INELASTIC COMPUTER SOLUTION

Group	Area	F _y	P _{ff} [*]	P _{pp} ^{**}	P _{test}
A	0.902	45.8	18.8	13.4	16.3
B	0.715	49.9	14.9	8.26	11.0
C	0.422	48.1	9.41	5.13	7.56
D	0.484	53.8	11.7	7.53	9.55
E	0.715	58.8	18.6	11.1	14.8
F	0.422	52.1	8.89	5.23	6.90

* fixed - fixed end conditions

** pinned - pinned end conditions

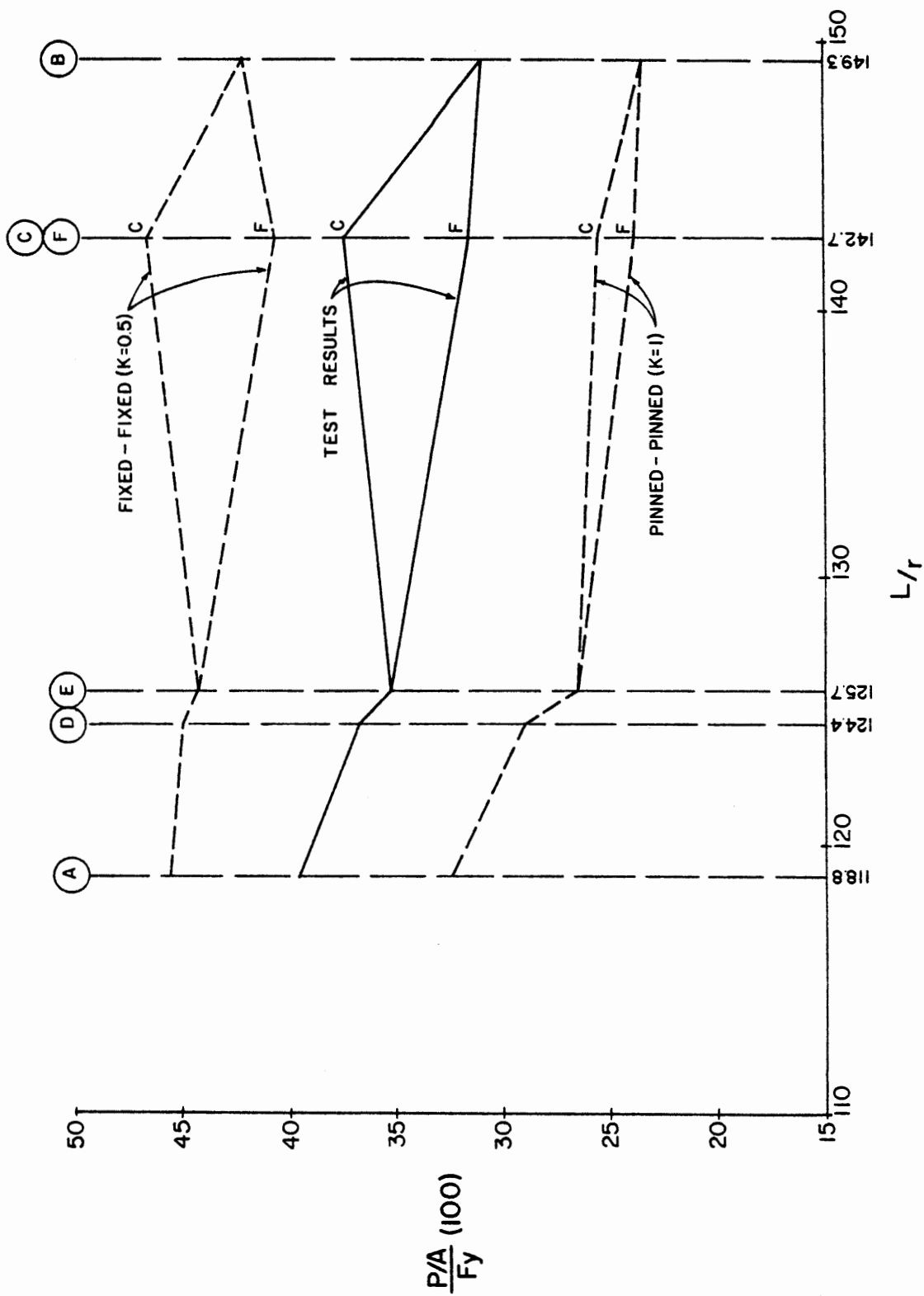


Figure 52. Plot of inelastic solution results.

By varying the K-factor utilized in the elastic solution technique, it is possible to alter the results of the solution and to model a certain amount of end fixity. Figure 51 shows the effects of specifying K-factors of 0.8 and 0.9. As can be observed, a K-factor of 0.8 gives slightly unconservative results whereas a K-factor of 0.9 gives results which are conservative but 50% closer than those resulting from the assumption of $K=1$.

The inelastic method, as developed by Mueller and Erzurumlu (7), can only model pinned or fixed end conditions. However, the test results indicated a significant amount of end fixity. By modeling both the fixed-fixed and pinned-pinned conditions, the inelastic solution provided an upper and lower bound on the test results.

The curves of Figure 52 show that the test results lie midway between the pinned-pinned and fixed-fixed end conditions.

For KL/r values less than 125, the elastic method gave results which were increasingly unconservative. This is readily apparent by looking at the plots of Figure 51. At KL/r ratios less than 125, the inelastic action of the test members becomes significant.

The elastic solution method attempts to predict the performance of the members through the use of amplification factors which modify the basic assumptions of classical elastic theory. For highly eccentric members who have large end moments and correspondingly large curvatures, these amplification factors do not adequately predict the member performance.

The inelastic solution technique gives excellent correlation for members whose KL/r ratio is less than 125. This technique recognizes

that portions of the member cross section may experience inelastic yielding. As Figure 52 shows, the results of the inelastic solution closely parallels the test results over all the range of tests.

CHAPTER V

CONCLUSIONS AND RECOMMENDATIONS

As discussed in the Introduction of this report, the ability to predict the buckling load of a single angle compression member is very difficult.

The results of the test program clearly indicate that the buckling load of a single angle member is very sensitive to the end connection eccentricity. For all of the test specimens of this report, the weak axis eccentricity was quite small, yet there were significant variations in the performance of some members which were fabricated from the same structural section, but with different bolt gaging, and therefore different eccentricities.

Over the L/r range of the group of test specimens, both analytical methods gave results which paralleled the test results. If a pinned-pinned end condition was assumed, both methods gave conservative results over the entire range of test specimen L/r ratios. For a fixed-fixed end condition both methods gave unconservative results.

The results of the elastic method paralleled the test results very well for the L/r range greater than 125. Below this range, the method gave progressively less conservative results. For the L/r range below 125, the elastic model cannot satisfactorily account for the inelastic behavior of a single angle member through the use of conventional elastic assumptions. The elastic method, however, can be safely

utilized for members whose L/r ratios are greater than 125. For this L/r range, failure would be predominately a result of Euler buckling and the effects of any inelastic action resulting from the end connection eccentricity would be minimal.

Both computer programs developed for solving the elastic combined stress equation are satisfactory provide the e_{xx} eccentricity is less than or equal to zero. Either of the two elastic solutions are simple enough to be implemented on a hand held calculator with the closed form solution, Figure 52, being the simplest to implement.

The inelastic solution gave values which paralleled the test results over the entire range of L/r values. Because this method accounts for inelastic behavior along with end connection eccentricity, it can consistently but conservatively predict the buckling load of single angle compression members over a wide L/r range. This technique cannot, however, model end fixity conditions other than pinned or fixed. It was obvious from the test results that some end fixity was present in the end connections.

The only limitations for the use of the inelastic method is the requirement for substantial computer resources. Because of its matrix formulation and iterative process it could not be easily implemented or utilized on currently available small micro computers.

It should be noted that the test frame, because of its massive size, relative to that of the test specimens, provided end support conditions which were effectively infinitely rigid. This would generally not be the case for a single angle diagonal member when it is bolted into a latticed tower structure. It is entirely possible that

the supporting members are only slightly larger than the diagonal member itself therefore providing only limited joint restraint. Therefore utilizing a K-factor of less than 1.0 is not recommended without specific tests to verify the values to be used.

The pinned-pinned buckling loads predicted by the inelastic method, as discussed in this report, can be assumed to be conservative values and, when modified by an appropriate safety factor, utilized as allowable design values for single angle compression members.

The values from the elastic combined stress technique when modified by an appropriate safety factor can also be utilized for single angle compression member design but its use should be limited to members whose L/r ratio is greater than 125.

BIBLIOGRAPHY

1. CHAJES, ALEXANDER, Principles of Structural Stability Theory, (Englewood Cliff, N.J.: Prentice-Hall Inc., 1974)
2. BLEICH, FRIEDRICH, Buckling Strength of Metal Structures, (New York, N.Y.: McGraw-Hill Book Company Inc., 1962)
3. JOHNSTON, BRUCE G., Guide to Stability Design Criteria for Metal Structures, 3rd Edition, (New York, N.Y.: John Wiley & Sons, 1976)
4. BLODGETT, OMER W., Design of Welded Structures, (Cleveland, Ohio: The James F. Lincoln Arc Welding Foundation, 1972)
5. AMERICAN INSTITUTE OF STEEL CONSTRUCTION, Manual of Steel Construction, 8th Edition, (Chicago, Illinois: American Institute of Steel Construction)
6. AMERICAN SOCIETY OF CIVIL ENGINEERS, Guide for the Design of Steel Transmission Towers, Manual No. 52, (New York, N.Y., 1971)
7. MUELLER, W.H. and ERZURUMLU, H., "Limit State Behavior of Steel Angle Columns," (Research Sponsored by Bonneville Power Administration, 1981)
8. BURDEN, R.L., FAIRES, J.D. and REYNOLDS, A.C., Numerical Analysis, (Boston, MA.: Prindle, Weber & Schmidt, 1978)